Force based inclinometry for navigation in legged robots inspired by the desert ant *Cataglyphis spec.*

Von der Fakultät für Ingenieurwissenschaften,
Abteilung Maschinenbau und Verfahrenstechnik der
Universität Duisburg-Essen
zur Erlangung des akademischen Grades einer

Doktorin der Ingenieurwissenschaften
Dr.-Ing.

genehmigte Dissertation

von
Barbara Schlögl
aus
Hamburg

Gutachter:
Univ.-Prof. Dr.-Ing. Dieter Schramm
Prof. Dr. sc. nat. Tobias Seidl
Dr. rer. nat. habil. Robert Martin

Tag der mündlichen Prüfung: 19. März 2021

Danksagung

Am Ende des Tages schreibt man die Doktorarbeit allein, aber nie einsam. An dieser Stelle mein Dank allen Wegbegleitern und Wegbereitern; allen Professoren, Kollegen, Studenten, Freunden und Familie, die mit Rat und Tat zur Seite standen und zum erfolgreichen Abschluss der Arbeit beigetragen haben.

Insbesondere danke ich Prof. Dr. Tobias Seidl für die Begleitung durch den gesamten Prozess der Promotion; für Feedback und gentle guidance in langen und kurzen Gesprächen, für die Gelegenheit im Dialog die Möglichkeiten zu entdecken und für die Freiheit am Ende meinen eigenen Weg zu gehen.

Prof. Dr.-Ing. Dieter Schramm danke ich für die erfolgreiche Kooperation und die freundliche Aufnahme an den Lehrstuhl; für das Einbinden und Anbinden an bewährte Strukturen und Bereitstellen notwendiger Ressourcen.

Dr. habil. Robert Martin danke ich für die Übernahme des Drittgutachtens.

Der Arbeitsgruppe Prof. Dr. Reinhard Blickhan, Dr. Lars Reinhardt und Toni Wöhrl der Friedrich Schiller Universität Jena danke ich für die Bereitstellung der Hochgeschwindigkeitsvideos und assoziierter Datensätze für meine eigene Forschung. Ebenso Dr. Thomas van de Kamp und Dr. Tomas Farago am Karlsruher Institut für Technologie für die Durchführung der μCT Scans.

Danke an alle Kollegen an dem Lehrstuhl für Mechatronik für die freundliche Aufnahme, die kollegiale Unterstützung und die Teilhabe am Flurfunk.

Meiner Arbeitsgruppe vor Ort in Bocholt und allen Professoren und Kollegen am Institut für Bionik sei gedankt für das angenehme Arbeitsklima im täglichen Betrieb.

Allen Studenten, die ich betreuen und begleiten durfte, danke ich für ihren Beitrag und wünsche alles Gute für den weiteren Weg.

Auch allen technisch und administrativ Unterstützenden möchte ich meinen Dank aussprechen.

Neben dem fachlichen Austausch gilt mein Dank allen Freunden, meiner Familie und den fleißigen Korrekturlesern, die je nach Bedarf mit konstruktiver Kritik oder bedingungsloser Aufmunterung unterstützt haben.

Danke.

Kurzfassung

Im Gegensatz zu heimischen Ameisenarten, welche zum Großteil bei der Futtersuche auf die bekannten Ameisenstraßen setzen, sind Vertreter der Art *Cataglyphis fortis* zu großen individuellen Navigationsleistungen gezwungen. In ihrem Lebensraum in der tunesischen Salzwüste ist die Orientierung mittels volatiler Pheromone gar nicht und die visueller Landmarken nur eingeschränkt möglich. Dennoch sind sie in der Lage, ihr Nest auch nach ausgedehnter Futtersuche in Entfernungen von bis zu mehreren zehntausend Körperlängen zuverlässig wiederzufinden. Diese herausragende Navigationsleistung, welche unter schwierigsten Bedingungen mit beschränkten neuronalen Fähigkeiten durchgeführt wird, macht sie zu einem geeigneten Vorbild für die Odometrie in Laufrobotern.

Der bionische Ansatz adressiert gängige Herausforderungen in autonomer Navigation von Laufrobotern. Das vorgeschlagene System ist robust gegenüber äußeren Einflüssen, sparsam im Rechenaufwand, in sich geschlossen und unabhängig von externer Infrastruktur. Das übergeordnete Ziel ist die Entwicklung eines generischen bionischen Systems, welches zu autonomer Lokomotion fähig ist. Im Speziellen befasst sich die vorliegende Arbeit mit dem Element der Bestimmung des Untergrundneigungswinkels, welcher ein entscheidender Baustein für die landgebundene Navigation im dreidimensionalen Raum ist. Mit dieser Information kann die Projektion des gelaufenen Weges auf eine zweidimensionale Ebene errechnet werden. In Kombination mit der Information über die Richtung kann so ein Odometer entwickelt werden, das eine zuverlässige Pfadintegration ermöglicht.

Basierend auf der bestehenden Forschung zu Verhaltensexperimenten bei den Wüstenameisen wird die Hypothese entwickelt und getestet, dass die Messung der Beinkräfte während der Bewegung der entscheidende Faktor ist, um ausreichend Information über den Untergrundneigungswinkel zu erhalten. Im Verlauf der Arbeit wird diese These zugespitzt auf die Messung der Drehmomente in den Gelenken, um das beschriebene Ziel zu erreichen.

Die vorliegende Arbeit folgt dem Prozess des bionischen Arbeitens. Der gewählte Modellorganismus wird analysiert hinsichtlich seiner Morphologie, insbesondere der Lage und Verteilung der Kraftsensoren Campaniforme Sensillen mittels eines Rasterelektronenmikroskops. Die Ergebnisse werden durch Röntgenmikrotomographie mit Synchrotronstrahlung validiert. Die wesentliche Beinbewegung wird aus Hochgeschwindigkeitsvideos extrahiert. Die digitalisierte Bewegung wird verwendet, um ein automatisiertes System zu schaffen, welches die Bewegung in Gelenkwinkel übersetzt. Die Randbedingungen, welche sich durch das Design der technischen Anwendung ergeben, werden direkt berücksichtigt.

Ein einbeiniger Prototyp wird konstruiert, um den zulässigen Grad an Abstraktion zu ermitteln und die Eignung von Drehmomentsensoren im Vergleich zu Kraftsensoren zu ermitteln. Die Ergebnisse werden in der Folge auf eine generische, handelsübliche Hexapodplattform der Mittelklasse übertragen. Die manuelle Auswertung der Drehmomente in allen Gelenken zeigt die grundlegende Möglichkeit der Verknüpfung von gemessenen Gelenk-Drehmomenten mit dem Untergrundneigungswinkel. Künstliche neuronale Netze werden eingesetzt, um die Notwendigkeit der Entwicklung immer neuer Expertensysteme für jede Eventualität, die in einer Forschungsmission auftreten kann, zu umgehen. Mit Hilfe von Datensätzen, die in einer Simulationsumgebung erzeugt werden, wird die optimale Topologie eines flachen feedforward Netzwerkes bestimmt. Be- und Entladeprozesse, sowie ungerade Pfade können so ohne zusätzlichen Aufwand abgefangen werden. Die Validierung erfolgt mittels experimentell ermittelter Datensätze.

Das abschließende Ergebnis bestätigt die eingangs formulierte Hypothese. Es ist möglich ein System zu entwickeln, welches den Untergrundneigungswinkels rein auf Grundlage idiothetischer Informationen bestimmt. Dieses System wird auf einem generischen Laufroboter in der Bewegung implementiert und benötigt nur Informationen über die Drehmomente der Gelenke. Das vorgestellte System ist ohne die Installation weiterer Sensoren funktionsfähig und durch den Einsatz künstlicher neuronaler Netze ressourcenschonend im Rechenaufwand. Die Bestimmung des Untergrundneigungswinkels kann mit einer zeitlichen Auflösung von mindestens einmal pro Schritt erfolgen und somit ist das System prinzipiell echtzeitfähig.

Die vorgestellte Methode hat Auswirkungen auf biologische Forschung sowie auch auf die Entwicklung eines generischen bionischen Systems. Neue Hypothesen über die Verhaltensweisen von Wüstenameisen können auf Basis der Plattform generiert und neue Versuchsdesigns erprobt werden. Darüber hinaus komplementiert das vorgeschlagene System die bestehende Forschung zweidimensionaler Navigationssysteme und kann zudem als redundantes System alternativer Navigationsansätze ohne hohen Aufwand implementiert werden.

Abstract

In the Tunisian desert ants of the species *Cataglyphis fortis* exhibit remarkable navigational abilities. They are able to home even under extreme conditions and rough terrain without the use of external guidance. This makes them ideal candidates for model organisms when developing biomimetic navigation strategies for mobile robots. This approach tackles challenges routinely faced in autonomous mobile robot navigation. The system is robust to external influences, computationally cheap, self-contained and independent of external infrastructure. The broader goal is the development of a generic biomimetic system capable of autonomous locomotion. In particular this thesis addresses the element of detecting the substrate inclination which is crucial information in earth-bound navigation in three-dimensional space. This information will be used in an odometer to determine the ground projection of the travelled distance and thus allow reliable path integration in conjunction with compass information.

Based on existing research like behavioural experiments on the desert ants the hypothesis is developed that measuring forces on the legs during movement is the determining factor to gain sufficient information about the substrate inclination. In the course of this thesis it is narrowed down to the measuring of only joint torques to reach that goal.

The thesis follows the biomimetic engineering process. The model organism is analysed with respect to morphology, location and distribution of force sensors campaniform sensilla with a scanning electron microscope. The findings are validated via synchrotron X-ray microtomography analysis. The essential leg movement is extracted from digitized high speed videos. The data is used to establish an automated system to translate the motion to joint angles under varying constrictions that can be chosen based on the design of the desired technical application.

A one legged prototype is constructed to evaluate the permissible level of abstraction and the suitability of force sensors versus torque sensors. The results are subsequently transferred to a generic commercially available mid range hexapod platform. Manual analysis of joint

torque proves the general feasibility of correlating the joint torque measurements with the substrate inclination. To eliminate designing expert systems for each eventuality encountered in an exploratory mission artificial neural networks are employed. Simulated data is used to optimize the topology of a shallow feedforward network sufficient for this task. Loading and unloading processes as well as slanted paths are covered in this approach. Validation is performed on experimental data.

The final conclusion of the thesis affirms the initial hypothesis. It is possible to implement a system on a generic mobile robot platform that allows detection of the substrate inclination based solely on idiothetic cues, i.e. joint torques. The proposed system works without installation of additional sensors and is computationally economical through the use of artificial neural networks. Determining the inclination is possible with a temporal resolution of once per step and as such suited for real time capable systems.

The presented method has implications on biological research as well as the development of generic biomimetic systems. New hypotheses about the desert ants can be generated and experiments designed with the use of the robotic platform. Furthermore the proposed method ties in seamlessly with existing research of two-dimensional navigation systems or as a redundant system to amend alternative navigation methods.

Contents

Kurzfassung **v**

Abstract **vii**

Notation **xiii**

I Introduction **1**

1 Motivation **5**

2 State of the Art **7**
2.1 Mobile Robot Navigation 7
2.2 Desert Ant Navigation 8

3 Structure **13**

II Analysis **17**

4 Morphology **21**
4.1 Introduction 21
4.2 Material and Methods 23
4.2.1 Samples 23
4.2.2 Scanning Electron Microscopy 23
4.2.3 Micro Computer Tomography 25
4.3 Results 25
4.3.1 Scanning Electron Microscopy 26
4.3.2 Micro Computer Tomography 26

4.4 Conclusions . . . 27

5 Kinematics **31**
5.1 Introduction . . . 31
5.2 Material and Methods . . . 32
5.2.1 Digitization . . . 32
5.2.2 Direct Kinematics . . . 34
5.2.3 Inverse Kinematics . . . 37
5.3 Results . . . 37
5.3.1 Direct Kinematics . . . 37
5.3.2 Inverse Kinematics . . . 38
5.4 Conclusions . . . 39

III Synthesis **43**

6 One Legged Platform **47**
6.1 Introduction . . . 47
6.2 Material and Methods . . . 48
6.2.1 Mechanical Components . . . 49
6.2.2 Simulated Environment . . . 50
6.2.3 Sensors . . . 50
6.2.4 Control and Movement . . . 52
6.2.5 Experimental Protocol . . . 53
6.3 Results . . . 54
6.4 Conclusions . . . 60
6.4.1 Experimental Setup . . . 60
6.4.2 Sensors . . . 61
6.4.3 Parameter Additional Weight . . . 62
6.4.4 Further Parameter Changes . . . 63
6.4.5 Influence on Further Research . . . 63

7 Hexapod Platform **65**
7.1 Introduction . . . 65
7.2 Material and Methods . . . 66
7.2.1 PhantomX Hexapod . . . 66
7.2.2 Experimental Setup . . . 67
7.2.3 Control . . . 68
7.2.4 Movement . . . 71
7.2.5 Sensors . . . 71
7.2.6 Data Preparation . . . 72
7.3 Results . . . 72
7.3.1 General Movement and Influence of Geometry . . . 73
7.3.2 Influence of Inclination . . . 74
7.4 Conclusions . . . 74
7.4.1 Influence of Previous Research . . . 76

7.4.2 Results . . . 76
7.4.3 Parameter Changes . . . 77
7.4.4 Influence on Further Research . . . 78

8 Artificial Neural Networks 79
8.1 Introduction . . . 79
8.2 Material and Methods . . . 81
8.2.1 Simulated Data . . . 81
8.2.2 Experimental Data . . . 83
8.2.3 Artificial Neural Network . . . 84
8.3 Results . . . 85
8.3.1 Simulated Data . . . 86
8.3.2 Experimental Data . . . 87
8.4 Conclusions . . . 93

IV Discussion 95

9 Summary 99

10 Scientific Contribution 103

11 Future Directions 105
11.1 Biological Model Organism . . . 105
11.2 Improvement on the Framework . . . 106
11.2.1 Photogrammetry . . . 106
11.2.2 DeepLabCut . . . 107
11.3 Generic Biomimetic System . . . 111

A Technical Drawings 113

B Supplementary Statistics 121

C Additional Measurements 133

List of Figures 135

List of Tables 144

Bibliography 147

Supervised Student Contribution to the Dissertation 155

Notation

3D three-dimensional

ANN artificial neural network

CAD computer-aided design

COM centre of mass

c.s. campaniform sensilla

csv comma separated values

DOF degrees of freedom

GPS global positioning system

μSR-CT synchrotron X-ray microtomography

MAE mean absolute error

MSE mean squared error

PLA polylactic acid

px pixel

RMSE root-mean-square error

ROS robot operating system

SEM scanning electron microscope

USB universal serial bus

Part I

Introduction

Contents

This part lays the necessary groundwork and introduces the relevant topics of the thesis.

Chapter 1 gives the necessary context to motivate the research.

Chapter 2 lays out the state of the art in desert ant research as well as on autonomous mobile robots. Based on this the research gap is identified.

Chapter 3 gives an overview over the structure of the thesis.

CHAPTER 1

Motivation

The fundamental motivation for the research topic is given.

Ever since the development of mobile robots one of the central research questions is their localization. For the robot to act truly autonomously it needs to be able to navigate on its own whether in an exploratory, delivery or service capacity. Current solutions for localization mostly rely on external infrastructure such as global positioning system (GPS), beacons or similar reference signals [Talluri and Aggarwal, 1999]. This of course inherently requires prior exploration of the environment and investment in infrastructure separately from the actual robot.

This thesis proposes a novel approach to the challenge based on biomimetic principles. In accordance with the biomimetic engineering process [VDI-Richtlinie 6220, 2012] the top-down approach aims to translate achievements observed in living nature to improve or enable technical applications.

Regarding navigational abilities one remarkable model organism is the desert ant *Cataglyphis fortis*. In contrast to the species prevalent in temperate climates they can not rely on coordination via pheromone trails. With the desert being their primary habitat the volatile scents evaporate too quickly to be useful and orientation along landmarks is limited in the sparse environment. Under the evolutionary pressure this species and other related species developed, amongst other, individual navigation strategies relying solely on idiothetic

cues. Thus foraging in extreme environmental conditions becomes feasible even with limited computing abilities due to small brain sizes. In their search the animals travel paths of up to a kilometre at distances of several hundred metres away from the nest which translates to several ten thousands body lengths for the ant [Ronacher, 2008].

The navigational ability of the desert ant, which convinces with its robustness to external disruptions, compact design and small computational effort, inspires the robot odometer developed in the presented thesis [Schlögl et al., 2018b]. In technical applications where external sensors or existing odometers are available the method based on ant odometry provides additional determination of the location in real time, thus increasing the redundancy of the system without requiring additional sensors.

CHAPTER 2

State of the Art

This chapter compiles the established navigational solutions in mobile robots to illustrate the advantages of the proposed approach. Subsequently the existing research in desert ant navigation is reviewed as foundation to the following original research.

2.1 Mobile Robot Navigation

Various systems for navigation in mobile robots have been developed with their unique sets of advantages and disadvantages. Generally they either rely on external infrastructure measuring the robot's position in relation to the known and fixed position of the beacons or on sensors fixed to the robot supplying it with information about its surroundings to infer its current position relative to a starting point or known configurations.

The disadvantage of external infrastructure is evident in the need to deploy the reference structures. Beacons would have to be installed in advance and thus the environment is already surveyed and in part explored. Even a global positioning system like GPS has drawbacks. For one the accuracy in standard, low cost, civilian applications is limited to around 3 m [McNamara, 2008]. Additionally the use is limited when considering applications within buildings, underground, underwater or extraterrestrial.

Systems that require the robot to follow markers along the way suffer from similar problems insofar that no exploration is possible, the territory has to be prepared in advance and limited flexibility in regards to unexpected obstacles is inherent. Additional systems to detect obstacles would be necessary.

A purely haptical approach based on impact sensors as they exist in the recently popularised cleaning robots proves impractical in unstructured terrain because of the late detection and risk of destruction on an unknown surface.

A possibility to gather data about the environment collision and destruction free is the use of lasers [Carmer and Peterson, 1996] to scan the surroundings. The use is limited by reflecting surfaces and viable only within a certain distance since high powered lasers could be incompatible in robot human interaction scenarios because of the risk of involuntary eye damage. Similar approaches based on other sensors include sonar and infra-red sensors [Hertzberg et al., 2012].

A less dangerous and very popular approach is the use of cameras [DeSouza and Kak, 2002]. While this seems very intuitive from a human perspective, the interpretation of the acquired data necessitates sophisticated algorithms for image recognition. Depending on the resolution of the pictures the computational requirements demand high energy consumption in addition to the consumption required to carry the additional weight of the camera and potential stabilizing equipment.

One of the easiest and commonly used methods for localization of wheeled autonomous robots is odometry. Using rotary encoders and compass information the current location is calculated relative to the starting point. Usually this information is supplemented by additional measurements because of its susceptibility to errors like sensor drift or slip effects [Hertzberg et al., 2012].

The proposed system joins the range of existing navigation techniques that are self-sufficient, focussing on the more versatile legged robots. Based on the biological model it encompasses several advantages such as low computational effort, robustness to external disturbances and independence of external infrastructure because it relies solely on idiothetic information. Since the solution does not need additional sensors it is possible to implement it as redundant odometer on existing commercial walking robots and thus obtain an additional control mechanism to improve the precision of the localization through sensor fusion.

2.2 Desert Ant Navigation

General Anatomy The desert ant *Cataglyphis fortis* has been subject to extensive biological research for several decades starting in the early 1900s [Forel, 1902, Santschi, 1929]. Their anatomy was already comprehensively described in 1983 [Wehner, 1983]. As usual

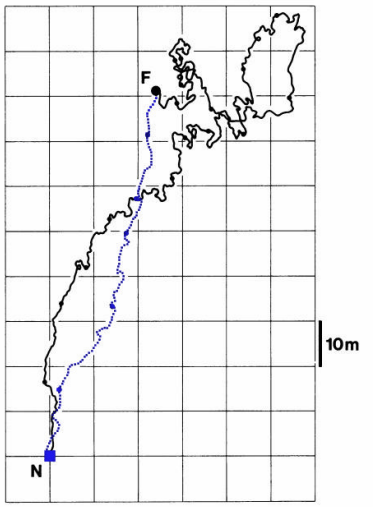

Figure 2.1: Path of a foraging desert ant after [Müller and Wehner, 1988]. N denotes the position of the nest, F denotes the position of the feeder. Black line is the foraging path. Blue line is the homing path.

with eusocial insects the members of different castes exhibit distinct characteristics depending on their tasks. For the navigational behaviour the focus lies on the foragers. They possess especially long legs which keep the body far from the ground since the foraging takes place during the hottest time of day [Sommer and Wehner, 2012]. Their compound eyes allow navigation along landmarks and optical flow [Fleischmann et al., 2016, Ronacher and Wehner, 1995] among other means of orientation. Of the various sensory systems of the ants they can use visual [Knaden and Wehner, 2005, Wehner and Räber, 1979], olfactory [Steck et al., 2009a, Steck et al., 2010, Steck et al., 2011] and tactile landmarks [Seidl and Wehner, 2006] as well as vibrations and magnetic cues [Bühlmann et al., 2012] to find the nest entrance which is only a small hole in the ground [Jeffery, 2003, Müller and Wehner, 1988]. All of these means are more useful in the vicinity of the nest entrance and hold little use for navigation at greater distances.

General Navigation While foraging the worker ants cover distances of several thousand body lengths [Ronacher, 2008]. In order to avoid retracing every step taken in the search pattern a robust homing method is necessary (Fig. 2.1). Path integration and the use of visual landmarks are two distinct and separate methods the ant uses to navigate. They work parallel and in competition with each other. Depending on distance to the nest their priority changes. The further from the nest, the more the ant relies on path integration, the closer to the nest, the more importance is given on recognition of landmarks [Hoinville and Wehner, 2018]. Since the two systems rely on completely separate sensors they can be investigated independently of each other. Accordingly, in this work no further investigation is made concerning visual navigation instead focussing on the path integration method.

Path Integration The principles of path integration in the desert ants are investigated through behavioural experiments (Fig. 2.2). The general setup of the experiment involves two parallel channels with one of the channels including the nest entrance. At the end of this training channel a feeder is installed. After the training period the ants are picked up at the feeder and transferred to the parallel test channel. Once the ant reaches the position in which it assumes the nest entrances but is unable to find it the animal starts a search in continuously widening turns. The most frequently passed position then corresponds to the assumed position of the nest entrance. To avoid giving the animals visual cues the channels are painted uniformly grey.

With this setup it is determined that path integration in desert ants *Cataglyphis fortis* consists of two parts. The ant is determining the direction through a sun compass and the distance by a step integrator. The sun compass works by detecting the polarization of the sunlight and extrapolating the direction the ant is heading [Wehner, 1982]. Though the compass constitutes an integral part of the path integration, it is not part of the following work since it is independent from all leg movement and the detection of inclination.

For the step counter on the other hand the leg movement is essential [Seidl et al., 2006]. While walking the ant integrates its steps to determine the distance travelled [Seidl, 2008, Wittlinger et al., 2006]. In a three-dimensional (3D) environment the substrate inclination has to be taken into consideration [Seidl and Wehner, 2008]. It is found that internally the ant does not use a full 3D representation of its surroundings but rather works with the ground projection [Wohlgemuth et al., 2002].

While this demonstrates that the ant has to measure the inclination the research question considering the function principle remains open. In this work based on the existing research the hypothesis is formulated that the forces on the ant's legs are detected and used to determine the angle of inclination.

Ground Reaction Forces Studies on the ground reaction forces of desert ants *Cataglyphis fortis* substantiate the formulated hypothesis. [Reinhardt, 2014] establishes a force measuring platform to determine the ground reaction forces in the desert ants while moving through a channel. The forces are analysed depending on the angle of inclination of the channel [Wöhrl et al., 2017]. Qualitative distinct forces occur depending on substrate inclination. If the desert ant is able to detect and interpret these forces on its legs it is possible for the animal to infer the inclination and use this information in navigation.

Conclusions Taken together the presented research suggests that the working principle of desert ant odometry relies on the forces on the legs. They are used to determine the angle of inclination of the substrate and subsequently to calculate the ground projection of the distance travelled from the starting point at the nest entrance. To implement a simple and effective solution to odometry in mobile robots the supposed principle is transferred to

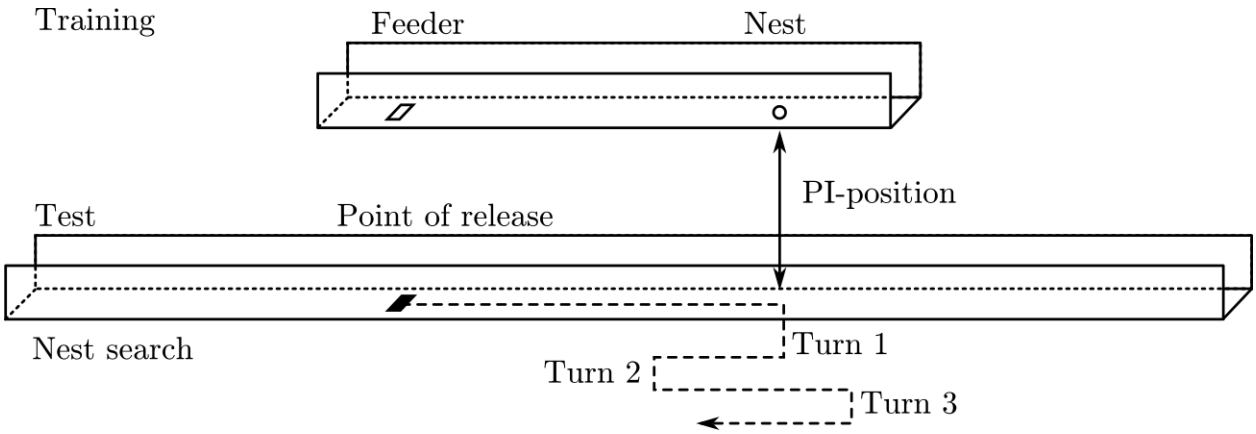

Figure 2.2: Experimental setup modified after [Seidl and Wehner, 2006]. Training and test channel are set up parallel to each other. After several trips between nest and feeder in the training channel the ants are transferred to the test channel. The position of the turns are recorded to determine the assumed position of the nest.

the technical application following the biomimetic engineering process [VDI-Richtlinie 6220, 2012]. The feasibility of the approach leads to insights on the plausibility of the suggested hypothesis in the biological model.

CHAPTER 3

Structure

The structure of the thesis is laid out and the central hypothesis formulated.

Based on the preliminary and existing research the central hypothesis is formulated:
It is possible to deduct the inclination of the substrate by measuring the forces occurring in the legs of a walking robot.
The information about the inclination allows the development of a robust odometer based on the navigation of desert ants with the goal of returning to the starting point after crossing structured terrain. The hypothesis is tested on a physical robot platform as well as in simulation. Joint torque is identified as suitable measure for the occurring forces [Schlögl et al., 2018a]. Implementing the technical solution allows generating new theories about the biological model.

The overall structure of the thesis follows the biomimetic engineering process of analysing the biological model, abstracting the findings, implementing them on a technical application and evaluate the findings. The thesis is structured into four parts: Introduction, Analysis, Synthesis and Discussion with the two middle parts containing the original research. Each of the chapters in those parts is in turn separated into four parts: Introduction, Material and Methods, Results, and Conclusions.

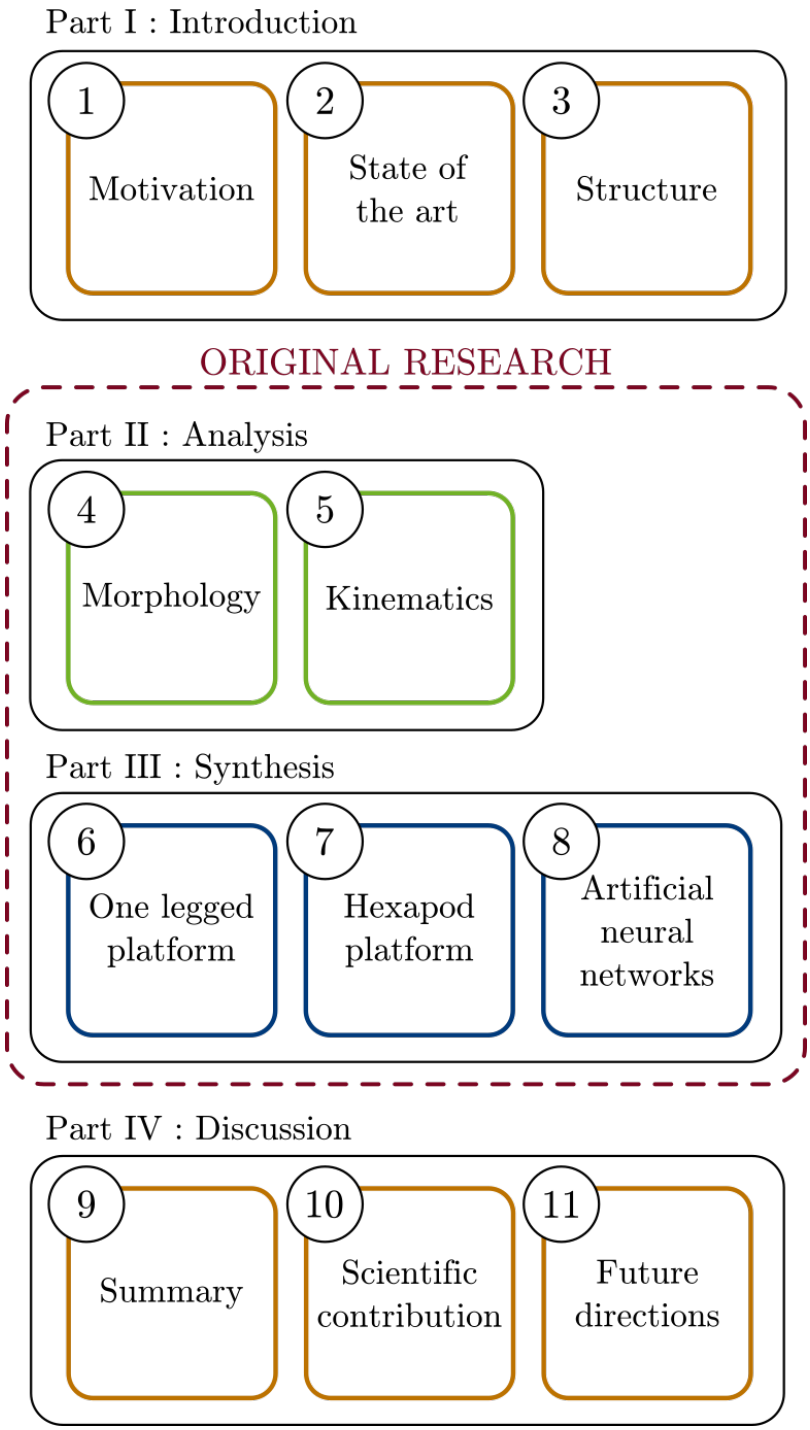

Figure 3.1: Structure of the thesis. Numbers denote chapter numbers. The thesis is structured in four parts with Part II and Part III comprising the original research.

Part I introduces the motivation for the thesis (Chapter 1). The state of the art in research regarding mobile robot navigation is detailed as well as the foundations of the research regarding the biological model (Chapter 2). Finally an overview over the structure of the thesis is given (Chapter 3).

Part II analyses the essential characteristics of the biological model. The ant morphology is investigated to substantiate the anatomical plausibility of the approach. Location and distribution of the force sensors on the legs are determined to be concentrated at the joints (Chapter 4).

Subsequently the kinematics of motion are analysed as they have been identified as crucial to the path integration (Chapter 5). The motion of single legs is abstracted and translated into a robot readable format.

Part III encompasses all aspects of the technical application. The limitations of the abstraction are determined to reduce the system complexity of the technical implementation. On a one legged platform (Chapter 6) emulating the proportions and the motion pattern of the biological model several sensors are evaluated to corroborate the hypothesis developed in Part II.

The results are translated to a generic six legged robot platform (Chapter 7). Manual analysis of the joint torque measurements when moving over various inclinations reveal that distinguishing them based on the measured values is possible. Based on the general feasibility of the task the expert knowledge necessary to differentiate the inclinations is replaced through the use of an artificial neural network (Chapter 8). The system is able to correct for weight differences and slanted paths in a simulated environment. The findings are validated on a real world dataset acquired from the robotic platform.

Part IV concludes with a summary of all original findings (Chapter 9) and states the scientific contribution (Chapter 10). Greater research contexts are considered with regards to the biological model organism and to improving the presented approach as well as an outlook to integrate the established system into other current research in order to gain a generic biomimetic robot system capable of autonomous navigation (Chapter 11).

Part II

Analysis

Contents

This part covers the necessary analysis of the biological model organism. The desert ant *Cataglyphis fortis* is investigated with regards to the morphology and kinematics of the legs. Thus the plausibility of the proposed approach is secured. The insights gained influence the design of the technical testing environments in the subsequent Part III.

Chapter 4 investigates the morphology of the desert ant's legs. In particular location and distribution of the force sensors campaniform sensilla is determined via scanning electron microscope and validated via synchrotron X-ray microtomography. They are concentrated at the joints, in particular the coxa-femur joint.

Chapter 5 presents a framework to translate digitized motion data to joint angles that can be used to control robotic platforms. The movement of desert ant front legs is shown to consist of four degrees of freedom. The motion can be reduced to three degrees of freedom without losing critical information. The system allows setting and adjusting constraints introduced by the limitations of technical implementations. The generated motion patterns are transferred in the subsequent part to the one legged robotic platform.

CHAPTER 4

Morphology

This chapter determines the position of force sensors campaniform sensilla on the legs of desert ants Cataglyphis fortis. Investigations are carried out via scanning electron microscope and validated via synchrotron X-ray microtomography. The force sensors are not spread evenly but are concentrated in fields around the joints, in particular the coxa-femur joint. This finding influences the further research as it is then concentrated on exploring the possibilities offered by measuring the joint torques via internal sensors.

4.1 Introduction

To successfully navigate uneven terrain it is necessary to know the angle of inclination of the substrate. In behavioural experiments several other anatomically plausible sensors were ruled out as mechanism to detect inclination. It was shown that leg movement is elementary since displacing the ant without the animal moving on its own prevented successful homing [Seidl et al., 2006]. Hair fields that gather information about the position of the legs could be shaved off without the ant losing the ability to navigate [Wittlinger et al., 2007]. Likewise duration and sequence of stance and swing phase does not correlate with change in inclination [Seidl and Wehner, 2008]. Visual signals are not at all processed in lateral direction and only to 10 % in ventral direction [Ronacher et al., 2000, Ronacher and Wehner, 1995]. In the experiments

optical flow is minimized by using corridors painted uniformly grey to prevent influencing the results of path integration. Energy consumption can be excluded as mechanism since distance estimation was not influenced by additional load while carrying food [Wehner, 1983].

Considering all this groundwork in excluding other possibilities and establishing the plausibility of measuring inclination through forces in the legs, the campaniform sensilla (c.s.) are probable candidates for being the basis of the measuring mechanism. Campaniform sensilla are known sensory systems in arthropods in general [Hoffmann, 1964] and in particular in insects [Kaib et al., 2010]. They are proprioceptive organs that usually occur in clusters on the body surface. This enables the measuring of tensile and compressive forces in the insect's rigid exoskeleton [Thurm, 2001].

In ants in particular c.s. are documented on the antenna [Dumpert, 1972]. Electrophysiological experiments on leaf-cutting ants show that they detect vibrations through the c.s. on their legs and use them to communicate [Markl, 1970] with the sensitivity decreasing from front to middle and hind legs.

Insects comprise the biggest class of animals with almost one million species having been scientifically described so far [Grimaldi et al., 2005] of which over 12 000 are classified as ants [Bolton, 2003]. Insofar it is not surprising that there is no extensive research published on the one specific species of *Cataglyphis fortis* particularly on the location of c.s. on their legs. Therefore original research has to be carried out before further investigations can commence.

With the research and insights gathered on the sensors on other insect species estimates concerning size and location can be carried over to the investigation of the desert ant *Cataglyphis fortis*. The small size of the sensors lends itself to only a limited amount of possible research methods. The ant legs are examined in detail with a scanning electron microscope (SEM). The locations of the sensors as identified with this method are validated in the 3D representation as acquired via synchrotron X-ray microtomography (μSR-CT). With both methods the location of the force sensors is determined to concentrate at the joints of the animal. This influences further research insofar as special consideration is given to the possibility of measuring joint torque in place of more elaborate force measuring schemes in or along the technical legs.

Chapter 3 introduces the hypothesis that measuring the leg forces is sufficient to determine said inclination. In this chapter the anatomic plausibility of that suggestion is investigated and the influence on the design of a robotic representation is evaluated. Without the anatomic prerequisites to measure leg forces the hypothesis would be insupportable for the desert ant *Cataglyphis fortis*. Distribution and location of the force sensors provide insight on possible technical recreations and limitations.

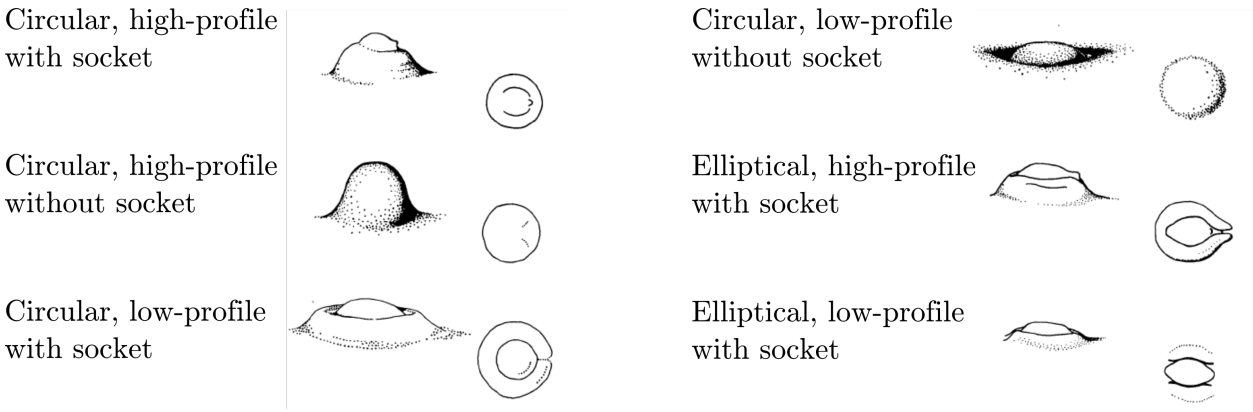

Figure 4.1: Various known shapes of campaniform sensilla as described on the wing and haltere of *drosophila melanogaster*. Modified after [Cole and Palka, 1982].

4.2 Material and Methods

Campaniform sensilla present in a variety of shapes (Fig. 4.1). Based on the findings on other ants and insects the size of the c.s. is expected to be in the order of micrometers. To examine them two methods for small scale investigations are employed. The SEM allows two-dimensional imaging of the ant legs in fixed positions. To cover the whole surface legs of various specimen are investigated. Finally the findings are validated in the three-dimensional imaging of a μSR-CT.

4.2.1 Samples

The desert ants were captured in the wild on an expedition in August of 2015 by Cornelia Bühlmann (University of Sussex) in a dry salt pan near the village of Menzel Chaker, Tunisia. They were put in an ethanol filled plastic test tube for conservation purposes and sent by mail to the laboratory in Bocholt. At time of conservation some of the animals were recently deceased, some still alive.

4.2.2 Scanning Electron Microscopy

Scanning Electron Microscopy is a method that was introduced in 1937 and is widely applied over a broad range of research topics. A focused electron beam is directed at the sample. Scattering electrons that leave the sample are caught on detectors. The higher the number of electrons, the higher the energy, the closer sample and cathode. Then the beam is moved a small bit and the scattering of the next piece of sample is examined. Bit by bit the whole sample is covered and the height of the surface is mapped. Crucial to this investigation method is the conductivity of the sample. If the sample is not very conductive, as is the case with a lot of biological samples, it is being charged over time which distorts

Figure 4.2: Prepared scanning electron microscope sample. Double sided tape is stuck to the sample holder and slices for the legs marked. The dried and dissected legs are placed and the whole holder is sputtered with gold.

the measurement. To prevent this the surfaces can be sputtered with conductive materials, which allows better resolution or more robust results. Prerequisite to this method producing faithful results is the sturdiness of the surface so that it doesn't deform in the preparation process. Another common problem with biological samples in SEM is the vacuum. The samples have to be dried. Fortunately the exoskeleton of ants is not overly wet and as such does not change too much in the drying process.

The SEM used in this investigation is a Hitachi model TM3030 (Hitachi High-Technologies Corporation, Japan). Its magnification ranges from 15 to 30 000. The maximum sample size is 70 mm in diameter and 50 mm in height.

Sample Preparation The specimen are air-dried overnight and the legs cut off with a razor blade. They are fixated on a SEM sample holder with conductive double sided tape. The samples are sputtered with gold on a Sputter Coater (Cressington 108auto, Cressington Scientific Instruments Ltd., England) at a current of 30 mA for 60 s. The legs of each specimen are distributed on a separate sample holder for easier identification. (Fig. 4.2) Four distinct specimen were investigated. For two of the samples the front, middle and hind legs of one side of the body are oriented with the dorsal side facing up while the legs of the opposite side of the body are oriented with the ventral side facing up. The other two samples are oriented with the caudal respective cranial side facing up (Fig. 4.3). This way the perspective of all anatomical planes are covered in at least two different specimen.

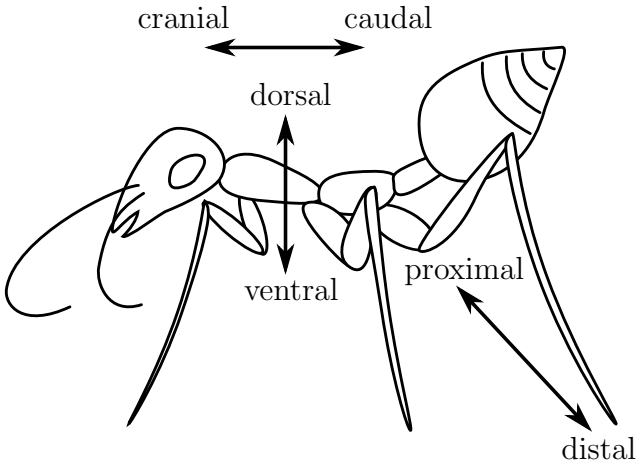

Figure 4.3: Anatomical directional reference of the ant. Cranial and caudal describe positions closer or farther from the head. Dorsal and ventral reference the distance to the back or stomach respectively. Proximal and distal denote the closeness to the body.

4.2.3 Micro Computer Tomography

A drawback of the SEM is, that the legs can only be examined from one perspective. After the legs are prepared their position can not be changed. To get a full 3D view of the whole leg this method is not appropriate. To validate the findings synchrotron X-ray microtomography is used which is an imaging technique that uses X-rays to get a three-dimensional reconstruction of an object, including internal structures in a non-destructive way [Flannery et al., 1987]. The sample was air-dried over night and the legs cut off with a razor blade. The legs and body were isolated in small plastic test tubes and sent to the Institute for Photon Science and Synchrotron Radiation of the Karlsruhe Institute of Technology (KIT). The imaging was performed by Thomas van de Kamp (KIT) and Tomás Faragó (KIT). The UFO imaging station of the KIT light source is used for synchrotron X-ray tomography. The parallel polychromatic X-ray beam is spectrally filtered to achieve a peak at 15 keV. Then 3 000 radiographic projections are taken. The magnification is adjusted to result in an effective X-ray pixel size of 2.44 µm. The tomographic reconstruction is performed with the GPU-accelerated filtered back projection algorithm implemented in the software framework UFO [Vogelgesang et al., 2012].

4.3 Results

With the SEM method it is possible to identify different c.s. fields with close resemblance along all legs and all specimen. The location of the fields are validated through the μSR-CT method.

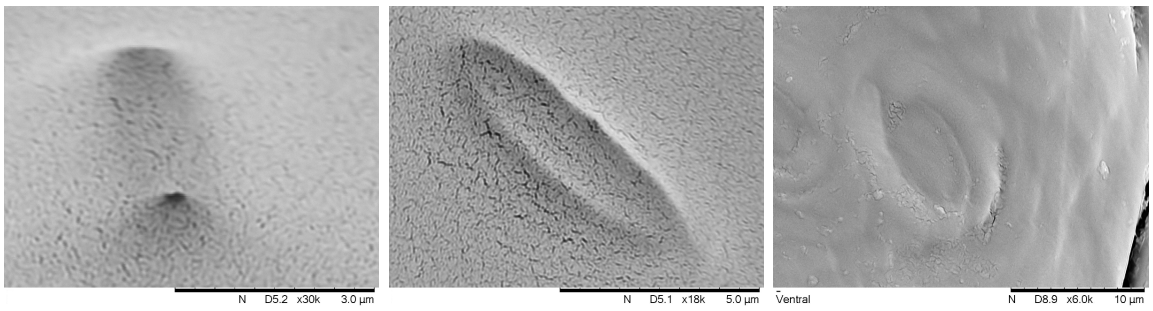

Figure 4.4: Three different shapes of campaniform sensilla on the legs of *Cataglyphis fortis*. All pictures taken on right middle legs. Left and middle pictures are from the same specimen, right picture from another specimen. Pictures taken as part of student work [Kreimeier, 2017].

4.3.1 Scanning Electron Microscopy

The Hitachi TM3030 SEM provides sufficient resolution to locate single c.s. on the prepared samples. The c.s. take distinct shapes (Fig. 4.4). They are either clustered in fields but also single c.s. are found. All discovered c.s. are elliptic in shape with the major axis (8.28 ± 0.15) µm and the minor axis (2.38 ± 0.29) µm in length. Most of the c.s. are arranged in fields with some single sensilla distributed in no particular pattern on the trochanter. The fields are the same over all legs in all examined specimen regarding location and orientation with only slight differences in number of c.s. per field (Fig. 4.7). One field is oriented ventrally on the femur and three on the trochanter are oriented in between caudal and dorsal direction. The rest of the leg is scanned with the same magnification but no further c.s. are discovered.

4.3.2 Micro Computer Tomography

The slices of the μSR-CT are reconstructed to a 3D volume in Drishti (Version 2.5.1) [Limaye, 2012] to visually check the validity of the acquired data (Fig. 4.8a). To closer examine the surface of the leg 3D Slicer (Version 4.10.1) [Kikinis et al., 2014, Fedorov et al., 2012] is used to reconstruct the exoskeleton. In this reconstruction the edge length of the voxels measures 2.44 µm. This is in the same order of magnitude as the size of the c.s. discovered by the SEM investigations (Subsection 4.3.1). Thus the c.s. appear as holes on the surface of the reconstructed exoskeleton (Subsection 4.3.2). The position of the fields as identified by the SEM results can be validated on another specimen. The resolution is not sufficient to reliably discover unknown single campaniform sensilla or c.s. fields.

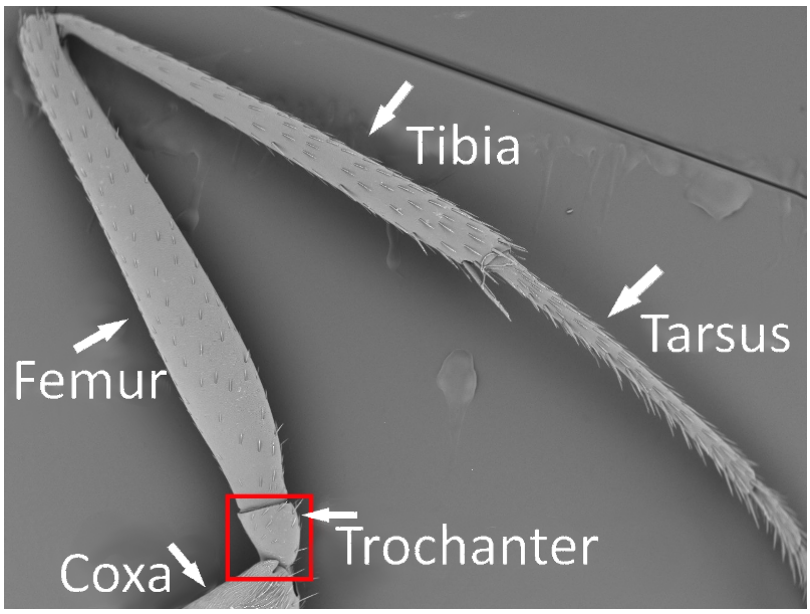

Figure 4.5: Overview of one dissected leg under the scanning electron microscope with the segments labelled accordingly. Campaniform sensilla are found mainly in the area marked with the red square. Fig. 4.6 shows magnifications of this area on different samples and thus different perspectives. Pictures taken as part of student work [Kreimeier, 2017].

4.4 Conclusions

Scanning electron microscopy The small sample size of four specimen examined with the SEM and one additional specimen with the μSR-CT does not permit generalization for the species of *Cataglyphis fortis* as a whole. Still the fact that the variations occurred less in placement but rather in number of c.s. per field suggests an underlying principle. Mechanically leverage effects are a plausible root cause for the concentration of the sensors near the joints especially the trochanter. This also suggests that knowledge of the detailed force profile along the whole leg is not necessary. Measuring at neuralgic points near the joints may be sufficient.

Micro Computer Tomography The resolution of 2.44 µm voxel size is sufficient to detect the campaniform sensilla as holes in the reconstructed surface. Since the c.s. are only between 5 µm and 10 µm long and about 2 µm wide it is not possible to reliably discern c.s. from reconstruction artefacts. Therefore it is not a suitable method to find new c.s. but it is suited to validate the known positions acquired via the SEM method. In this way the drawback of the latter method of not providing a full three-dimensional model can be eliminated.

Influence on further research The final objective of investigating the force sensors in this context is not the lifelike replica of a desert ant or their campaniform sensilla but

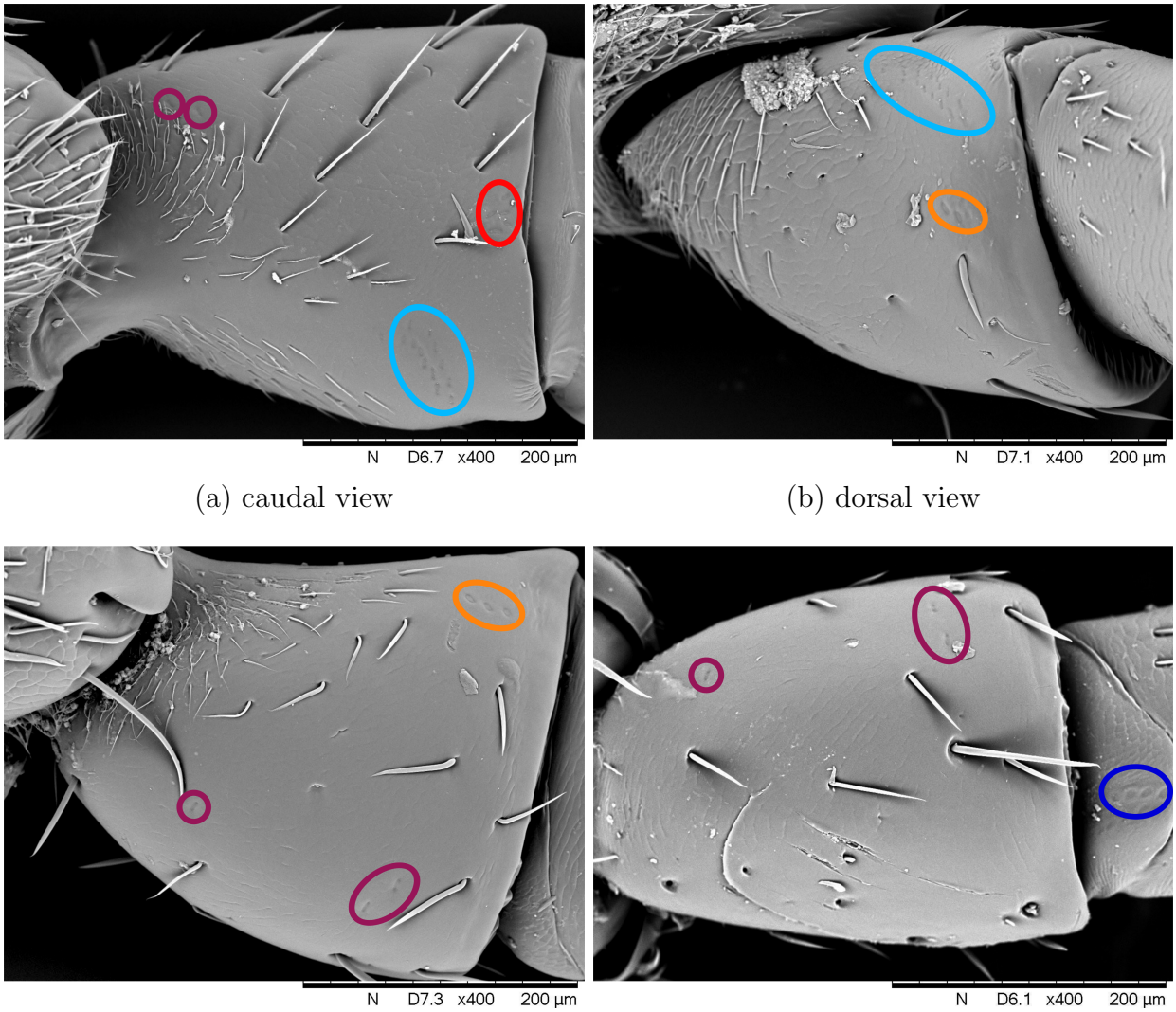

(a) caudal view (b) dorsal view

(c) cranial view (d) ventral view

Figure 4.6: All available views of the trochanter on the samples. Views according to the subcaptions. Circles mark fields and single campaniform sensilla with color according to Fig. 4.7. Modified after student work [Kreimeier, 2017].

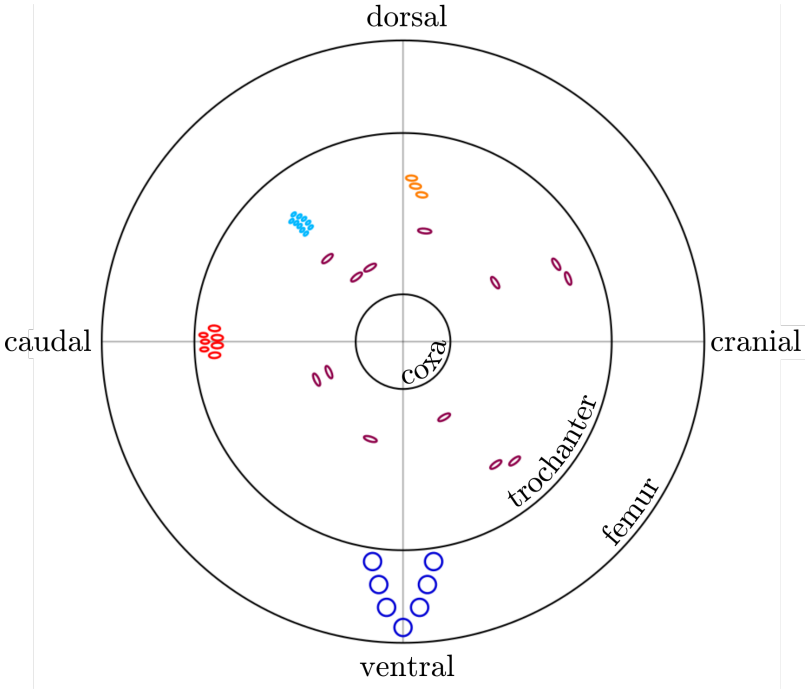

Figure 4.7: Polar projection of discovered fields and single campaniform sensilla. Pictures taken as part of student work [Kreimeier, 2017].

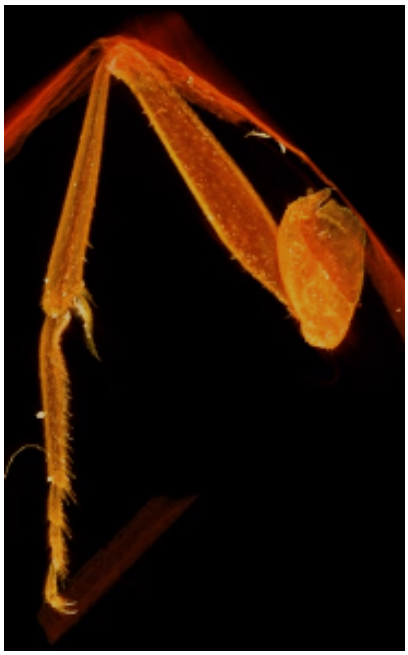

(a) Reconstruction via Drishti.

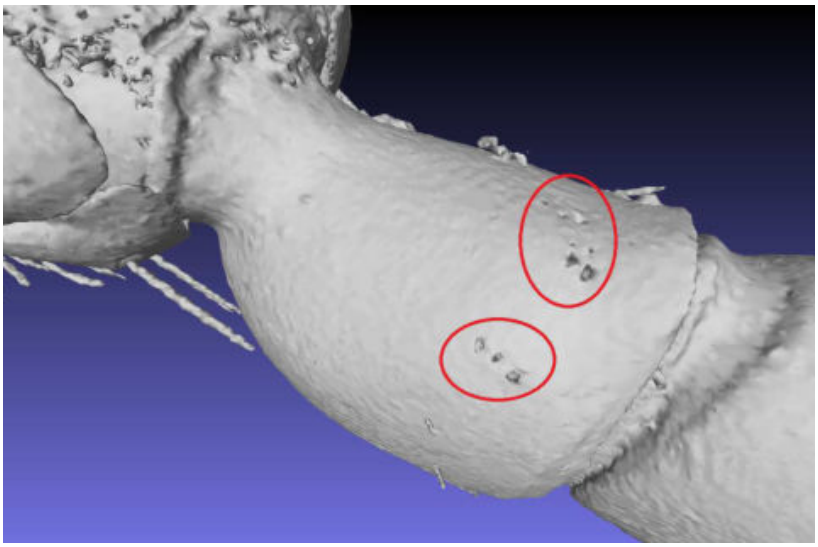

(b) Reconstruction via 3D Slicer. Pictures taken as part of student work [Hügel, 2018].

Figure 4.8: Reconstructed synchrotron X-ray microtomography images. Holes on the surface (marked with red circles) correspond to the positions of the campaniform sensilla as determined via scanning electron microscope.

rather the abstraction and further application of underlying principles. A replication of the full sensory system of the desert ant is not expedient in realizing the implementation on a technical application. The research questions that could be answered with investigating the sensilla more thoroughly, though interesting, do not contribute to the development of a cheap, fast and widely applicable odometer. The production cost and time and resources spent on development are disproportionate to the expected benefits considering the ongoing research in the field of c.s. in various insects [Vincent et al., 2007].

In the original research presented in this chapter the c.s. on the legs of the desert ant *Cataglyphis fortis* are concentrated on the joints, in particular the trochanter. This leads to the hypothesis, that measuring the global flow of the forces from the ground through all of the exoskeleton of the legs is redundant. Concentrating on the forces emerging at or around the joints would be sufficient which is corroborated by mechanical considerations of leverage effects. Further support for this simplification is given in Chapter 6 where strain gauges and internal joint torque measurements are compared and the latter are found sufficient. This solution is less complex than additional sensors measuring the force flow through the whole leg and is easier to implement on already existing robots.

CHAPTER 5

Kinematics

The core of this chapter is to extract the biological movement of the ant legs and transform it into a format that can be deployed on robotic applications. A generic framework is established that allows the translation of movement digitized from high speed videos to joint angles. Different constraints can be introduced that mirror the limitations of the respective technical implementation. Thus new motion patterns are automatically generated based on the chosen biological model organism. The generated pattern is used to control the one legged platform designed in Chapter 6.

5.1 Introduction

Behavioural experiments on desert ants *Cataglyphis fortis* have shown that the movement of the legs is fundamental for their navigational abilities [Seidl et al., 2006]. The kinematics of the desert ant are investigated in order to gauge the impact of the leg movement on the navigation and subsequently determine how closely that movement has to be replicated on the technical application.

Like many other insects ants primarily use an alternating tripod gait [Zollikofer, 1994]. It is characterised by the front and hind leg of one side and middle leg of the other side on the ground forming a tripod. This ensures stable footing, while the opposing tripod moves

forward. Then the stance and swing phases are switched. This mode of walking constitutes an advantageous trade off between stability and speed. This tripod gait is widely employed and seldom deviated from, even over a wide range of external and internal influences [Wahl et al., 2015]. It is not changed depending on step length, frequency or posture, including no conclusive change over substrate inclination [Seidl and Wehner, 2008].

Comparative studies on the gait of desert ants *Cataglyphis fortis* and wood ants *Formica polyctena* were conducted with respect to substrate inclination and ground reaction forces. *Formica polyctena* consistently employ the tripod gait in a grounded running strategy maintaining stable ground contact. They do not change their running strategy or kinematics depending on the inclination [Reinhardt, 2014].

Detailed investigation of the ground reaction forces of *Cataglyphis fortis* find high variability of temporal parameters over all inclinations leading to hypothesize a consistent motor programme independent of the substrate inclination [Wöhrl et al., 2017].

Based on the foundational findings that the ant kinematics do not vary systematically with the substrate inclination the leg movement is extracted and reconstructed for further investigations. The videos are digitized to gain a three-dimensional representation of the movement of the ant legs. This information is translated into joint angles to drive the robots while adhering to industry standards of robot control. The insights gained on the kinematics of the biological model is used to generate new research questions specifically which influence the design of the robotic application in Chapter 6.

5.2 Material and Methods

The movement is extracted from high speed videos. Neuralgic points are identified and digitized. The setup translates into 3D coordinates. This spatial information is translated into rotational angles between elements of a chain to adhere to standards used in robotic descriptions. The final representation of the movement allows identification of the relevant degrees of freedom (DOF) for the implementation of a robotic leg.

5.2.1 Digitization

The movement of the ant legs is extracted from high speed video material of desert and wood ants moving through a canal. The data is used as the base in the subsequent modelling and generation of new motion patterns. The digitized data of the front leg of *Cataglyphis fortis* is provided by the group of Blickhan, Reinhardt and Wöhrl (Friedrich-Schiller-Universität Jena) for the following investigations.

Also a set of high speed videos captured while investigating a bordering research topic is provided by the same group for further analysis. The videos were shot as part of a study of ant kinematics with special focus on the associated ground reaction forces. Wood ants *Formica polyctena* and desert ants *Cataglyphis fortis* are compared with respect to changing ground reaction forces on different inclinations [Reinhardt and Blickhan, 2014, Wöhrl et al., 2017].

The filming setup consists of a high speed video system (HCC-1000, VDS Vosskühler GmbH; Osnabrück, Germany) with a resolution of 1 024 px × 512 px at a sample rate of 922 frames/s. It is placed directly over a narrow channel of 15 mm width at a distance of 15 cm. The narrow channel promotes walking in a straight line. A mirror is placed next to the channel to enable simultaneous views from the top and side. In the middle of the running track a small force measuring plate is located [Reinhardt, 2014]. The ants are introduced to one side and cross the channel.

The animals show a variety of exploratory behaviours. For the investigations these videos are excluded. Only videos where the ants exhibit the typical tripod moving pattern and run in a straight path at a constant speed without touching the canal walls are considered. The ants climbed inclinations of $-60°$ to $60°$. The ants of *Cataglyphis fortis* exhibited mean running speeds between 54 $\frac{\text{mm}}{\text{s}}$ to 87 $\frac{\text{mm}}{\text{s}}$ which is slow compared to their top speeds of up to 700 $\frac{\text{mm}}{\text{s}}$ [Wehner, 1983].

The ants are not marked. To digitize the movement easily identifiable body parts are identified and digitized. On the body the junction between caput and thorax as well as the centre of mass (COM) at the junction of thorax and gaster are chosen (Fig. 5.1). This establishes the proper movement of the ant, i.e. speed and direction of the body, which can then be subtracted to obtain the leg movement relative to the body as frame of reference.

The leg movement is specified by three points: the position of the coxa joint to determine the connection point to the body, the easily identifiable femur-tibia joint and the tip of the tarsus as the position of the end effector (Fig. 5.1).

The described points are traced manually in WINanalyze Version 2.5.0 3D (Mikromak, Germany) and analysed in MATLAB R2009b (The MathWorks, Inc., USA). The reference frame fixed to the ant body is defined by the center of origin located in the center of mass of the ant, the x-axis corresponds to the cranial direction, the y-axis to the distal direction and the z-axis to the dorsal direction (Fig. 5.1). The synchronous information of top and side view allows the reconstruction of the spatial coordinates in all three dimensions. One step cycle is determined by the consecutive touchdown of the left or right middle leg. Each step is standardized to 100 % of the step cycle and smoothed with a Savitzky-Golay filter [Wöhrl et al., 2017]. The average coordinates for each marker are extracted (Fig. 5.2).

The data is used to analyse and model the motion pattern of the ant on a robotic platform.

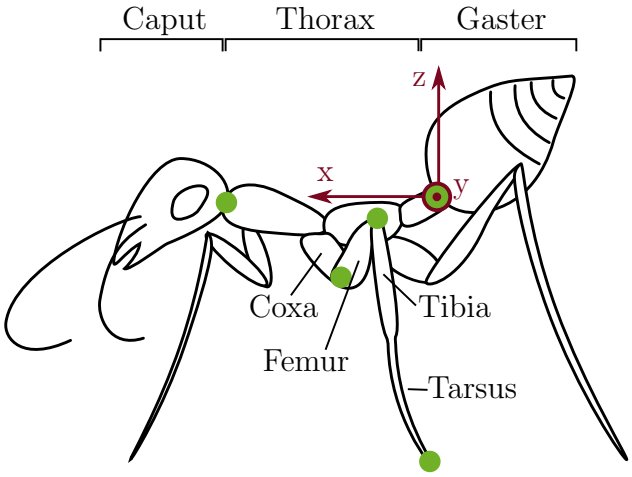

Figure 5.1: Digitized points and fixed reference frame on the desert ant. Green points mark the characteristic points that are identified to digitize the movement. On the body the junction between caput and thorax as well as the junction between thorax and gaster are chosen. Exemplary for all legs the points on the middle leg are marked. The coxa-femur and tibia-tarsus joints as well as the tip of the tarsus are chosen for digitizing. The body-fixed reference frame is centred in the centre of mass. The x-axis corresponds to the cranial direction, the y-axis to the distal direction and the z-axis to the dorsal direction.

5.2.2 Direct Kinematics

To generate motion patterns the digitized data is translated into a kinematic chain. The direct kinematics are modelled and characteristic parameters identified.

In order to control a robot the spatial coordinates of the digitized points are transformed into a common format used in robotics. Since robots are described as kinematic chains the accepted format are rotational angles between the the elements of the chain. With the angles a physical or simulated robot can be driven.

The digitized data is imported into MATLAB 2015b. The modified Denavit-Hartenberg parameters [Craig, 2009] are calculated by the DHFactor function of the Robotics Toolbox (v9.10) [Corke, 2002]. This MATLAB toolbox provides functions and classes necessary in arm-type robotics. Kinematics and dynamics of serial-link manipulators are represented in a general fashion and functions to manipulate and convert between common representations of orientation and poses are provided. The links are established as the connection lines between the digitized points (Fig. 5.3). Key characteristics such as link length and number of DOF are identified.

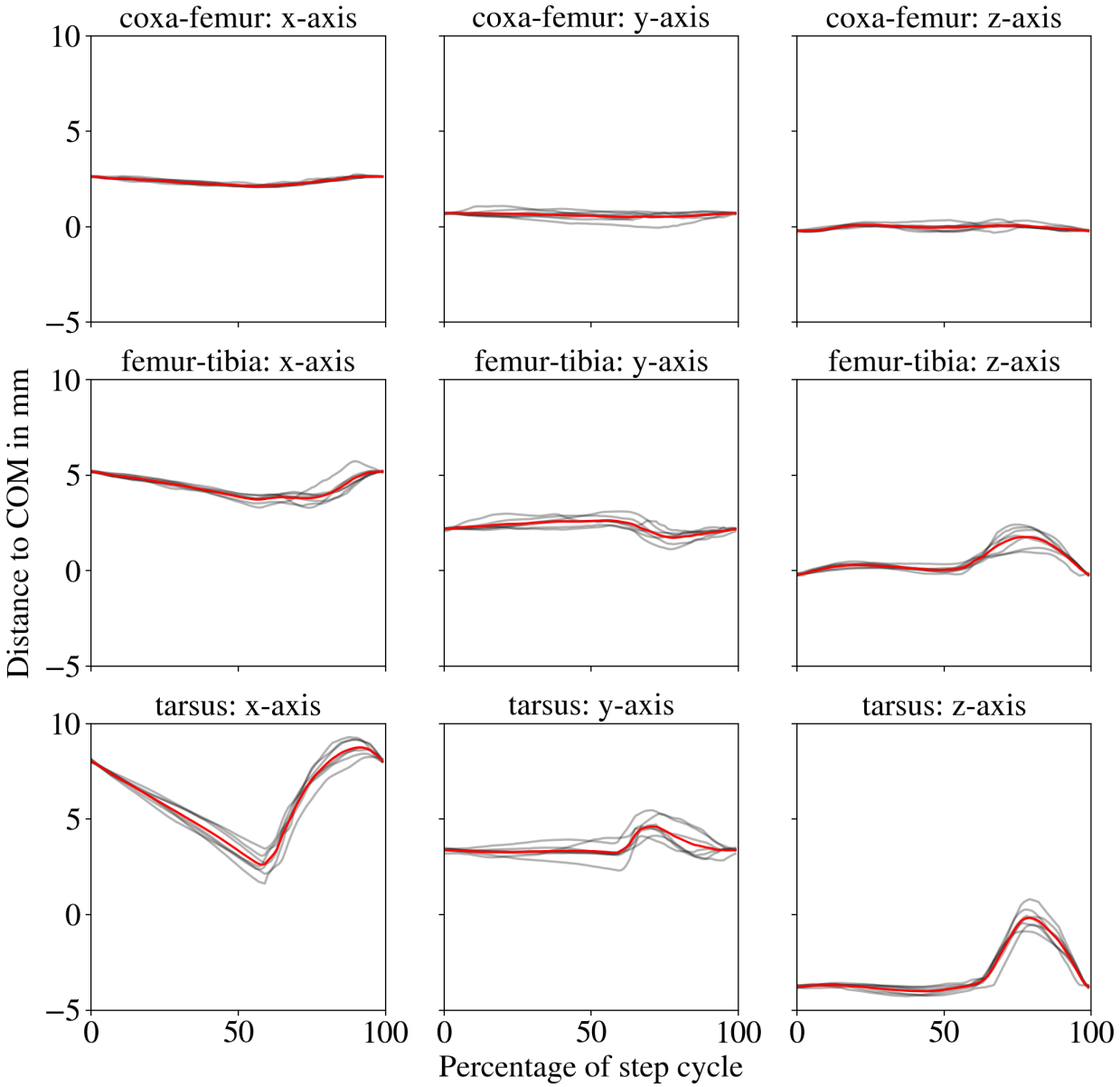

Figure 5.2: Positions of the digitized markers of the front left leg in the body-fixed reference frame of the ant. From top to bottom the coxa-femur joint, femur-tibia joint and tarsus tip are shown. Left to right break down the cranial(x), distal(y) and dorsal(z)-axis. On the x-axis of every graph the progress through the step cycle normalized to 100 % is marked. The y-axis shows the distance from the ant's centre of mass on the axis denoted in the title of the sub-plot. Grey lines represent data of different steps while the red lines are the respective average over all steps for the marker.

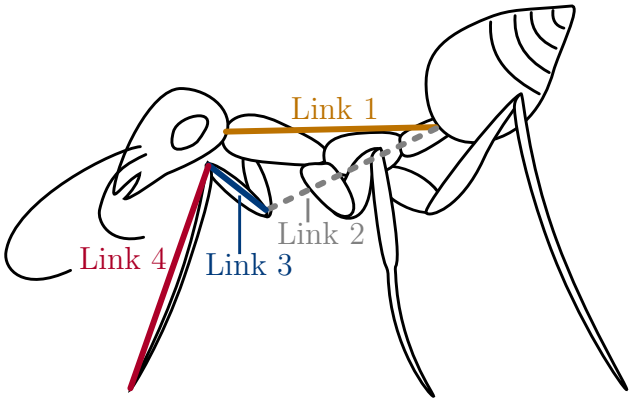

(a) Links as located in the ant.

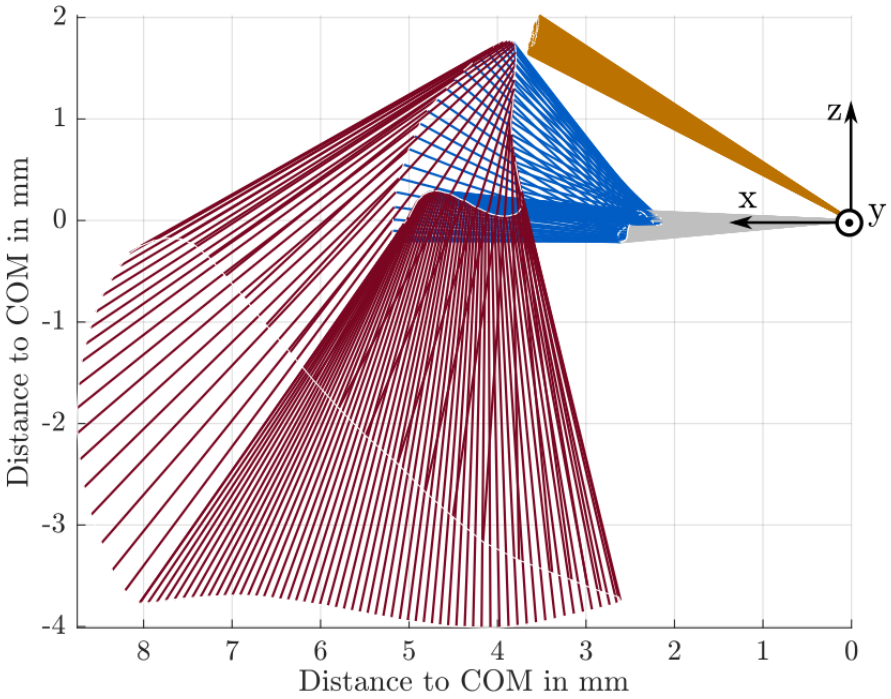

(b) Digitized links over the normalized step cycle in the body-fixed reference frame. Each link is drawn for every 1 % of the step cycle.

Figure 5.3: The digitized points are connected to links. The first link (1) connects the head with the ant's centre of mass. A virtual link (2) is drawn from there to the coxa-femur joint to establish the junction of body and respective leg. The next link (3) represents the thigh and runs to the femur-tibia joint. The final link (4) covers tibia and tarsus and ends in the tarsus tip.

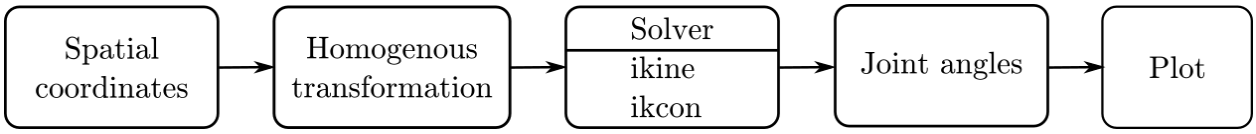

Figure 5.4: Sequence to determine the inverse kinematic. The spatial coordinates of the digitized points are transformed homogeneously and entered into the solver. Two solvers are evaluated: ikine and ikcon and compared with the digitized data (Fig. 5.8). The solver determines the joint angles. For visual screening of undesired behaviour like jerking motions the generated motion is plotted (Fig. 5.7).

5.2.3 Inverse Kinematics

The constraints as identified in the direct kinematics and posed inherently by a technical application are applied to a framework that is able to calculate varying inverse kinematics within a given set of parameters. One suitable set of parameters is chosen to be applied on a one legged robotic platform (Chapter 6).

To calculate different motion patterns depending on initial parameter sets a framework is implemented in MATLAB and Simulink (Fig. 5.4). The constraints identified in the direct kinematics considering link length and DOF are taken into account. Additional restraints can be introduced if desired. The inverse kinematic is implemented to follow the digitized path of the end effector as closely as possible under the constraints. Its spatial coordinates are imported and the transformation matrix calculated. Two different solvers are tested to calculate the inverse kinematics numerically and result in the joint coordinates. The results are saved for implementation on a robotics platform and additionally plotted for visual screening for undesired behaviour like jerking motions.

5.3 Results

The digitized data allows reconstruction of the leg movement excluding rotation within the leg. The direct kinematics provide insight into the changing link length and the number of required DOF to reconstruct the movement on a robotic platform. The inverse kinematic framework allows calculation of different motion patterns under a given set of parameters. The results are dependent on the initial parameters. A solution with three free and one fixed DOF is chosen to be implemented on a one legged robotic platform.

5.3.1 Direct Kinematics

The legs are represented individually as kinematic chains starting at the joint with the ant body and ending in the tarsus tip as the end effector. The direct kinematics are calculated and reveal changes in link length of up to 11 % (Fig. 5.5). Following the Denavit-Hartenberg

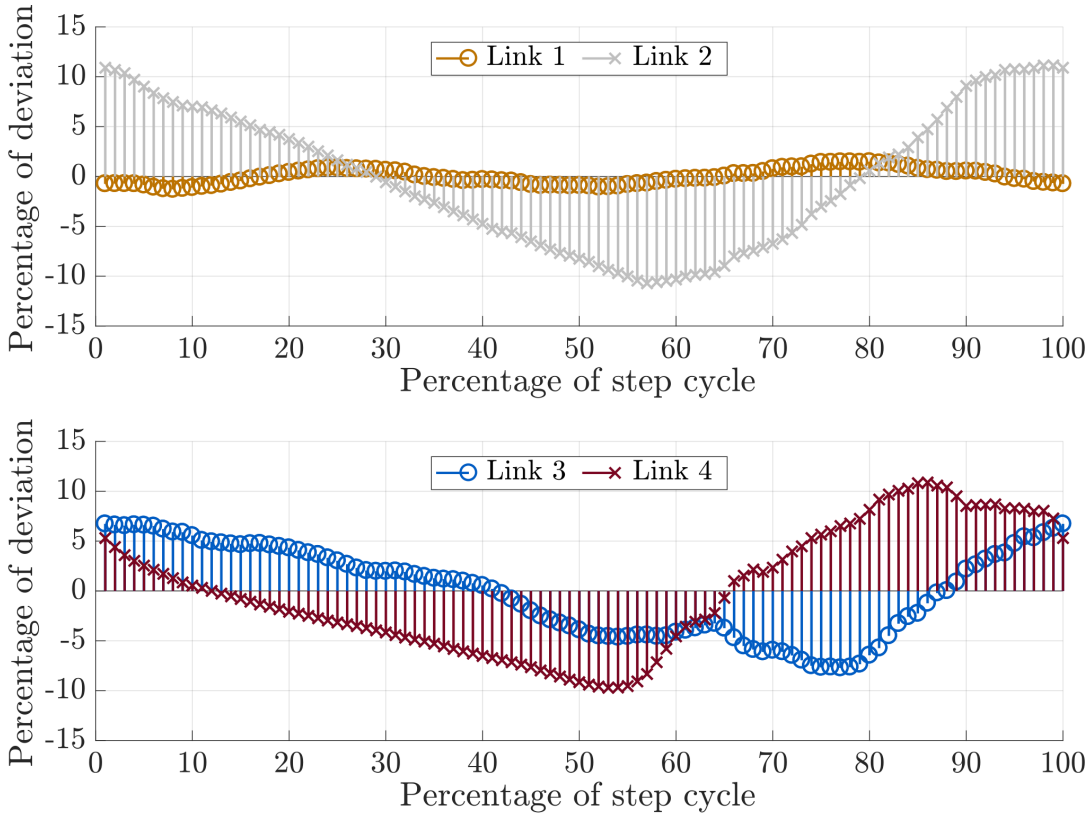

Figure 5.5: Percentage of deviation of the links to their respective averages.

convention four perpendicular DOF can be identified. Rotating two of the DOF by each 90° yields an equivalent but simplified representation of the kinematic chain (Fig. 5.6). The second DOF remains at an absolute value of $(41.9 \pm 1.4)°$. Relaxing the constraint that DOF need to be perpendicular, a simplified model with one fixed and three free DOF is possible with two of the DOF oriented at the corresponding fixed angle to each other.

5.3.2 Inverse Kinematics

For the modelling the link lengths are assumed to be fixed at the average link length as determined by the direct kinematics. This abstraction leads to an aberration between the digitized and modelled behaviour (Fig. 5.7). The solution to the angle calculations is not unique. This leads to several possible configurations of the kinematic chain resulting in the same position of the end effector. For the employed solvers the calculations depend on the initially chosen pose. Undesirable results, such as jerking motions and flipping of the kinematic chain are identifiable in the visual representation and a different more suitable set of initial pose can be chosen. While none of the two solvers are able to completely reproduce the digitized data either one is suited to solve the posed task. For further development the

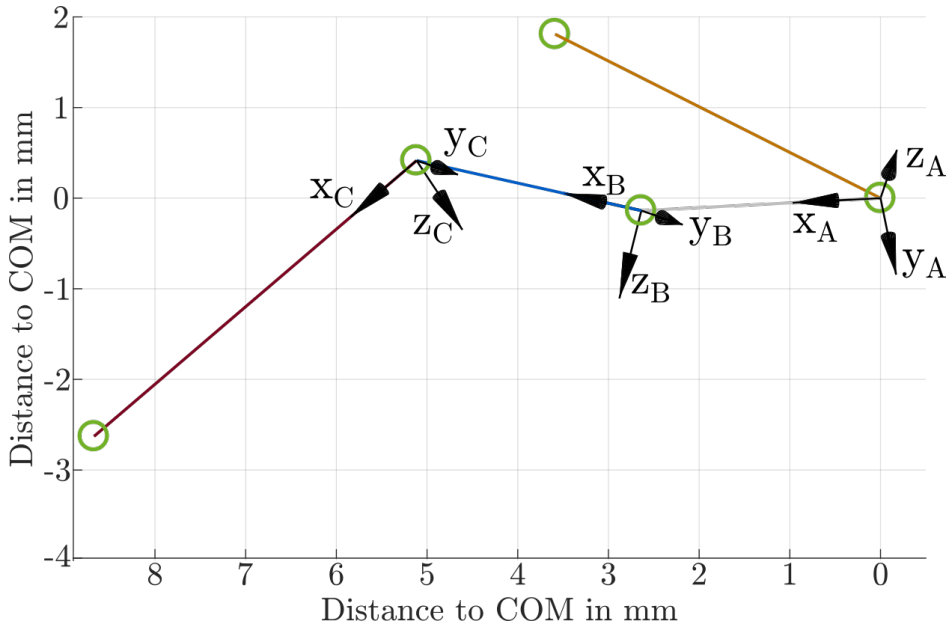

Figure 5.6: Modified kinematic chain following the Denavit-Hartenberg convention at 95 % of the normalized step cycle. The x-axis follows along the links connecting the digitized points. The origin of the frames is located at the beginning of the links. Green circles denote the digitized points that are connected by the links.

solver ikine is chosen, as it exhibits smoother motions (Fig. 5.8) and faster computation time.

5.4 Conclusions

The method established in this chapter provides a framework to digitize the ant movement and generate possible motion patterns to deploy on a robotic platform. In the direct kinematics the transformation of spatial coordinates to rotational angles reveals new findings about the mobility of ant legs. It also allows driving the physical and simulated representations in further research. Developing a robotic application poses limits on the faithfulness of the representation of the natural movement. This limits the explanatory power of inferences to the biological model but does not render the findings useless. As of now the passive flexibility of the leg is not represented and inner rotation of the leg can not be detected from the source material. To investigate these aspects a simulated environment may be most suitable to determine the cost-benefit considerations of a more natural implementation. However the framework as established, enables the generation of motion patterns as close to the biological model as the technical constraints allow. The findings are immediately applied to a one legged robotic platform in Chapter 6. The quasi four DOF solution is implemented with a connection pieces between motors representing the free DOF angled at 42°. The platform is then equipped with various sensors based on the findings of the ant's sensors as estab-

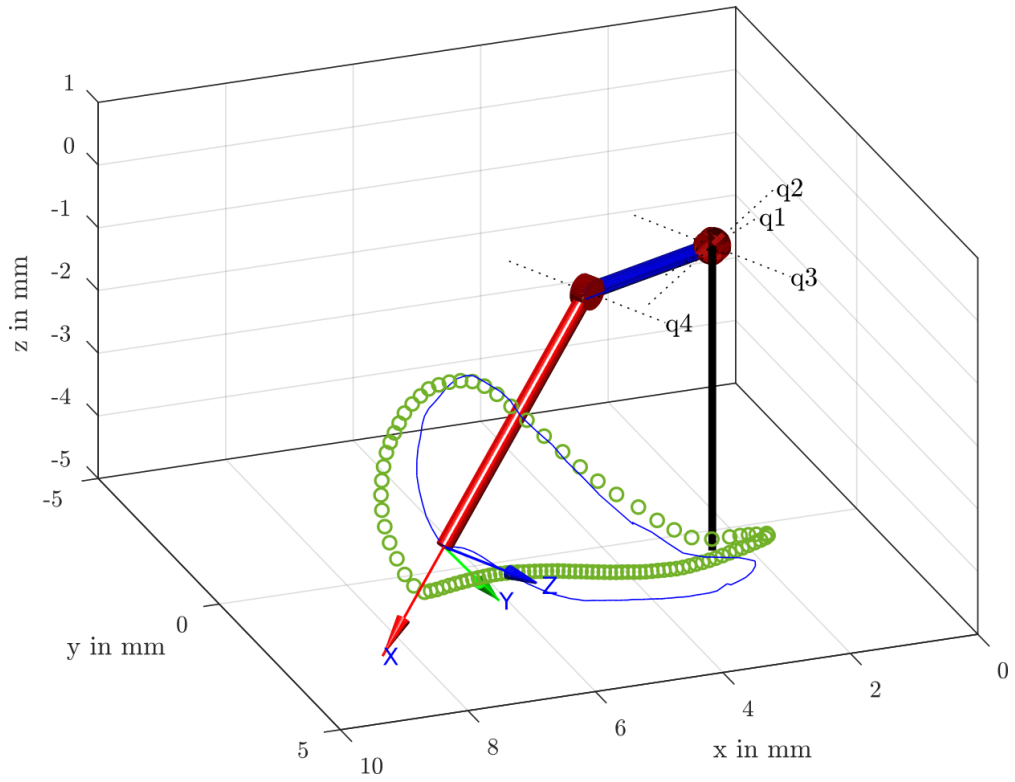

Figure 5.7: Visual representation of the solution of the inverse kinematic solver. Green circles represent the digitized data. Blue line shows the path of the end effector during the simulation. q_n denote the degrees of freedom. The difference in the paths stem from abstractions assumed in the robotic model, like fixed link length. Blue link corresponds to Link 3 in the ant, red link to Link 4 (Fig. 5.3). The movement is relative to the coxa. The frame of reference denotes the distances to the ant's centre of mass in mm.

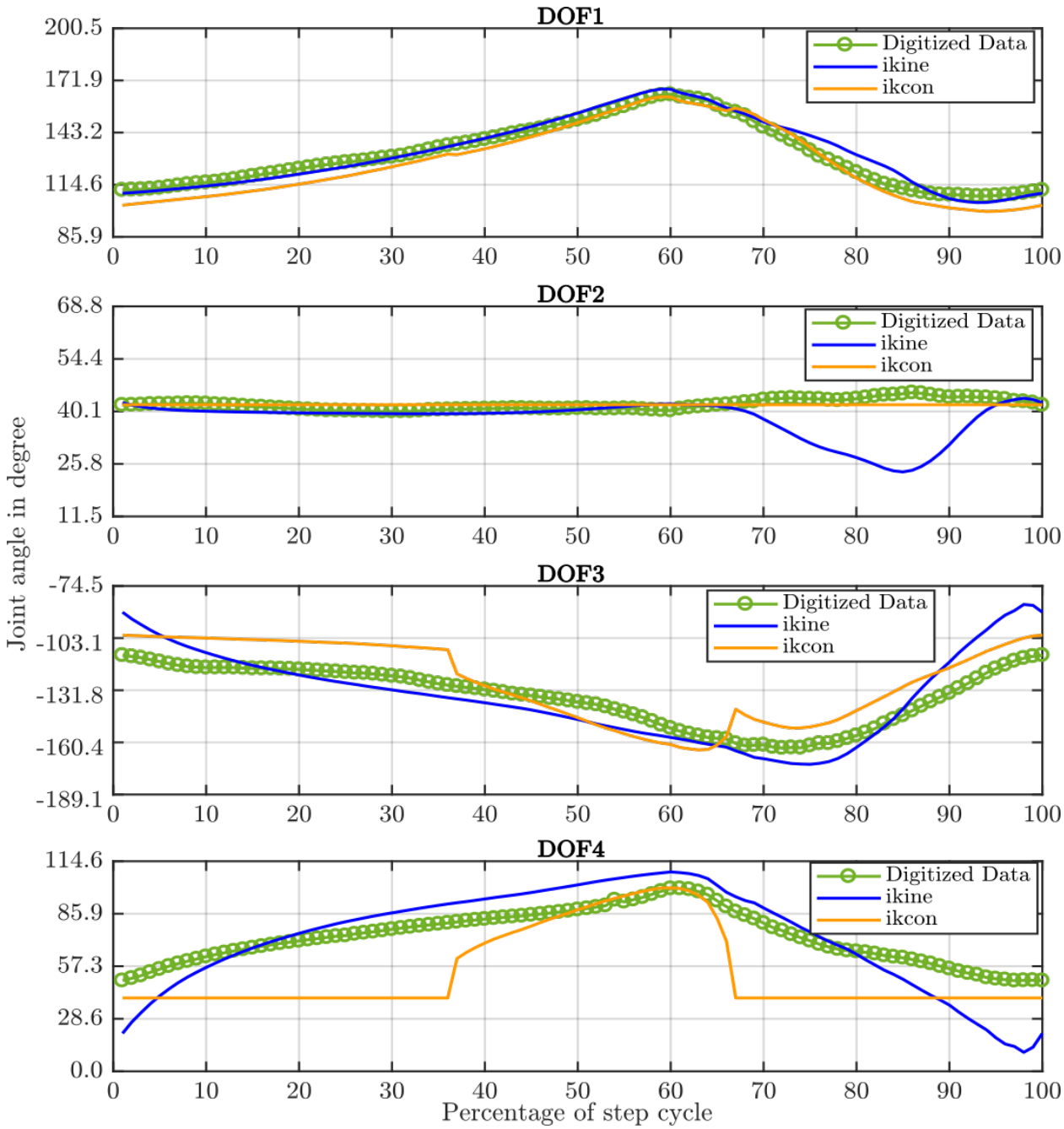

Figure 5.8: Comparison of the performance of the solvers ikine and ikcon. The reference curve "Digitized Data" is generated by the forward kinematics of the digitized points. The four degrees of freedom are shown in degree over the percentage of the step cycle. The closer the curves to the respective digitized data points, the more faithful the reproduction. Another desired trait is a smooth curve to avoid jerking motions in the robot. Pictures taken as part of student work [Giugno, 2016], slight modifications.

lished in Chapter 4 in order to establish the best implementation for detection of substrate inclination.

The leg length is determined using the digitization of the high-speed videos. This seemingly introduces a change in leg length. This stems from the way the data is obtained and the flexibility of the leg. The digitized points are at the coxa joint, the femur-tibia joint and the tip of the tarsus (Fig. 5.1). If the leg is in the air, it is fully stretched and tarsus end and femur are at maximum distance. When the leg touches the ground, the tarsus bends. Since the traced points do not reflect this bending, the effective distance between tarsus end and femur diminishes. The first implementation of the simulation does not mirror this level of complexity. The leg is assumed to be rigid and of fixed length. The systematic error is accepted consciously. It is possible to model the bending but no apparent pay-off is expected. Observing the animals the primary function is damping the footfall, more secure footing due to greater support area and thus also the avoidance of tripping and slipping [Federle and Endlein, 2004]. The results obtained in the simplified approach of rigid legs demonstrate that the general function principle is not reliant on the leg compliance. Still there exists a field of research dedicated to behaviour of robots and the influence of compliance on their walking on slippery and soft surfaces like snow, grass or sand [Xiong et al., 2014]. Depending on the outcome of experiments specifically taking compliant and flexible feet into account, incorporating these characteristics opens the possibility of improved stability as seen in the biological model.

Part III

Synthesis

Contents

Following the completed analysis of the biological model, iterative optimizations of different prototypes are developed in this generative part. Based on the findings of the analytical Part II a one legged prototype is designed that serves as proof of concept. Afterwards the insights gained are transferred to a generic commercially available hexapod platform. Approaches to correlate substrate inclination and sensor readings manually and via artificial neural network are evaluated.

Chapter 6 compares internal torque sensors and external strain gauges with respect to their ability to detect the substrate inclination. The sensors are deployed on a one legged platform based on the desert ant leg's proportions and motion patterns as established in the analytical Part II. Internal and external sensors perform with comparable precision but the internal torque sensors offer the benefit of avoiding installation of additional sensors.

Chapter 7 establishes the general feasibility of extracting substrate inclination from internal joint torque sensors on a moving hexapod platform.

Chapter 8 replaces the manual analysis with an artificial neural network. The topology is optimized on datasets acquired in a simulated environment and validated on the real world datasets. The correlation of substrate inclination with sensor readings of internal torque sensors is demonstrated. The ability remains under varying weight and on slanted paths.

CHAPTER 6

One Legged Platform

After analysing the biological model the findings and hypotheses are implemented on a technical platform. A robotic leg is constructed that mirrors the ant leg's proportions and an abstracted movement. Internal torque sensors and external strain gauges are compared with respect to their ability to discriminate the substrate inclination while the leg moves along a track. The results are validated with the measurements of a spring scale. The experiments are repeated with additional weight on the setup. The performance of internal and external sensors is comparable. However internal sensors offer the benefit of avoiding installation of additional sensors.

6.1 Introduction

The one legged platform is iteratively optimized to find the maximum permissible level of abstraction from the biological model. The goal is not to reconstruct a desert ant in detail but rather to develop an application as far removed from the biological model as necessary to facilitate industrial manufacturing. At the same time the key properties of the underlying principle have to be identified and preserved for the system to work. In the present case this translates to identifying a generic robotic system which mirrors the ant closely enough to

allow for the determination of the substrate inclination to work while being as generic and easily fabricated and assembled as possible.

Several aspects influence the design of the technical platform. Considering the production process the design should be simple and robust. A modular setup and the possibility of rapid prototyping facilitate iterative adaptations as they arise from the measurements. Taking these requirements into account a modular 3D print of a singular leg is produced and tested in a simplified environment. Thus building costs and programming effort is minimized compared to a full hexapod setup because less materials and simplified controls are used. The need for external force sensors resembling the ones in desert ants is tested and rejected in favour of easier to implement internal motor readings.

It is possible to correlate the sensor readings with the inclination of the substrate. This allows for finding a reverse function to determine the susbtrate inclination from the sensors. The feasibility of a setup devoid of external sensors is demonstrated. This simplifies the hexapod setup in the following chapter. A simplified movement can be used without adoption to environmental influences.

6.2 Material and Methods

The experimental setup consists of three main parts (Fig. 6.1). The movable modular leg is made up of three motors connected by 3D printed connector pieces (Subsection 6.2.1). The leg moves along a linear track of variable inclination (Subsection 6.2.2). It is equipped with various sensors (Subsection 6.2.3). Test procedure checks for correlation of track inclination with sensor read outs. Additionally the influence of parameter change regarding total weight is investigated (Subsection 6.2.5).

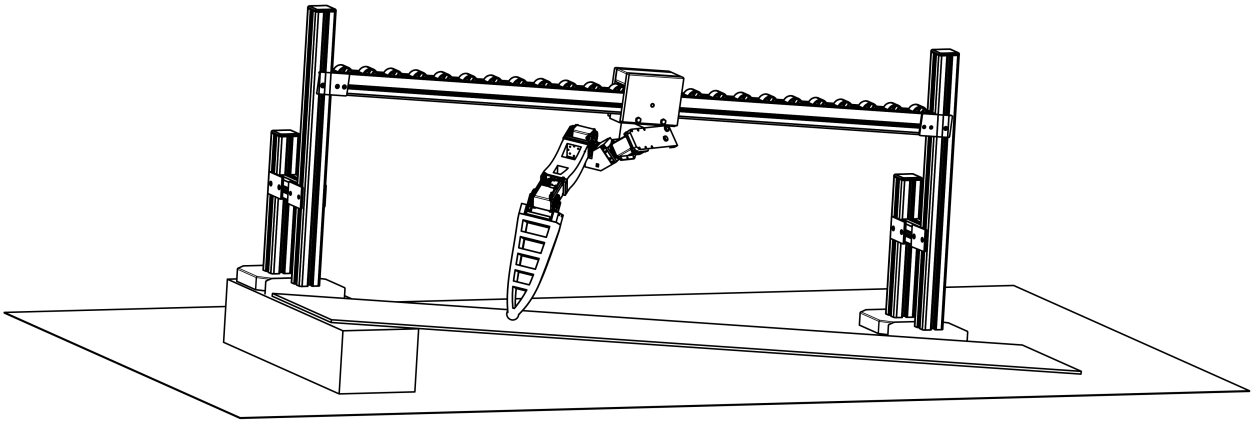

Figure 6.1: Overview of the experimental setup for the one legged platform. The modular leg is movable along the angle-adjustable linear track. The substrate is pictured simplified as an inclined plane. Substrate and track are fixed at the same angle for each run. Dimensioned drawing in appendix (Fig. A.1).

6.2.1 Mechanical Components

The modular leg design consists of three basic shapes connected by motors to allow movement.

Connectors The leg shape is derived from the biological model. Abstracted versions of the crucial parts coxa, femur and tibia are modelled and 3D printed. Their respective lengths are proportional to their counterparts in the front leg of *Cataglyphis fortis*. The printer used is a MakerBot Replicator 2 and the material for femur and tibia is polylactic acid (PLA) filament 1.75 mm (Renkforce). Due to the stress on the coxa it is printed in carbon fibre reinforced nylon filament. It exhibits a 42° angle to represent the mean of the fourth DOF present in the ants movement (Chapter 5).

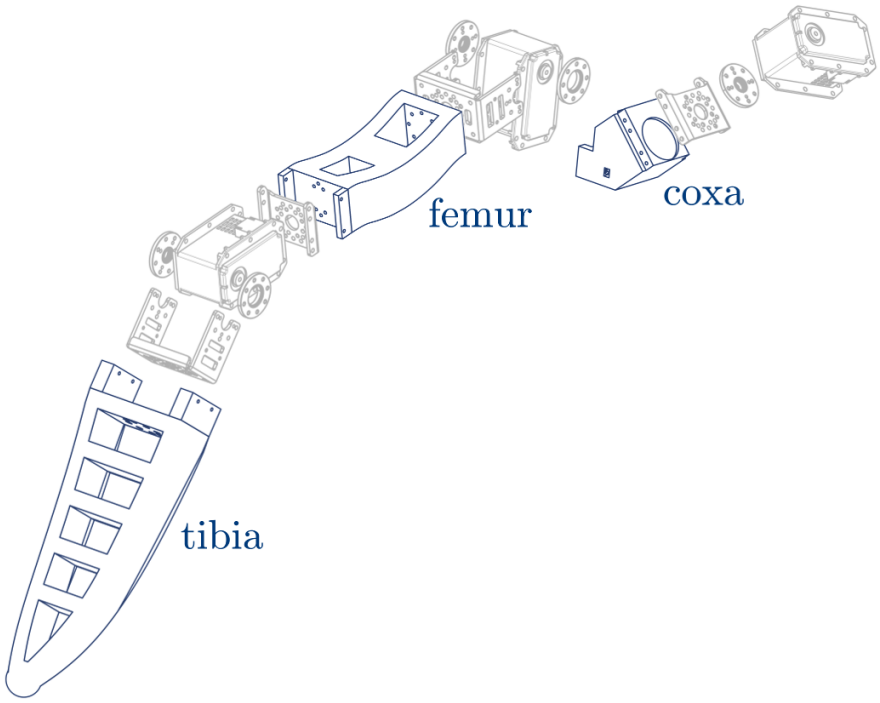

Figure 6.2: 3D-printed connector pieces. The nomenclature follows the established names in hexapod research which is based on the biological counterparts. Dimensioned drawing in appendix (Fig. A.4, A.5 and A.6).

Motors The motors used are Dynamixel motors model MX-64 AT (ROBOTIS INC, USA) (Fig. 6.3). They are compatible to the robot operating system (ROS) interface and offer internal sensors for motor torque. The motors also provide a timestamp. The motors are daisy chained and connected via universal serial bus (USB) to the laptop that controls the movement. The motors are fixed to brackets (model FR05-H101) which in turn are screwed to the 3D printed connector pieces.

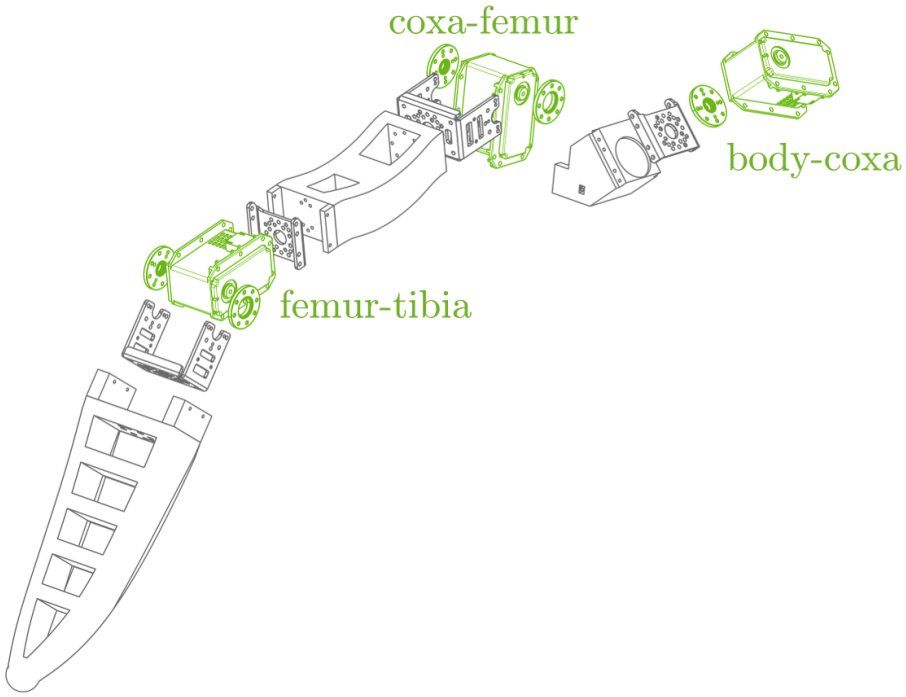

Figure 6.3: Motors link the connector pieces with each other and to wagon representing the body. The nomenclature denotes which parts are linked. Dimensioned drawing in appendix (Fig. A.2).

6.2.2 Simulated Environment

The modular leg (Subsection 6.2.1) is fixed by a bracket to a custom made wagon mounted on the linear track. The wagon encases an aluminium profile with a roller conveyor at the top enabling linear movement along the track (Fig. 6.1). An additional weight can be attached to the underside of the wagon. Inclination is realized by raising one side to a higher level corresponding to the desired angle. The substrate is realized by a stationary treadmill that allows for easy adjustment of inclination according to the angle determined by the angle of the linear track.

6.2.3 Sensors

The platform is equipped with various sensors. In preliminary experiments the most useful ones are determined, taking into account measuring technique and stability, robustness, price, size, and ease of application. The final measurements are conducted with three different kinds of sensors (Fig. 6.4). A spring scale at the foot serves for validation purposes. Strain gauges are applied as external sensors while the torque sensors supplied by the motors themselves are evaluated as internal sensors. All sensors are recorded simultaneously to ensure comparability. The correlation of respective sensor read out with substrate inclination is

determined to evaluate the usefulness of the sensor in a final application. Additional criteria in a final evaluation are cost, energy consumption, installation, ease of calibration and read out.

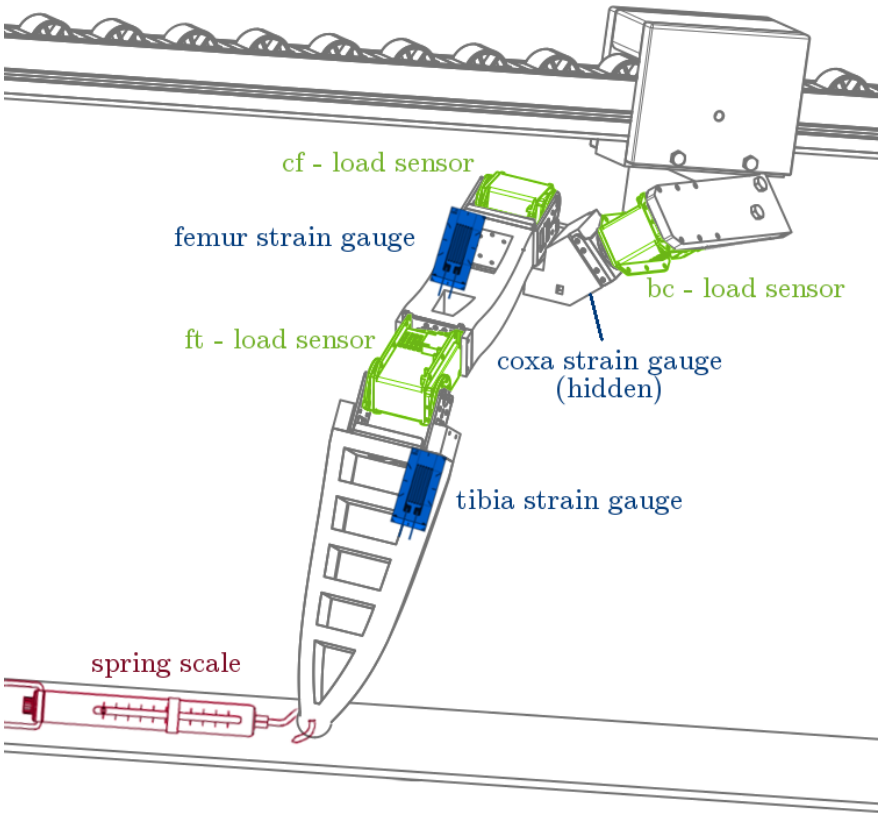

Figure 6.4: Schematic illustration of sensor placement. Sensor sizes are not to scale. The nomenclature of the sensors corresponds to the respective connectors or motors they belong to.

Spring scale A spring scale Medio-Line 40025 (PESOLA) is attached to the tip of the foot to ensure constant and reliable data acquisition. It is aligned with the substrate inclination to record the main forward driving forces. The scale is read during the movement of the leg along the linear track. The maximum value is noted and confirmed via video recording of the experiment. The measured values are averaged over 15 repetitions. The result is used to check the plausibility of the other sensor readings because the real world applicability of this approach is not given.

Strain gauges Strain gauges 6/120 LY11 (HBM GmbH, Darmstadt) are installed on each of the three connector pieces. Their position near the movable joints (Fig. 6.4) is chosen in accordance with the findings of Chapter 4. The sensor values of the strain gauge are read

via a measuring amplifier QuantumX Modul MX840 A (HBM GmbH, Darmstadt) and the corresponding software catmanEasyAP (Version 3.4, HBM GmbH, Darmstadt).

Internal torque sensors The motors Dynamixel MX 64-AT provide a way to measure the torque internally. Current and torque are directly proportional. This allows conversion from one measure to the other via linear transfer function (Fig. 6.5). The motors are daisy chained to each other and connected to the measurement laptop (Latitude E5550, Dell) via USB2Dynamixel (ROBOTIS INC, USA). The sensor readings and corresponding timestamps are recorded via the same ROS interface used to control the motor movement (Subsection 6.2.4).

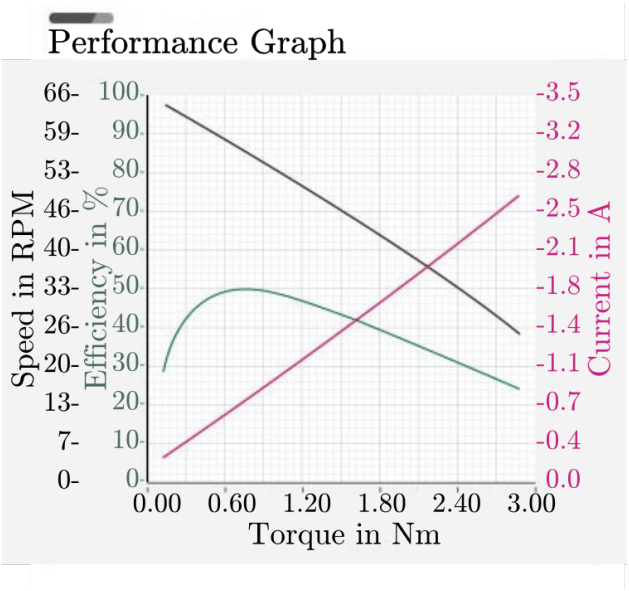

Figure 6.5: Transfer function showing the correlation of the applied torque and the measured current in the motor (pink line) [ROBOTIS, 2020]. The linearity allows using the current as measure for the joint torque. Also pictured: Efficiency in percent (green) and speed in revolutions per minute (black) as a function of torque.

6.2.4 Control and Movement

Control The leg movement is controlled via ROS protocol. The motors are connected via USB to the measuring laptop running Ubuntu 16.04 and ROS kinetic. The digitized angles of the desert ant front leg (Chapter 5) are looped and replayed constantly. No feedback or adaptation is performed. The motor commands are sent out via *dynamixel_manager* node and information about the state of the motors is received in the reverse direction (Fig. 6.6).

Movement The movement is modelled after the movement of the front leg of *Cataglyphis fortis*. Chapter 5 provides the detailed description of capturing and converting the movement

from ant to robot. The movement chosen follows the quasi four DOF movement realized by shape of the coxa (Fig. 6.2). The immovable connector piece angles the two DOF at 42° to each other and thus acts as the fixed quasi DOF.

The trajectory is replayed constantly. From the neutral initial position the leg lifts up and forward. When it touches down on the surface the wagon is pushed along the linear track. The friction between wagon and track prevents sliding back while the leg once again lifts so that the subsequent push starts further along the track. In this way the leg is moved along the track. Depending on the angle of track and substrate the resulting movement is classed as an upward (positive angles) or downward (negative angles) movement.

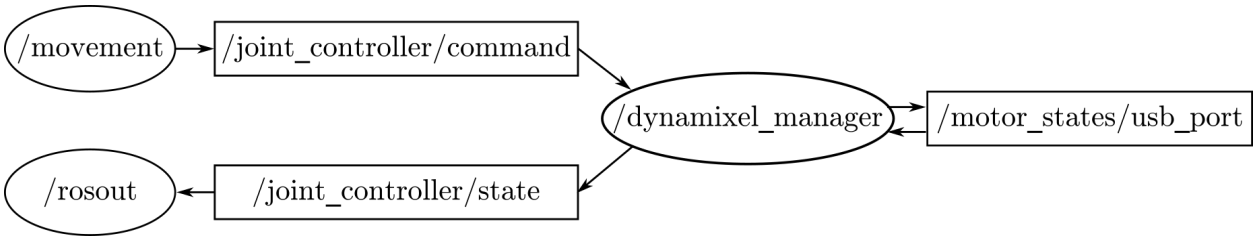

Figure 6.6: Simplified overview of ROS nodes. The three joints are summarised to one node in this illustration. Circles represent nodes, squares represent topics. The fixed movement is generated in the *movement* node and published to the *command* topic. This topic is processed in the *dynamixel_manager* node into commands readable by the Dynamixel motors and published to the *motor_state* topic that gets published to the USB port and thus the motors. In the reverse direction the information from the motors via the USB port is read in at the *motor_state* topic and published by the *dynamixel_manager* node to the *state* topic where it is recorded for further analysis.

6.2.5 Experimental Protocol

While the modular leg moves along the linear track all sensors are recorded simultaneously and saved for further evaluation. The internal torque sensors are recorded via the ROS interface while the other sensors are independent of the control system.

Each run consists of the leg executing five steps along the track. After that the wagon is reset to the initial position at the beginning of the track and the leg is reset into its initial neutral position. This sequence is repeated three times.

The whole set is carried out for 10 different inclinations from $-20°$ to $+25°$ in $5°$ increments. Positive angles denote a upward movement of the leg, negative angles a downward movement.

For each inclination the experiments are conducted as described and every run is repeated with an additional weight of 417 g fixed to the underside of the wagon.

Sensor readings are averaged over the accumulated 15 steps for each inclination and weight. The average measurement for each sensor is plotted against the respective inclination. This allows investigation of possible correlation of the factors.

Statistical investigations are conducted to investigate the correlation of sensor reading to inclination as well as the inverse. This gives a measure of how well the inverse function works.

6.3 Results

The sensor readings are averaged over the 15 repetitions and presented as function of the set inclinations. Error bars denote the standard deviation of the average and as such show the variability between repetitions. The smaller the error, the more reliably reproducible is the sensor read out. The sensors are grouped by their type. The readings of the spring scale serve as validation set. The three external strain gauges and the three internal torque sensors are grouped and compared. Each inclination is tested with and without additional weight. The respective datasets are shown next to each other. Each dataset is fitted to a linear regression as the simplest bijective inverse function. The correlation of both sensor read out with inclination as well as the reverse are calculated to quantify the fit.

Spring scale While the leg moves the maximum pulling force necessary to propel it forward along the linear track is recorded via the spring scale. The values go up to a maximum of 15 N(Fig. 6.7a). The measured values are stable over several repetitions as can be seen by the small standard deviation of the average. One notable exception is the movement on a level surface without additional weight with a standard deviation of (1.31 ± 0.01) N. The higher the inclination the more pulling force is recorded. The sensor reading show a strong linear correlation to the chosen inclination. The correlation coefficient of 0.9787 far exceeds the 0.6021 necessary for a significance level of 5 % (Tab. 6.1). Adding additional weight reveals a similar picture in terms of value spread and errors (Fig. 6.7b). Although the abnormally high standard deviation at 0° is not present when the experimental setup is weighed down. Increasing the inclination still leads to higher values of the sensor readings but the rate of increase changes. Negative inclinations result in similar sensor readings but the higher the inclination, the bigger the spread between sensor readings with and without additional weight. This leads to an increase in the slope of the linear regression line by 26 %. The sensor readings continue to show a strong linear correlation (Tab. 6.1).

Strain gauges The forces acting on the leg result in a slight deformation of the 3D printed material. The strain gauges measure this deformation. The measure is the relative deformation, that is to say the deformation compared to the neutral resting position without additional force on the sensor. Depending on their position the deformation is differently

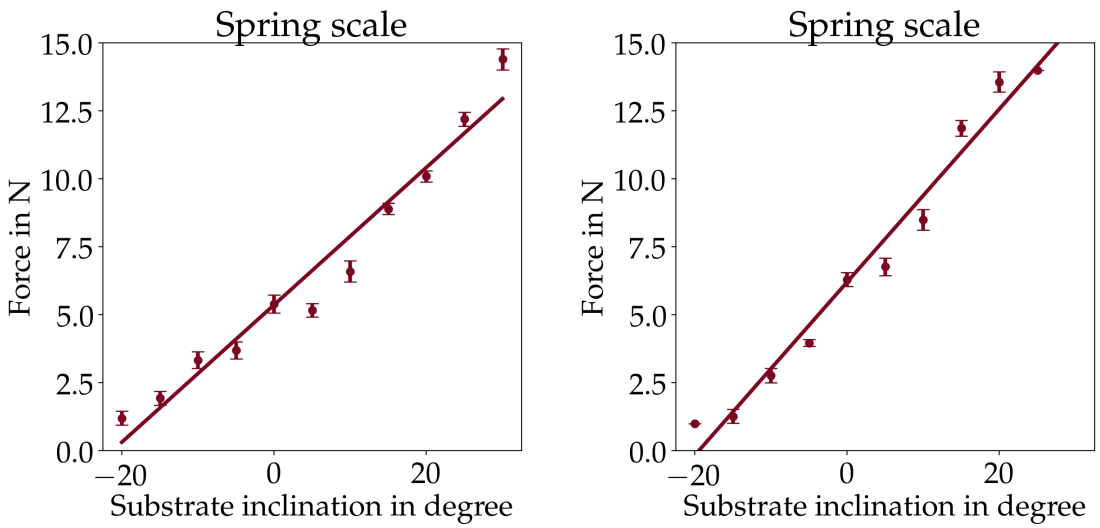

(a) without additional weight (b) with additional weight

Figure 6.7: Forces measured with the spring scale in dependence on the substrate inclination. Mean and standard deviation over 15 repetitions are shown. The line represents the linear regression fit. Precise model parameters can be found in Tab. 6.1. Adding weight to the experimental setup leads to 26 % increase in the slope.

pronounced. This manifests in the different range of read out values (Fig. 6.8a). The strain gauge on the coxa only expresses values from $-25\,\frac{\mu m}{m}$ to $-275\,\frac{\mu m}{m}$. At the same time the strain gauge at the femur experiences higher forces resulting in deformations starting at $-150\,\frac{\mu m}{m}$ and up to $-650\,\frac{\mu m}{m}$. The strain gauge at the coxa is subject to the highest deformations starting in the same range as the one on the femur but going up to $900\,\frac{\mu m}{m}$.

In comparison with the validation measurement of the spring scale the values of the strain gauges exhibit a higher variation of values between different repetitions as indicated by the error bars. While there is a wide spread in the precision, the accuracy remains constant which can be seen especially well on the tibia strain gauge with the averages following the linear regression rigorously. The other two while showing more scattering follow this general pattern. The precision decreases from tibia over femur to the coxa strain gauge.

Despite the low precision the high accuracy results in a strong linear correlation of the averages with the chosen inclination. The correlation coefficients for all three strain gauges far exceed 0.6021 and are as such strongly correlated on a 5 % significance level (Tab. 6.1). Still they can be ordered on their accuracy. The strain gauge on the tibia shows the least scattering and as such exhibits the highest correlation coefficient, followed by the sensor on the coxa and finally the sensor on the femur. The change in deformation with changing inclination is also different between the three sensors. The higher the slope of the linear regression line, the greater the sensor response to the changing parameter. For the strain gauges the slopes of the sensor readings at the coxa is the greatest, after that the femur and the smallest is at the tibia.

Adding weight to the setup results in a similar picture regarding the scattering of the averaged values as well as their precision (Fig. 6.8b). Negative inclinations result in similar sensor readings but the higher the inclination the bigger is the spread between sensor readings with and without additional weight. This leads to an increase in the slope of the linear regression line on average by 50 % for all three sensors (Tab. 6.1).

The accuracy especially in the femur and coxa increases which can be seen visually by the spread around the linear regression line being less than without additional weight (Fig. 6.8) and quantitatively this is expressed in a higher correlation coefficient (Tab. 6.1). In the case of additional weight all three correlation coefficients even exceed 0.90. One notable exception is the measurement at +10° inclination. For all three sensors this sensor reading diverts from the regression line.

Internal torque sensors The forces on the leg change the torque on the joints realized by motors. The change in torque is measured by the internal torque sensors. The sensor read outs are calibrated on the maximum torque of 6 Nm. As such all values are positive and less than 6 Nm.

The range of measured values of the body-coxa joint and the femur-tibia joint spreads between 1 Nm to 4 Nm. The read outs of the coxa-femur joint on the other hand shows almost no spread with values ranging only from 0.0 Nm to 1.5 Nm (Fig. 6.9a).

Errors on the coxa-femur joint are smaller than on the other two but the scattering is more pronounced. In combination with the small range of values overall this leads to no discernible correlation of sensor read out and inclination. This is shown as well in the correlation coefficient well below 0.6021 and as such a correlation can be rejected on a 5 % significance level (Tab. 6.1).

The precision on the body-coxa and femur-tibia joint is lower than the one on the validation set of the spring scale measurement. This indicates a higher aberration of values between different repetitions. While there is a wide spread in the precision the accuracy remains constant with the averages following the linear regression line. The relative error is comparable to the ones on the strain gauges. The higher the inclination, the higher the responding sensor read out. This direct proportionality is quantified in correlation coefficients of over 0.95 (Tab. 6.1). While the correlation coefficient of the body-coxa joint is higher than that of the femur-tibia joint, the difference is small and the relation is inverse for the measurement with additional weight. The slopes of the regression lines of body-coxa and femur-tibia joint are of comparable order of magnitude.

Adding weight to the experimental setup results in similar values regarding accuracy and precision (Fig. 6.9b). The slope of the linear regression line doubles for both the body-coxa and femur-tibia joint with an additional weight of 417 g. The spread of sensor read outs in relation to the chosen inclination is more pronounced on higher inclinations. No significant

Table 6.1: Model parameters of the linear regression of the respective sensor reading x and the substrate inclination α

(a) Without additional weight

sensor		linear regression		correlation
type	position	$x(\alpha)$	$\alpha(x)$	coefficient
strain gauge	tibia	$x = -2.8255\alpha - 136.14$	$\alpha = -0.3467x - 47.101$	0.9897
	femur	$x = -4.9528\alpha - 334.14$	$\alpha = -0.1540x - 50.273$	0.8734
	coxa	$x = -7.8825\alpha - 390.33$	$\alpha = -0.1046x - 39.937$	0.9079
torque	femur-tibia	$x = 0.0569\alpha + 2.1023$	$\alpha = 16.590x - 34.598$	0.9716
	coxa-femur	$x = 0.0029\alpha + 0.7182$	$\alpha = 6.7083x + 0.0834$	0.1407
	body-coxa	$x = 0.0377\alpha + 2.1010$	$\alpha = 24.151x - 50.291$	0.9540
spring scale		$x = 0.2533\alpha + 5.3336$	$\alpha = 3.7819x - 19.961$	0.9787

(b) With additional weight

sensor		linear regression		correlation
type	position	$x(\alpha)$	$\alpha(x)$	coefficient
strain gauge	tibia	$x = -04.1287\alpha - 149.87$	$\alpha = -0.2353x - 35.187$	0.9855
	femur	$x = -08.5021\alpha - 365.99$	$\alpha = -0.1021x - 37.026$	0.9316
	coxa	$x = -12.8060\alpha - 433.20$	$\alpha = -0.0729x - 31.431$	0.9664
torque	femur-tibia	$x = 0.0984\alpha + 2.4666$	$\alpha = 09.538x - 23.373$	0.9690
	coxa-femur	$x = 0.0047\alpha + 0.8647$	$\alpha = 10.287x - 06.516$	0.2202
	body-coxa	$x = 0.0724\alpha + 2.3021$	$\alpha = 13.158x - 30.174$	0.9763
spring scale		$x = 0.3184\alpha + 6.204$	$\alpha = 3.0601x - 18.92$	0.9871

improvement in accuracy and consequently in the correlation coefficient is discernible after adding weight (Fig. 6.9 and Tab. 6.1).

Key findings All sensors except the coxa-femur internal torque sensor show a strong linear correlation of sensor read out to inclination. Even if the relative error on the internal and external sensors is higher than on the validation set the high correlation coefficient shows high accuracy of the averages on a linear regression line. Adding weight to the experimental setup changes the slope of the linear regression line. The underlying principle that the sensor read outs can be correlated to the chosen inclination remains. The accuracy of external and internal sensors are of comparable magnitude.

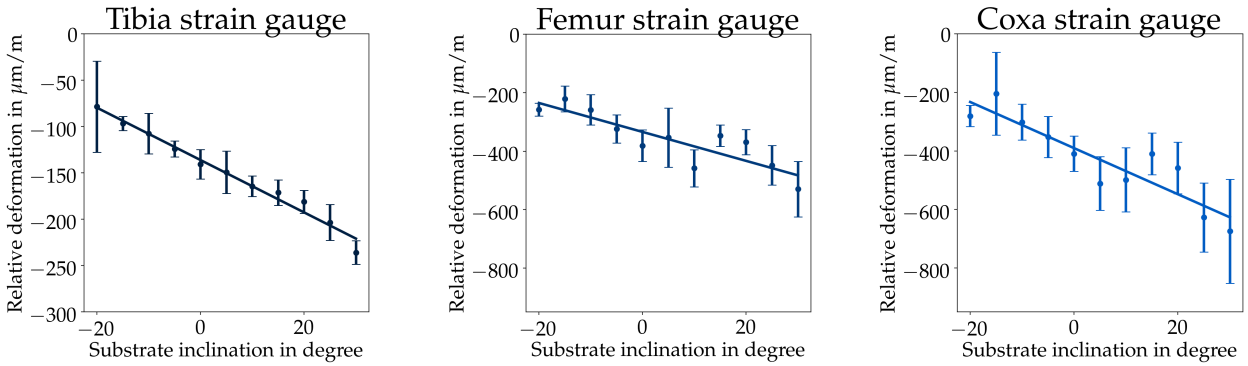

(a) without additional weight

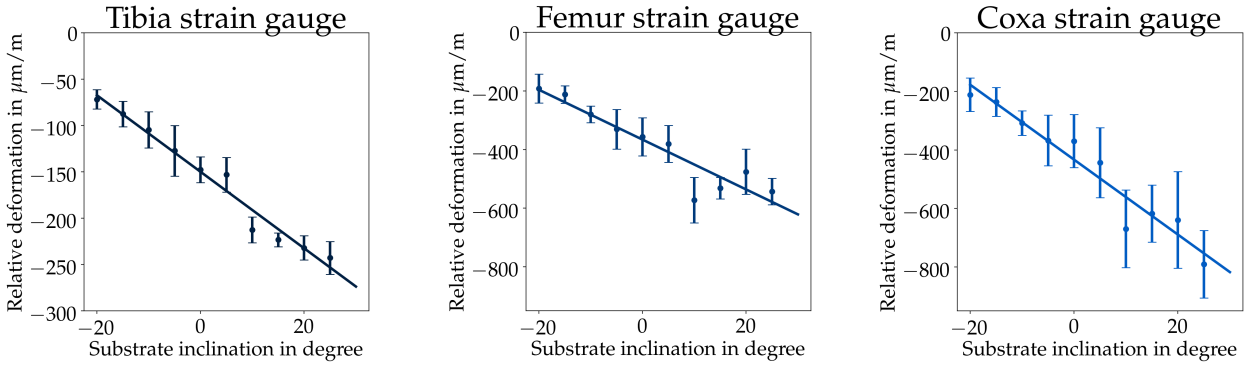

(b) with additional weight

Figure 6.8: Relative deformation of the strain gauges over the substrate inclinations. Mean and standard deviation over 15 repetitions are shown. The lines represent the linear regression fits. Precise model parameters can be found in Tab. 6.1. Adding weight to the experimental setup results in a steeper slope for all strain gauges.

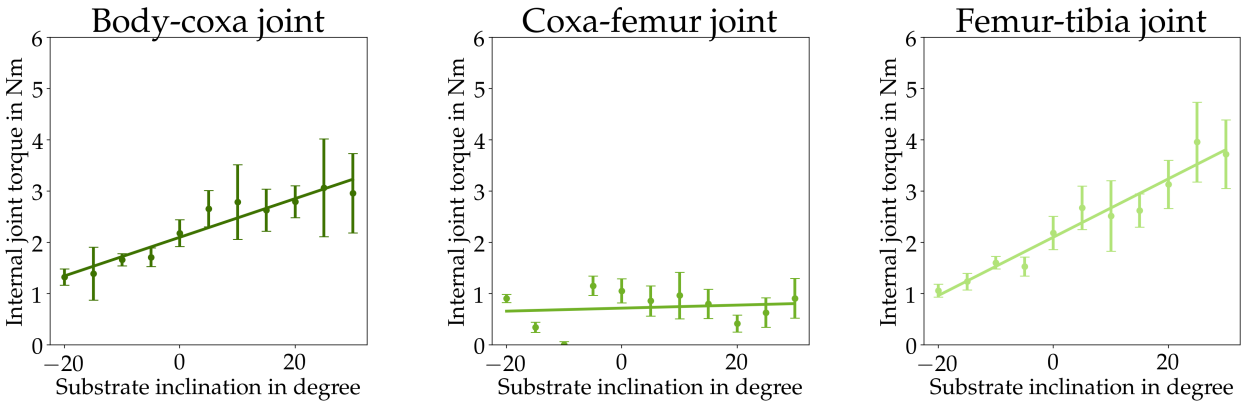

(a) without additional weight

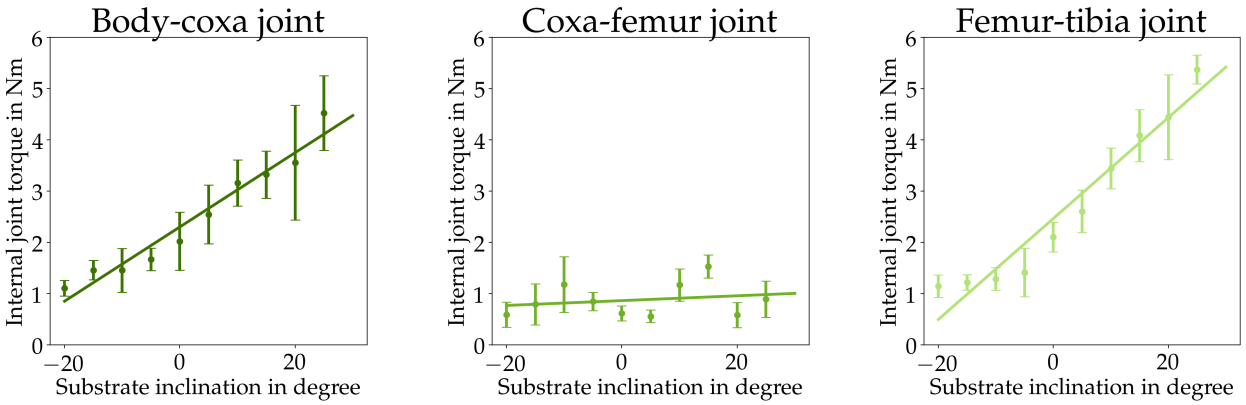

(b) with additional weight

Figure 6.9: Internal joint torque over the substrate inclinations. Mean and standard deviation over 15 repetitions are shown. The lines represent the linear regression fits. Precise model parameters can be found in Tab. 6.1. Adding weight to the experimental setup results in a steeper slope for body-coxa and femur-tibia joint. The coxa-femur joint shows no dependance on the substrate inclination.

6.4 Conclusions

This chapter outlines the development and experiments performed on the simplified one legged setup. It is shown that a correlation of substrate inclination and sensor read outs measuring the forces on the leg can be found. The goal is to find a bijective inverse function, that allows the translation of sensor read out to substrate inclination. Then the idiothetic cues from the robot's own sensors allow determining the substrate inclination which can be used in the odometry and consequently for navigation. Three different sensors are tested and the best suited for further development is identified. External sensors, which are inspired by the biological model, exhibit comparable results to the internal ones, with the later additionally offering advantages in usability. The technical abstraction offers insight into the permissible level of abstraction while retaining the underlying principle. The modularity of the platform allows for quick testing on the influence of varying parameters.

6.4.1 Experimental Setup

The experimental setup is influenced by the results of the analysis (Part II). The campaniform sensilla measure the deformation of the ant's exoskeleton. To determine if it is necessary to model this behaviour two types of sensors are considered. Strain gauges are technical instruments to measure the deformation on the surface of the robotic leg. Thus, they are closer to the biological model. Since the campaniform sensilla are located near the joints and as such effectively measure the joint torque (Chapter 4) the internal sensing mechanism of the robotic leg is examined. Using the internal sensors offers advantages concerning usability.

The movement of the leg is modelled after the kinematics of the front leg of *Cataglyphis fortis* (Chapter 5). The front leg is identified in literature as the main motor on steep inclinations when moving upwards [Wöhrl et al., 2017]. Additionally the normal ground reaction forces change continuously with the substrate inclination [Reinhardt, 2014]. Thus it is a promising candidate for a simple correlation between forces measured and inclination. In its kinematics of the front leg the desert ant reveals a four DOF system. One of them is quasi stationary, only assuming values of $(42 \pm 1)^\circ$. Thus the system can be reduced to a three DOF system by affixing the freely movable elements at this angle to each other. In the robotic leg this is realized by the coxa connector pieces being angled by 42°.

The foot shape of the robotic leg was chosen to be round so that the angle of contact with the ground is independent from the leg stance and inclination of the substrate. To counteract the resulting small area of contact the foot was encased in rubber-like material which raised the friction sufficiently to propel the leg forward along the linear track.

6.4.2 Sensors

The sensors are considered in their usefulness at detecting the substrate inclination. To achieve this, there needs to be a strong correlation of sensor read out with the inclination on a bijective function. All but one sensor show this correlation on a simple linear line. They differ in their applicability for further research. The influence of added weight which relates to load changes in the final application is covered by the experimental setup. It influences the slope but not the overall shape of the inverse function. The underlying principle proves robust to repeated execution of experiments and along parameter change as can be evoked by loading the robot.

Validation The spring scale serves as validation measurement. The forces on the leg change with changing inclination. A linear correlation can be found which is mirrored in the results of the internal and external sensors. The small error bars express a high precision over repeated measurement. It suggests that the general idea of correlating substrate inclination with sensor readings is valid even though the spring scale is not suited for a real world application.

External sensors The differing ranges of sensor read out of the strain gauges, even though they are the same type and fixed on the same material, is a result of the forces acting on the different connector pieces. According to their position and the leg geometry the basic leverage changes and as such some sensors experience higher strain than the others.

The anomaly at $+10°$ with added weight (Fig. 6.8b) is probably a systematic error in experimental procedure. The anomaly occurring in all strain sensors at the same inclination in the same direction and same order of magnitude of deviation from the linear regression line points to a faulty preparation or execution for this particular inclination. Also it is not visible in the experiment without added weight which rules out a direct relation to the specific value of inclination. Closer examination and greater sample size in this range of inclination are needed to ascertain a real systematic effect over an experimental error.

The higher accuracy with added weight is a result of the smoother movement of the leg which leads to less variation in the sensor readings and as such to a better reproducibility. This in turn improves the correlation coefficient.

Internal sensors The coxa-femur joint shows no correlation of sensor read outs with the inclination. The body-coxa and the femur-tibia joint are comparable in performance as seen by the similar correlation coefficients and similar relative errors. The accuracy and the precision are in the same order of magnitude as those of the strain gauges. This means the two sensor types are similarly suited for the application. Adding weight does not improve

the accuracy of the internal torque sensors. This signifies a robustness against less smooth movements which is an advantage over the strain gauges.

Evaluation of sensors The sensors are evaluated on their applicability in a technical realization. The requirements are low cost and low energy consumption while still being easy to install, calibrate and read out. A solution with already pre-equipped internal sensors is favoured.

The external strain gauges are lightweight and exhibit low energy consumption. Their real world applicability is nevertheless limited. Errors can be introduced by the accuracy of placement. The sensor readings are temperature dependent so additional sensors to correct for this influence have to be installed. The sensors are on the surface of the legs so that they are exposed to environmental influences.

The motors are pre-equipped with the sensing capability for internal torque. This means there is no need for additional sensors and no additional power supply is necessary.

Comparing the results of the internal sensors with the external strain gauges the external ones show only a marginally better performance. Weighing the complicated installation, the added costs for the sensors, the additional wiring, the measuring amplifier and the energy consumption the benefit of the higher performance becomes negligible.

In summary since the internal sensor offer advantages in usability at comparable performance they are exclusively used in further experimental setups.

6.4.3 Parameter Additional Weight

The modular setup of the one legged platform allows for quick parameter change. One parameter considered explicitly are different weights. In the sensor readings of all types of sensors this is expressed in a higher slope of the linear regression line. This means with additional weight the response of the sensors increase. The effect is less pronounced on negative inclinations because gravity already favours the downward movement and additional weight just adds additional pull. On the positive inclinations the influence of the added weight is more pronounced. The leg moves against the additional gravitational pull of the extra weight and as such the forces on the leg increase.

Since the added weight does not change the shape of the inverse function, the underlying principle is robust against this parameter change. Still the specific measurements are influenced and a high load as well as a steep substrate inclination both lead to an increase in sensor read out. Thus factors like loading have to be considered such as to not confuse the influences.

6.4.4 Further Parameter Changes

Although the modularity of the setup allows for rapid changing of parameters and examining their influence on measurements explicitly, additional parameter changes are covered in alternative ways. Since all results on the one legged platform are inherently limited in their significance and have to be repeated in real world application, changes in leg geometry, shape and material are implicitly covered in the following research on a full hexapod platform in Chapter 7.

Hooks, claws and adhesive pads as suggested by the biological model are subject of research [Palmer III et al., 2010, Endlein and Federle, 2015, Federle and Endlein, 2004]. They offer interesting insights into the necessary adhesive principles successfully employed in nature. Biomimetic principles exploiting anisotropic friction are shown to improve slipping and energy consumption [Manoonpong et al., 2016]. All these solutions were discarded because they introduce unnecessary levels of complexity into the experimental design. Coating the foot with a rubber-like material enhanced the friction to the substrate sufficiently for measurements while retaining maximum simplicity in design and production.

Experiments concerning leg compliance and different substrate materials are covered by other research groups [Xiong and Manoonpong, 2015, Xiong et al., 2014]. In a real world application both these influences have to be considered and unified in an all-encompassing approach.

6.4.5 Influence on Further Research

In summary this chapter shows that internal sensors are as useful as external sensors and offer additional benefits. This influences the design of the hexapod platform (Chapter 7) as only the internal torque sensors of the motors are used as idiothetic cues to determine the substrate inclination.

Since the underlying principle proved robust and stable over repeated experiments on a variety of inclinations, jerky movement and additional load the design of the hexapod platform is further removed from the biological model. It exhibits three perpendicular DOF as compared to the pseudo four DOF setup introduced in this chapter. The leg shape is further simplified to straighter lines that are easier to produce. While the filament used in 3D printing allows for rapid prototyping as seen in the preliminary experiments it is not very stable. Thus the commercially available PhantomX hexapod employs aluminium as connector pieces between the motors. The underlying principle proves to be robust to changes in these parameters.

Pressure sensors at the foot tip to measure ground reaction forces proved to be impractical because shear forces prevented usable readings. Thus this approach also proved unusable in the final application.

CHAPTER 7

Hexapod Platform

The findings acquired on the one legged platform are further generalized to a generic hexapod platform. The internal torque sensors are recorded for the robot moving along a ramp set at varying inclinations. On a subset of the motors it is possible to discriminate the inclination from the sensor readings. The hind legs' bc- and cf-joint as well as the middle legs' bc- and ft-joint are especially suited. This chapter is a proof of concept of the possibility to detect the substrate inclination with solely idiothetic cues from the joint torques.

7.1 Introduction

Hexapod platforms are well established in research and application of walking robots. They exhibit a variety of sizes and complexities, just like insects, their biological counterparts. In contrast to wheeled platforms the use of legs offers great stability and the possibility to overcome higher obstacles in relation to body height. This predestines them for missions on uneven and unknown terrain. The absence of established knowledge on such exploratory missions leads to the need for navigational abilities.

The overall goal is to establish an ant inspired path integrator that takes the substrate inclination into account to enable precise homing. To ensure reliable detection of substrate

inclination a correlation function between measured idiothetic cues on the platform and the inclination has to be established.

The one legged platform (Chapter 6) already presented valuable insights for the mobile six legged platform. In an abstracted technical adaptation of an ant leg the internal sensors of the motors are sufficient in establishing a correlation to the substrate inclination. Based on the robustness of the findings the construction of the hexapod platform is further simplified to counteract the increased complexity of movement coordination and control of the additional legs.

The idiothetic cue on the hexapod platform is the power consumption of the motors which is related to the torque on its joints. The motors in which this measure allows a correlation to the substrate inclination are identified and quantified. A generic system is chosen as the platform to demonstrate the viability on low cost off the shelf components and thus the wide applicability of the solution.

7.2 Material and Methods

The experimental setup consists of a hexapod walking on a ramp with variable inclination (Fig. 7.2). The data is acquired by internal sensors of the hexapod's motors. The experiments on each inclination are repeated to account for imprecisions in the setup. From the raw data average step cycles are extracted. The change in the average step cycle is correlated to the change in substrate inclination.

7.2.1 PhantomX Hexapod

Experiments are conducted on the PhantomX Mark III hexapod kit (Trossen Robotics, USA) (Fig. 7.1). The body is made from aluminium and the motors are Dynamixel AX-18A (ROBOTIS INC, USA). The nomenclature follows the pattern established on the one legged platform (Chapter 6, Fig. 6.2 and 6.3). The connector pieces are labelled in order coxa, femur, tibia going from the closest to the body to farthest. In total the hexapod is equipped with 18 motors. The sides of the robot are denoted left and right referring to a top view perspective with the forward walking direction facing upward. The legs on each side are numbered 1 to 3 from front to back (Fig. 7.1). The three motors on each leg are labelled with respect to the connecting pieces body-coxa (bc), coxa-femur (cf) and femur-tibia (ft) joint (Fig. 7.1). The bc-joint controls the forward to backward range, the cf-joint lifts the leg up and the ft-joint determines the width of the stance. The motors of each leg are daisy chained and intersect on the ArbotiX-M robocontroller (Trossen Robotics, USA) and the 6 Port AX/MX Power Hub (Trossen Robotics, USA) which is in turn connected to the measurement laptop

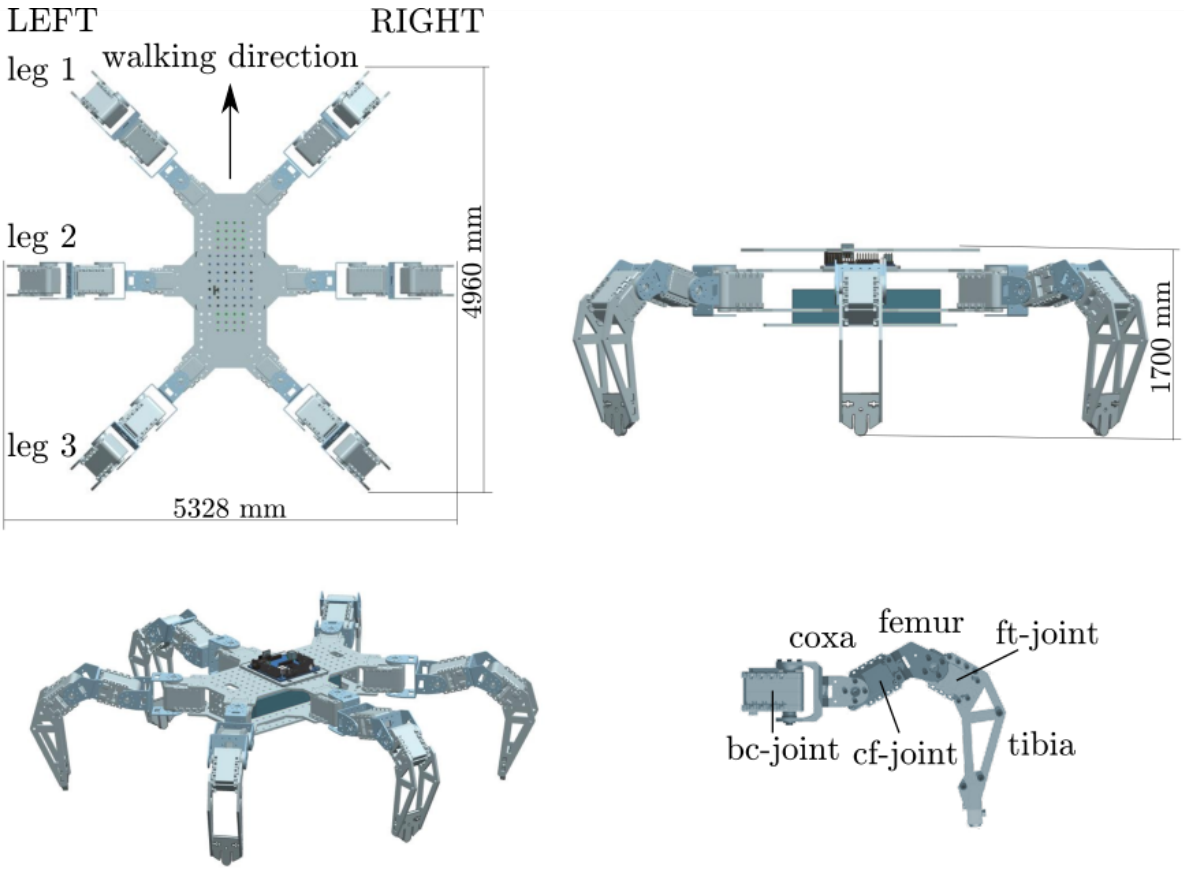

Figure 7.1: Dimensions and nomenclature of the PhantomX platform. The walking direction determines the front of the robot. From front to back the legs are numbered consecutively. The sides left and right are determined looking from the top with the walking direction oriented upwards. All legs consist of three connectors labelled from the body outward: coxa, femur and tibia. The joints are labelled with shortened forms of the connectors that they border: body-coxa (bc), coxa-femur (cf) and femur-tibia (ft). This nomenclature is consistent with Chapter 6.

(Latitude E5550, Dell) via USB2Dynamixel (ROBOTIS INC, USA) (Fig. 7.4). The robot is powered by a 11.1 V 5 300 mAh Lithium Polymer (LiPo) battery (Gens Ace, China).

7.2.2 Experimental Setup

The experimental environment consists of a ramp made from a 19 mm wooden plank. The platform measures 2.4 m × 1.0 m. A rubber mat is fixed on top to enhance friction. The inclination is changed by elevating one end of the ramp. The angle is measured with a digital inclinometer (Toolcraft Model No: 110914) against the plane floor of the laboratory.

The hexapod is placed at one end of the ramp and powered on. It assumes the neutral starting position with all six legs on the ground. The controls and data recording nodes

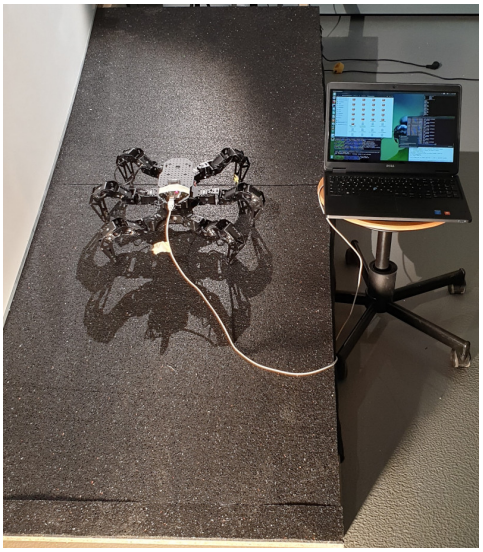

(a) top view

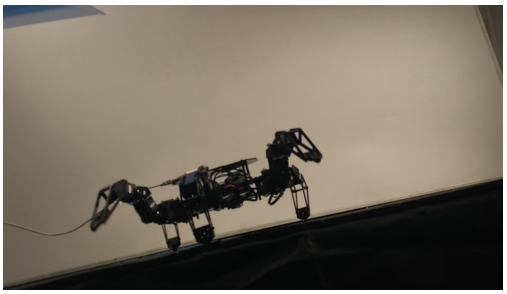

(b) side view

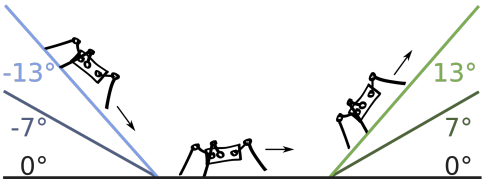

(c) inclinations

Figure 7.2: Overview over the experimental setup. The robot is placed on a ramp of varying inclination. Walking upwards is denoted with positive angles, walking downwards is denoted with negative angles. The robot is powered by batteries, the USB cable connects to the laptop controlling the movement and logging the measurements of the internal torque sensors.

are started. The forward moving command is sent and the measurements stored for later examination. The hexapod moves along the ramp in a straight line perpendicular to the inclination for 10 to 14 steps. The stop command is sent and the robot powered down. The hexapod is reset to the initial starting position and the next run is recorded.

Readings of the internal load sensors of all 18 motors are recorded continuously over the whole length of each run. The recording is done via the ROS interface and saved for further evaluation.

The sequence is repeated up to 15 times before adjusting the inclination of the ramp. The runs are recorded on a horizontal ramp corresponding to 0° inclination as well as on 7° and 13° and their inverse (Fig. 7.2). This covers the maximum range of inclinations the hexapod can safely travel without excessive slipping of the legs. Positive angles denote a upward movement of the hexapod, negative angles a downward movement (Fig. 7.2c).

7.2.3 Control

In addition to the sensor readings the ROS interface controls and coordinates the leg movement. The motors are connected via USB to the measuring laptop running Ubuntu 16.04 and ROS kinetic. A script continuously replays a loop of the motors positions without feed-

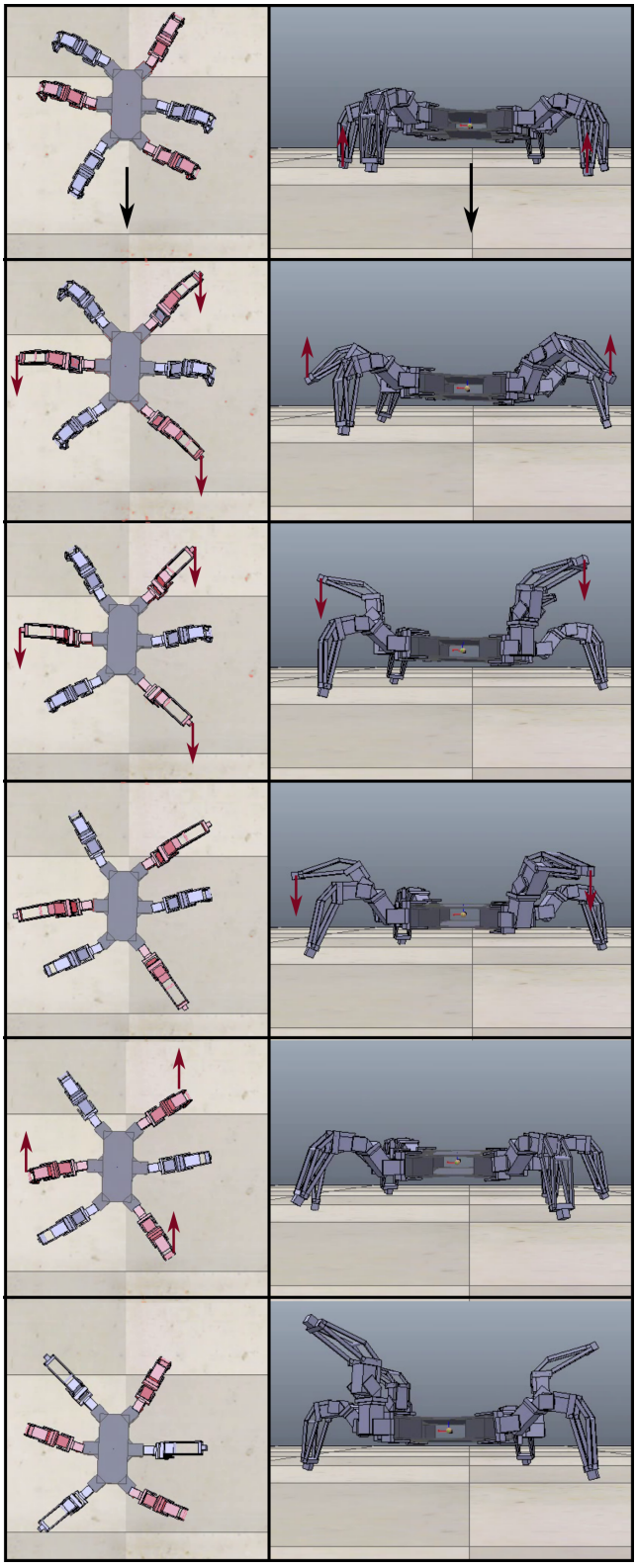

Figure 7.3: Sketch of the robot movement. The black arrow indicates the walking direction. Legs in motion are colored red in the top view. Red arrows indicate the motion direction of the legs. The step cycle of one tripod is shown, afterwards the analoguous movement is repeated on the opposing tripod.

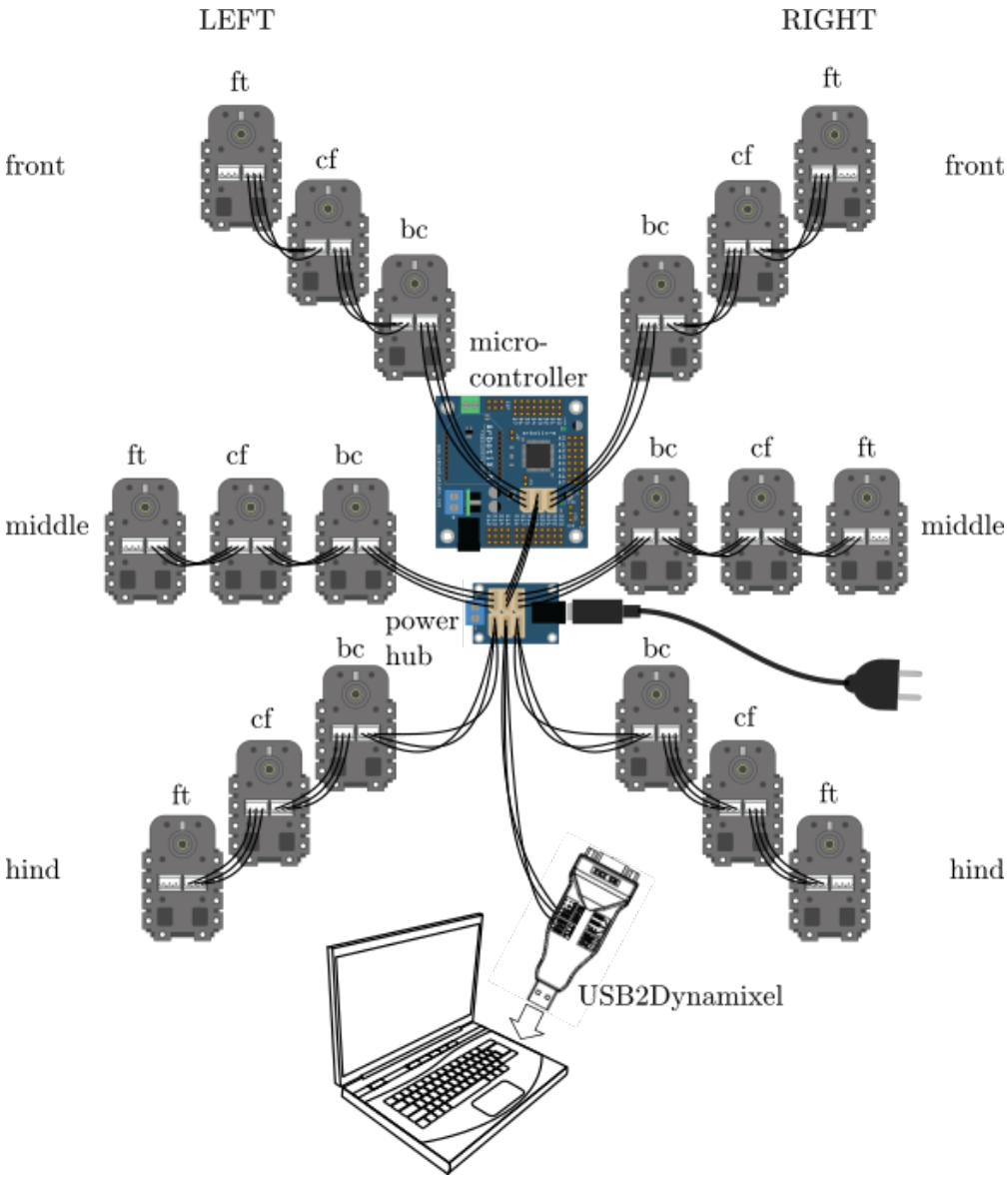

Figure 7.4: Schematic of the wiring. The motors of each leg are daisychained and connected to the microcontroller. The robot is powered by a battery pack indicated by the power plug in this image. The microcontroller is connected through the power hub to the USB2Dynamixel device that allows communication to the laptop via the USB-port.

back or adaptation to environmental cues while at the same time storing the timestamps of sending the first signal of the swing phase of each tripod.

7.2.4 Movement

The footfall pattern is modelled after the ant's tripod gait. A tripod consists of the front and hind legs of one side and the middle leg of the opposite side. The movement of the tripods is identical but shifted in time by half a period. This leads to one tripod staying on the ground and providing stable footing while the opposing tripod moves forward, touches down and forms the new support tripod.

The legs are equipped with three motors each, corresponding to three perpendicular DOF. In a coordinated movement the cf-joint lifts the leg up, while the bc-joint moves it forward. The ft-joint keeps the width of the stance stable. At the end of the forward trajectory the cf-joint returns to its neutral state, resulting in a touchdown of the leg. By turning backward the bc-joints push the robot further forward in the stance phase.

A full step cycle consists of a full swing phase and the following stance phase of one tripod with the other tripod experiencing first the stance and then the swing phase. More precisely it starts at the beginning of the swing phase of one tripod which is counted from first lift-off of the corresponding legs until their touch down. The cycle lasts through the stance phase of the same tripod with the other tripod in swing phase and ends at the touch down of the opposing tripod. This also marks the end of the stance phase of the first tripod where a new swing phase would commence and thus a new step cycle. The movement is repeated cyclically (Fig. 7.3).

7.2.5 Sensors

The Dynamixel AX-18A provides an internal sensor for the current. This measure is correlated to the sum of all forces inducing a torque along the motor's main axis in the following labelled load on the motor. The sign indicates the direction of the resulting force either clockwise or counter-clockwise around the main axis. In a controlled environment this measurement exhibits a linear transfer function to the joint torque (Fig. C.1).

The data is recorded by a script echoing the respective ROS topics continuously over the whole duration of the runs. Since the motors are daisy chained the measurements are taken at marginally different times. Each data point consists of the sensor reading and corresponding timestamp. The ROS script used to control the movement additionally logs the timestamps at the start of the swing phase of each tripod.

7.2.6 Data Preparation

The goal of the data preparation is to extract a clean average step cycle to examine the impact of the ramp's inclination free from other interferences. To control against external influences the data is screened for the hexapod walking in a straight line along the ramp for more than nine steps without slipping and without error messages on the ROS interface. For each inclination the first 11 runs that meet these criteria are selected. The first step of each run moving the robot from the initial neutral position to the walking position is dropped. The dataset of each run consists of the nine steps following the initial one. This ensures equal weighting in the statistical evaluations. Preliminary statistical investigations on the inter- and intra-run aberrations conclude that the aberration of any step from the average step during one run is smaller than the aberration of the average step cycles between runs (Fig. B.3). Thus the confidence interval is calculated with all steps of all runs accumulated into one dataset.

To extract an average step cycle for each inclination the measured data is cut into separate steps, normalized and averaged. The data points are classified as belonging to the swing or stance phase of the respective motor based on the timestamps of the corresponding tripod lift-off. The duration between lift-off of one tripod and lift-off of the other one is set to be 100 % of the swing phase. The swing phase of one tripod is counted as stance phase of the opposing tripod. The internal load sensors of all motors continuously measure the load over time but the daisy chaining leads to asynchronous timestamps for each measured value. Thus the timestamps are normalized to the duration of the respective swing or stance phase and accumulated into bins of size 10 %.

To align the frames of reference on both sides of the body and adjust for the mirror symmetry in the hexapod's construction the sign of all values of the left body side is flipped.

The average step cycle consisting of swing and stance phase is calculated over all steps of all runs on a particular inclination. It is calculated separately for all 18 motors on all five inclinations.

All average step cycles are presented as function of the inclination to determine if it is possible to distinguish the surface inclination solely from the measured joint loads.

7.3 Results

Sensor readings are accumulated into average step cycles for each tested inclination as a function of the time elapsed in swing and stance phase. Where the 95 % intervals don't overlap, the difference in average load on the motor at that time point is statistically significant.

The measured load is a combination of the motors' proper movement and external torque. The size of the external torque is influenced by the geometry of the hexapod, specifically the

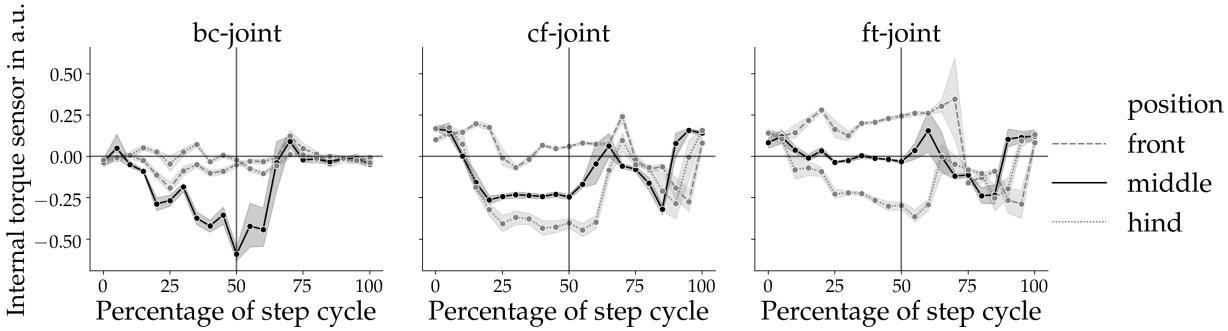

Figure 7.5: The internal torque sensor is read in arbitrary units. The course over a whole step cycle is recorded and averaged over all steps and all runs. The shadows indicate the 95 % confidence interval. The results shown are at 0° inclination and for the right front, middle and hind legs. From left to right the joints are further from the body. The shift from stance to swing phase is marked with a vertical line.

alignment of the legs in relation to the direction of movement (Subsection 7.3.1) as well as the inclination of the ramp and thus the alignment of the robot in three-dimensional space (Subsection 7.3.2).

Corresponding motors on the left and right side of the hexapod exhibit the same progression of the average load over time. While it follows the same pattern of plateaus and local extrema, a non-negligible amount of averages are statistically distinct between left and right side (Fig. B.2). In the following the left side is discussed in detail with all results applicable analogous on the right side.

7.3.1 General Movement and Influence of Geometry

The **bc-joint** (Fig. 7.5A) moves in a front to back direction, a negative sign indicates movement to the back. The gradual fall of the load during the stance phase corresponds to the proper movement of this motor pushing to the back and thus moving the body forward. In the swing phase a smaller peak in the opposite direction corresponds to the shorter movement of moving the leg forward in the swing phase. This movement is overlaid by the forces introduced by the other two motors of the leg that move up and out at the same time. Thus this peak is less pronounced. After moving the leg forward this motor does not move for the rest of the duration of the swing phase as reflected by the plateau at zero load. The middle leg is oriented perpendicular to the direction of movement and as such experiences the greatest changes in load for the bc-joint.

Negative values of the **cf-joint** (Fig. 7.5B) denote an upward movement of the leg or the sum of the external forces pointing upward. In stance phase the joint exhibits a plateau at negative values. This corresponds to the motor counteracting the gravitational forces acting

on the legs and keeping the robot in a stable position. In swing phase a pronounced spike in the same direction is visible that corresponds to the lifting of the leg so that it doesn't hit obstacles when moving forward. The sign is the same because the forces acting on the motor stemming from counteracting gravity and its proper movement act in the same direction. When the leg moves back down values in the positive load range are recorded.

The **ft-joint** (Fig. 7.5C) determines the width of the stance. Negative values of load denote a movement of the tip further away from the body. In stance phase the ft-joint also keeps the leg stable against gravity. Because of its alignment the absolute value differs from the cf-joint but the plateau is also visible. In swing phase in order to extend the leg even more and avoid obstacles it also performs a movement stretching the end effector further upwards as can be seen by the valley in swing phase. When the leg moves back down values in the positive load range are measured.

This general sequence of movement can be observed on all legs. Differences arise from the different alignment of front and hind legs, which rotate the axis along which the loads are measured.

7.3.2 Influence of Inclination

A change in inclination changes the intensity of the load with the overall progression over time staying the same for all motors (Fig. 7.6).

Sensor readings during the stance phase show greater discrimination over different inclinations. The hind legs' bc- and cf-joint as well as the middle legs' bc- and ft-joint are especially suited to recognize the substrate inclination. A combination of the information of at least these four motors yields higher accuracy than each on its own, because middle bc- and hind cf-joint show clearer differentiation on negative inclinations and the other two mentioned on positive inclinations.

None of the motors alone allows the discrimination of the substrate inclination at each point in time over the whole step cycle.

7.4 Conclusions

This chapter outlines the development and experiments performed on the hexapod platform. Manual correlation of the measured joint torques to the substrate inclination is possible. The findings lay the groundwork for the following chapter that pursues the same goal with an automated approach. A full analytical modelling of the 18 interdependent, time-dependent signals proves to be a highly complex and multi-parametric task to which an artificial neural networks is well suited. The complexity is furthered by considering the introduction of

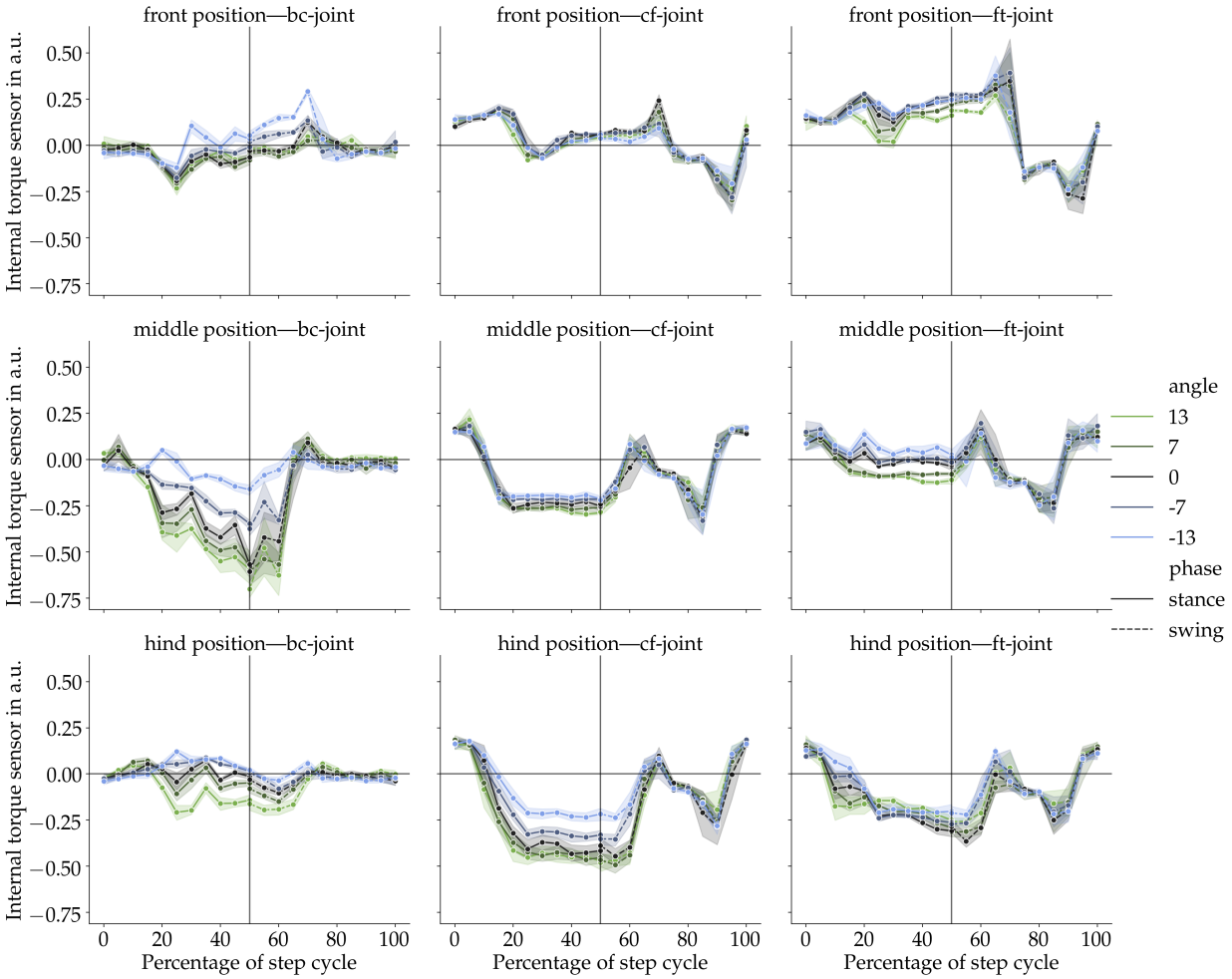

Figure 7.6: The internal torque sensor is read in arbitrary units. The course over a whole step cycle is recorded and averaged over all steps and all runs. The shadows indicate the 95 % confidence interval. The results are shown from top to bottom for the right front, middle and hind legs. From left to right the joints are further from the body. Colours indicate the inclination of the ramp. The shift from stance to swing phase is marked with a vertical line. The results for the left leg can be found in the appendix (Fig. B.1).

additional influences like loading and unloading of payload or slanted paths, which are also handled in Chapter 8.

7.4.1 Influence of Previous Research

Taking the previous research into account and the proof of concept on the one legged platform (Chapter 6) the insights are transferred to the hexapod platform. Since the concept proved to be robust to the abstractions realized in the one legged platform further abstractions and variations are implemented on the hexapod platform. A change in motors from the more powerful model MX-64 AT to the smaller AX-18A did not impede the general function principle.

The load bearing structures in the PhantomX hexapod are made from aluminium. This does not pose any problems for the underlying principles.

The movement is abstracted further. In the PhantomX the fourth pseudo DOF is not present. Instead it only possesses three perpendicular DOF. Only the most basic principles of the ant locomotion are preserved. The tripod gait with its alternating support triangles is still present and sufficient to exhibit the desired properties. A closer look on the actual movement and resulting forces present in ants and other insects is conducted in [Guo et al., 2014a, Guo et al., 2014b, Guo, 2015, Guo et al., 2018]. The final application is the deciding factor if the additional effort to reconstruct the biological model closely is warranted. For simple navigational tasks it is shown to not be necessary. This saves on computing costs in control and assembly cost in construction of the hexapod platform. An additional fourth DOF is not crucial to the navigation task.

Another real world influence is the inertia of the legs. This introduces additional movement transmitted along the joints and even the body. The legs with around 200 g each introduce non-negligible inertia effects considering the total weight of the robot with battery of 2.4 kg. Thus all legs together account for half of the total weight in contrast with the desert ant where the legs only contribute 14.94 % of the body weight [Guo et al., 2018]. The inertia effects introduce movements that the motors of the tripod currently in stance phase have to balance.

7.4.2 Results

The movement for each step is repeated without feedback loops. Thus, the steps are stable over each run as can be seen in the statistical evaluation (Fig. B.3). The small error bars in the results section indicate that the steps are also stable over several runs. This indicates little to no sensor drift or challenges with resetting the motors between each experiment.

The constant shape with varying intensity is explained by the fact that each step cycle is executed the same. No feedback is collected and no adaptations are performed to the movement. Thus the contributions to the measured load stemming from the proper motion of the motors remain constant. The influence of the shifting weight stemming from the geometrical change in the measuring setup introduced by the lifting of the ramp is observable in the changing amplitudes especially in the stance phases.

The statistical differences in the left-right-symmetry does not allow for combining both datasets to obtain an average step cycle for each type of motor discriminating only the position of the leg and the type of joint (Fig. B.2). Differences in the averages can be attributed to manufacturing differences in the motors and precision of the experimental setup. The robot exhibited a tendency to pull to the right side when walking upwards on the ramp. This indicates either a systematic error in the ramp setup resulting in a slanting ramp or an imbalance in the motor forces resulting in a drift to the right side. Independent of the source of the error the theoretical symmetry is broken in real world conditions as witnessed by the sensor readings. However both sides individually still permit the discrimination of the inclination, proving the robustness of the underlying principle against these influences. Thus the hypothesis that it is possible to discern the substrate inclination from solely the internal sensor readings of the motors continues to hold up even with small symmetry breaks and real world conditions.

7.4.3 Parameter Changes

When changing the inclination the curve progression, especially in the swing phase, remains constant for all joints of the same type and position as the executed motion remains the same (Fig. 7.6). In stance phase however the cf- and ft-motors do not move so that the proper movements do not overlay the torque measurement. Thus in this phase the change in torque on the leg stemming from the shift in weight can be observed and evaluated. This force changes with the inclination. On positive inclinations the bc-joints need to push the body forward against the gravity, whereas on negative inclinations less force is necessary because of gravity already pulling the body forward. These effects can be observed in the splitting of the measured bc-loads. On negative inclinations the relief of the hind legs is visible especially in the cf-joint. Apart from that the cf- and ft-joints remain comparably stable over all inclinations since their main task is stabilising the robot against the gravity.

Joints that only allow discrimination of positive inclinations are gradually more loaded by the shifting weight distribution. On the negative inclinations they are almost not loaded as expressed by the zero load. Joints that only allow discrimination of negative inclinations are gradually unloaded when the weight shifts forward. On the positive inclinations they are fully loaded and thus not permitting their differentiation.

In a real world application the sensor fusion of several motors is advised. The joints differ in their ability to differentiate the tested angles. The reduction of the influence of sensor noise, the reliability of the estimation and introducing redundancy are the apparent advantages of this approach.

The resolution of inclination discrimination is half a step cycle because the discrimination is mainly possible in the stance phase but not over each time step. The slower the inclination changes along the complete walking path, the more reliable the measurement because several step cycles can be recorded. The inclination change is measured on the scale of the hexapods length of 50 cm (Fig. 7.2). Smaller structuring of the surface is not identifiable.

7.4.4 Influence on Further Research

The hexapod model is chosen due to its close resemblance to the biological model. Hexapods are also widely used in robotic applications. Their six legged setup offers an advantageous trade off in terms of stability, complexity, speed and versatility in rough terrains.

In the presented results the effect of sensor noise is diminished by the averaging over many time steps. In applying the results to an odometry system filtering the noise becomes necessary to get a clear reading of the current load.

To get a reliable result in the manual analysis at least half a step cycle is necessary. This corresponds to 1 s in real time. This leaves enough time for processing the measured values for a real time application. The measurements however provide a validation to the approach with artificial neural networks that it is fundamentally possible to discriminate the inclination solely on the proprioceptive signals recorded by the motor's internal load sensors. The hexapod exhibited a tendency to drifting to the right side of the ramp. This impeded the recording of long straight walks. The runs that were too slanted are excluded in this analysis and the runs are cut to short instances. The influence of walking on a ramp in a line that is not perpendicular to the ramp is investigated in a simulated environment in Chapter 8.

CHAPTER 8

Artificial Neural Networks

Based on the general feasibility to correlate substrate inclination and joint torque sensor readings as demonstrated in the previous chapter an artificial neural network is designed to take over this task. This eliminates the need to design and alter expert systems for every eventuality encountered in an exploratory mission. Datasets are generated in a simulated environment to determine the optimal topology of a shallow feedforward network. The artificial neural network is able to discriminate the substrate inclination based on the joint torques even when additional parameters like weight of the robot model and its alignment on the ramp are altered. The findings are validated under real world conditions with the dataset acquired on the physical robot platform of the previous chapter.

8.1 Introduction

Analysing the joint torque on a generic hexapod platform (Chapter 7) revealed the general feasibility of correlating the measured value to the substrate inclination. It also exposed the complexity of a manual modelling approach to this multi-parametric, 18-dimensional, time-dependent task. For such a challenge, that is shown to be fundamentally solvable but hard to model explicitly under varying conditions, artificial neural network prove a useful tool. Due to their trainable nature external influences can easily be incorporated into the

problem definition, as shown in this chapter with varying the payload and introducing slanted paths.

Inspired by the powerful capacities of the human brain artificial neural networks (ANNs) consist of simple basic components. Abstracted neurons are connected by simple synapses. Activated neurons influence each other with a dedicated subset of the neurons representing the solution. With a big enough sample set of corresponding input and expected output the ANN can be trained to recognize patterns in the input data and correlate them to a certain solution. This principle has been well established since the groundwork was laid in [McCulloch and Pitts, 1943] but it wasn't until the rise of advanced computing power that ANNs experienced a renaissance and enabled previously unknown possibilities in a variety of areas of application. Arguably they rang in the current era of machine learning and artificial intelligence. Their primary function is to detect patterns in large amounts of data. Their full potential unfolds in generalizing new patterns to established solutions. In the context of this work the application on the multi-parametric problem of mapping the signals received by the hexapod's 18 motors to the current substrate inclination as established in Chapter 7 is apparent.

The goal is to find a suitable artificial neural network that correlates the idiothetic cues of the motors to the current substrate inclination. Although ANNs are inherently black boxes the manual analysis in Chapter 7 demonstrates that the measured data exhibits recognizable patterns that are statistically relevant and reproducible. While this does not preclude the ANN from identifying and utilizing additional hidden patterns the previous findings motivate the use of ANNs in demonstrating the general existence of patterns.

Since the measurements on the hexapod platform are limited by the necessary manual labour in repeating the measurements the dataset is supplemented by simulated datasets. The simulated environment allows additional parameter changes. The ANN proves robust to generalizations as introduced by varying weights of the hexapod and slight changes in alignment on the ramp, thus eliminating the need of elaborate and costly expert systems to account for all these influences.

The idiothetic cues of hexapods in a real and simulated implementation are recorded on ramps of differing inclinations and the datasets are used to train ANNs of various topologies. A shallow feedforward neural network with just one hidden layer is sufficient to discriminate the inclination in the experimental resolution of 7° and indicating the possibility of even finer results. The ANN proves robust to additional influences introduced by loading and skewed walking paths.

8.2 Material and Methods

The artificial neural network is tested on two distinct but related datasets: the experimentally obtained measurements of the hexapod platform and simulated joint torque measurements on the simulated recreation of the experimental platform. In both cases the setup consists of the hexapod and ramps with varying degrees of inclination. The ramps are climbed up or down by the hexapod and the idiothetic cues measured. The measured values are fed into a shallow feedforward neural network and it's performance in discriminating the inclination is evaluated. Different topologies of the ANN are varied to find the best fit for the problem. The general experimental setup remains the same in the physical experiments as well as in the simulated environment. A hexapod platform is placed on an inclined ramp and performs a series of steps along the ramp.

8.2.1 Simulated Data

The large datasets required to train an artificial neural network are produced in a simulated environment.

Simulation Setup The robot simulator CoppeliaSim (Ubuntu release V 4.0.0, rev 2, 64 bit, Coppelia Robotics AG, Switzerland) [Rohmer et al., 2013] is used to obtain the simulated datasets (Fig. 8.1). The simulator is based on a modular architecture. The suitable physics simulation library can be chosen for the rigid body simulation while built-in modules provide forward and backward kinematics, collision detection and motion planning. Plug-ins enable further functionality and customization to control each model individually. In the conducted experiments Bullet 2.78 is used as dynamics engine. The simulation time steps are set to 25 ms. The dynamics setting remains at the default Accurate setting. An existing model focussing on static and dynamic modelling [Nguyenová et al., 2018] represents the hexapod in the simulation. The weight is set to 2.393 kg to mirror the real world conditions.

Ramps of different angles are modelled in the 3D computer-aided design (CAD) programme SolidWorks and imported into the CoppeliaSim Simulation. 0°, 3°, 4.5°, 6.5°, 10°, 13°, 16° and 20° ramps are used. For the hexapod walking up these ramps the angles are labelled with a positive sign, for downwards movement the angles are denoted with a negative sign.

The hexapod model is placed above the ramp with a small gap between both models to eliminate the risk of interference. When starting the simulation the hexapod model drops until it comes in contact with the surface and starts its movement. The commands to the motors are the same as in the real hexapod (Subsection 7.2.4) and are sent out in a continuous loop to the motors. The joint torques are retrieved and exported into a comma separated values (csv) file to be presented to the ANN.

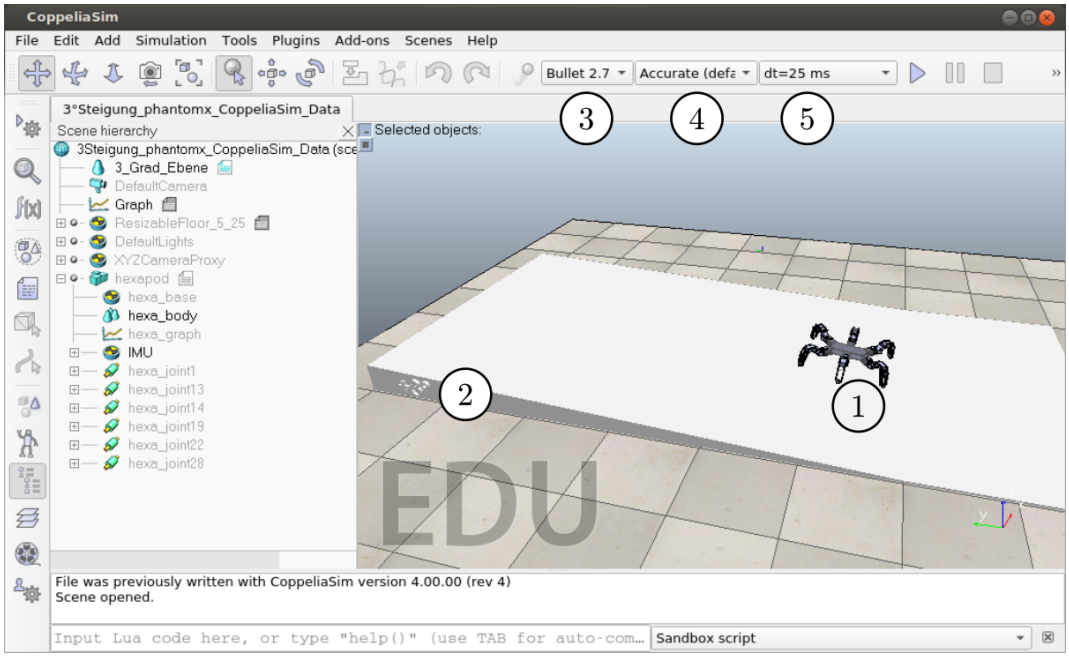

Figure 8.1: Simulated environment in CoppeliaSim. The scene hierarchy is accessible on the left side. On the right side the graphical representation of the simulation is visible. The model of the robot (1) is placed on the model of the ramp (2). The dynamics engine (3), the accuracy (4) and the time step size within the simulation (4) can be chosen in the drop-down menus at the top.

Experimental Protocol The simulation is set up to allow manipulation of the total weight of the hexapod and the alignment of the ramp (Fig. 8.2). To automate the data acquisition and prevent the introduction of unconscious bias to the datasets the simulation is set up in three configurations. The first configuration randomly adds between 0 g and 400 g to the total body weight of the hexapod. This weight is constant for the remainder of the simulation. The second configuration randomly changes the initial alignment of the ramp between ±35° (Fig. 8.2). The third configuration is a superposition of the previous two. Both the weight and the alignment are changed randomly and independently.

The simulation is run for 15 s simulation time. The first second is excluded from consideration to account for the time needed for the models to make contact. The following 10 s simulation time are used to train and evaluate the ANNs. The remaining seconds are recorded to ensure safe shutdown of the simulation without data loss but are not considered for training because on high inclinations the hexapod has already reached the end of the ramp by that time.

The simulation is then restarted to record another randomized data sample. The procedure is repeated 1 000 times. The final dataset for each of the three test conditions is made up of 1 000 repetitions with 40 time steps each of 0.25 s intervals on 15 different inclinations. So for all 18 motors 600 000 corresponding joint torques are used to train the ANNs. The target data is set to the true inclination of the corresponding modelled ramps.

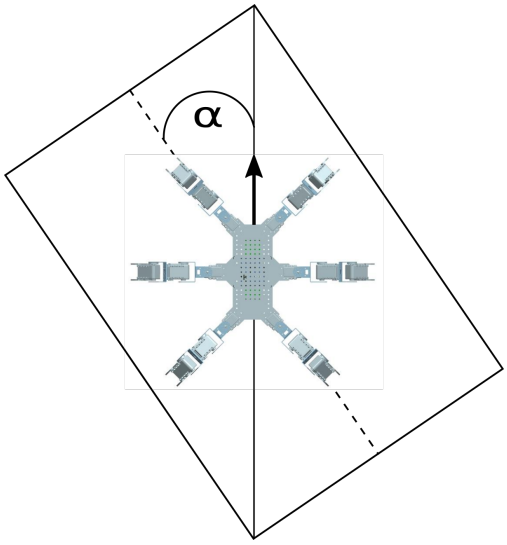

Figure 8.2: Schematic illustration of the alignment of the robot model on the ramp. The arrow denotes the walking direction of the robot model. The gradient of inclination is oriented along the dotted line. The angle α between these two orientations is used to describe the alignment. Positive angles denote clockwise rotation of the walking direction against the ramp. Negative angles denote a counter clockwise rotation.

8.2.2 Experimental Data

To validate the ANN approach the concept is tested on the data acquired under real world conditions. The detailed description of the experimental setup including coordination of movement and control and measuring interface can be found in Section 7.2. The hexapod PhantomX traverses ramps with inclinations of 13°, 7°, 0°, −7° and −13°. The motors continually measure the load, which is effectively a combination of proper movement and external joint torques.

The data is recorded by the control interface that records the current loads for all 18 motors each time all six legs touch the ground. This corresponds to a rate of once per second which in turn corresponds to twice per step cycle. To increase the frequency of the predictions a different set of ANN are trained on the data as described in Subsection 7.2.6. The continuously measured data is grouped by their timestamps to corresponding phases of the step cycle. The rate is consequently at 20 times/step cycle. To improve the prediction on the continuously measured data, the dataset is extended by an additional input representing the percentage of the current step cycle. This way the ANN can weigh the information depending on if the legs are actively moving at that moment or not.

The target dataset in both cases is the known pre-set angle of the ramp. The angle is verified before data collection with a digital inclinometer (Toolcraft Model No: 110914).

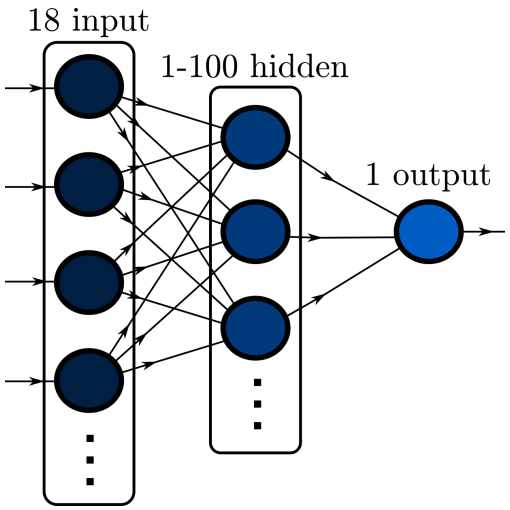

Figure 8.3: Schematic illustration of the artificial neural network. Circles denote neurons, arrows denote connections. All neurons are fully connected and the information is propagated forward through the ANN. The 18 input neurons represent the signals received from each of the 18 motors. In one case an additional input neuron is introduced to represent the current percentage of the step cycle. The number of hidden neurons is varied from 1 to 100 to determine the optimal topology. The output neuron is interpreted as the predicted angle of substrate inclination in degree.

The dataset of all time steps contains 2 951 data points, the reduced dataset of only the double support phases contains 1 568 data points.

8.2.3 Artificial Neural Network

A shallow feedforward neural network consists of three layers (Fig. 8.3). The input to the ANN is encoded in the neurons of the input layer. The information is passed through and processed in the neurons of the hidden layer. The neurons of the output layer in turn encode the answer of the ANN.

Topology The ANNs are implemented with the Neural Fitting App of the Deep Learning Toolbox in MATLAB 2017a (Fig. 8.3). In the presented application the input layer is comprised of 18 neurons representing the load or torque on the motors at one time step. Each time step is considered an independent sample. The output layer consists of just one neuron that encodes the predicted inclination of the ramp based on the input from the motors. For the hidden layer different topologies are evaluated ranging from 1 to a maximum of 100 neurons. The target data needed to train the ANN is either the measured inclination of the ramp in case of the real world experiments or the chosen inclination of the ramp model in case of the simulated data.

Training To train an ANN three datasets are necessary: the input that is fed into the ANN, the predicted values the ANN produces and the true output values corresponding to the chosen input. Depending on the aberration between the predicted and the true values the connection between the neurons is adjusted. This is done by varying the weight and the biases of the neurons according to the learning algorithm. Various such algorithms exist, depending on the structure of the problem and the size of the datasets. Here the Levenberg-Marquardt algorithm is chosen as it is a versatile approach for a wide variety of applications [Moré, 1978].

For each tested condition, the two real world datasets as well as the three simulated datasets, separate ANNs are constructed. The overall training and testing procedure remains the same. Of the dataset 70 % is randomly assigned as training samples. 15 % is used as validation sample and the remaining 15 % comprise the test sample. During training the weights and biases of the neurons are adjusted according to the Levenberg-Marquardt algorithm to improve the performance. The validation set assures that the ANN generalizes the problem and prevents overfitting. When the performance on the validation set is worse than on the training set six times in a row the training is stopped. A good performance on training data with bad performance on validation data is indicative of overfitting. The other criterion to stop training is a maximum of 1 000 epochs.

Evaluation To evaluate the performance of the ANN two measures are determined, the expenditure to train and the performance of the fully trained ANN.

Presenting the whole training set and calculation of new weights and biases is termed one epoch. This is a measure how fast the ANN learns. The number of epochs the ANN undergoes before meeting one of the stop criteria is recorded.

To determine the performance of the ANN the test data is presented and the difference between the predicted and the true values is calculated. The test data is used exclusively to determine the ANN's ability to generalize to new problems. These samples are never presented in the training phase. The performance is evaluated on the root-mean-square error (RMSE) of the whole dataset.

8.3 Results

In general an increase in the number of hidden neurons decreases the RMSE but this effect is not unlimited. As a counter effect with increasing size of the hidden layer the time necessary to train the artificial neural network increases.

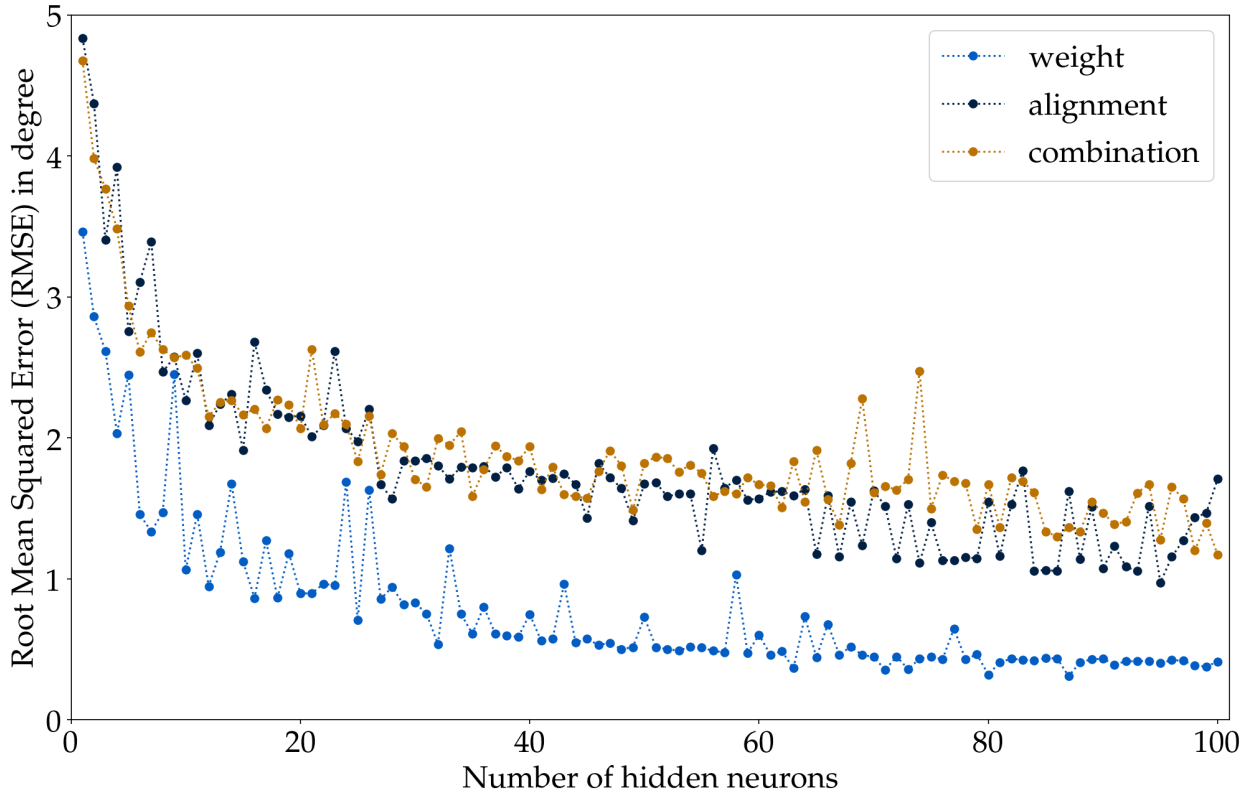

Figure 8.4: For each of the three conditions of varying weight (light blue), varying alignment (dark blue) and their combination (orange) artificial neural networks are trained for 20 epochs. The ANNs differ in number of hidden neurons. For each condition from 1 to 100 hidden neurons are evaluated after training with respect to the root-mean-square error in degree. The lines serve as guides to identify the general trend but do not represent relation between measured values.

8.3.1 Simulated Data

In order to identify the topology best suited for the task the ANNs are trained for 20 epochs and the trend in performance is evaluated. Then the ANN with the best performance is fully trained and the results analysed.

Topology With increasing number of hidden neurons the RMSE decreases and thus the performance increases under all tested conditions (Fig. 8.4). After a certain size of the hidden layer the performance plateaus and no further improvement is discernible. Under all conditions this size is reached at around 70 hidden neurons. The RMSE for the condition of differing alignments is bigger than the one for the differing weight condition and acts as lower limit for the performance of the combined weight and alignment condition.

Performance For the weight condition the optimal topology is at 87 hidden neurons with a RMSE of 0.174°. For the alignment condition the optimal topology is at 95 hidden neurons with a RMSE of 0.569° and for the combined condition at 100 hidden neurons with a RMSE of 0.840° (Tab. 8.1). Changes in alignment lead to worse predicting performance of the ANN which sets the lower limit in the prediction abilities for the combined condition. Three ANNs with these topologies are fully trained until the mean squared error (MSE) of the validation dataset exceeds the training set six times in a row (Fig. 8.5). The necessary epochs to fully train the ANNs are for the weight condition 1 451, for the alignment condition 681 and for the combined condition 552. To closer evaluate the performance the predictions depending on the initial input is considered. For the weight condition the response at 0° inclination exhibits a greater spread than the other tested inclinations (Fig. 8.6a). In contrast for the alignment condition the response at 0° as well shows a more precise prediction performance (Fig. 8.6b). For the combined condition no considerable deviations of the prediction are discernible (Fig. 8.6c).

8.3.2 Experimental Data

The stop criterion for the experimental data was set to 1 000 epochs. All nets reached the validation stop criterion in less epochs and thus are fully trained. For each topology 100 ANNs are trained and evaluated.

Topology For all conditions the performance increases with the number of hidden neurons until a plateau is reached (Fig. 8.7). Providing context about the percentage of the step cycle passed by adding the additional input neuron improves the performance of the ANN (Fig. 8.7b). In this case a tendency towards a decline in performance is seen with excessive number of hidden neurons. If only the points in time of the double support phase are presented to the network, the performance increases even further (Fig. 8.7c). The random initialization and short training periods lead to different levels of performance of the fully trained ANNs as evident by the standard deviation when averaging over 100 repetitions (Fig. 8.7). Considering the training epochs necessary to reach the stop criterion all conditions exhibit an early peak at less than 10 neurons which then levels off onto a plateau with increasing number of neurons. The best net is at the intersection of little complexity, good performance and fast training. This is reached at the lowest number of neurons that coincide with the start of the plateau in performance where the necessary epochs drop. For all conditions this is reached at 20 to 40 hidden neurons.

Performance Fully training the ANN used for the real world data takes less epochs than on the simulated data in all tested conditions (Fig. 8.8). The prediction of all inclinations is equally good under all real world conditions (Fig. 8.9). The RMSE is greater than on the simulated data.

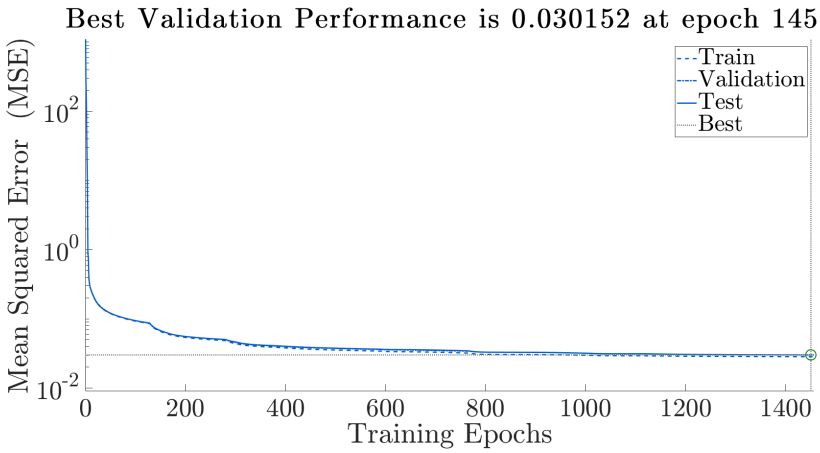

(a) varying weight

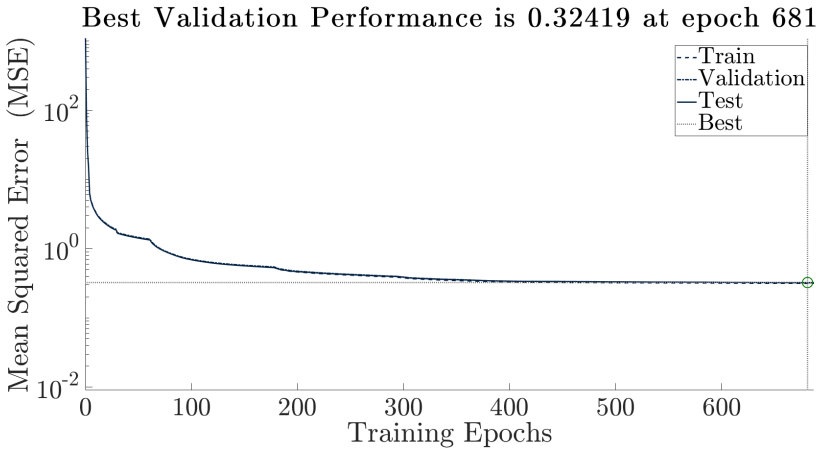

(b) varying alignment

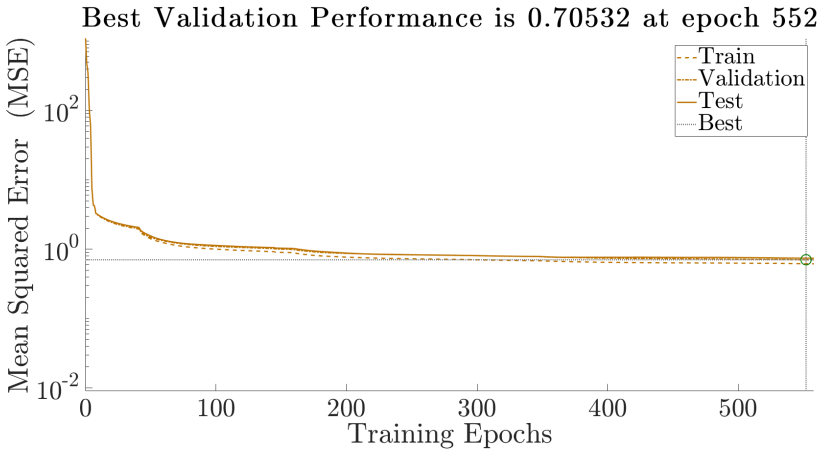

(c) varying both parameters

Figure 8.5: Training sequences for the fully trained artificial neural networks on the simulated environment for the three conditions varying weight, varying alignment and their combination. The performance as measured by the mean squared error for the data subsets training, validation and test are shown separately but run almost identically. The training stops when performance on the validation set is worse than on the training set six times in a row. The best validation performance is marked by a green circle and dotted lines.

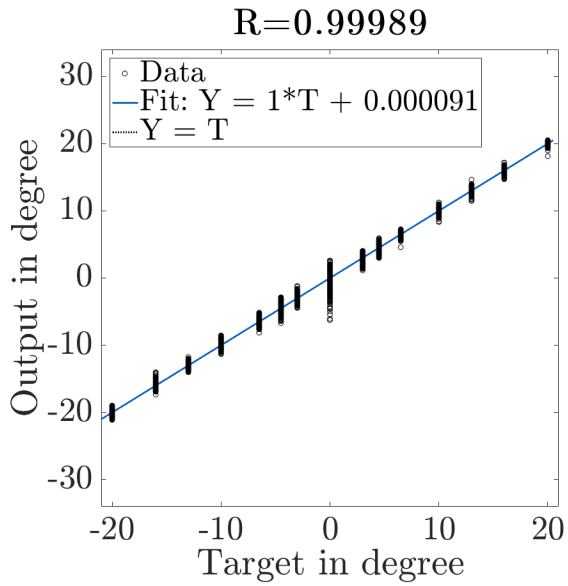

(a) varying weight

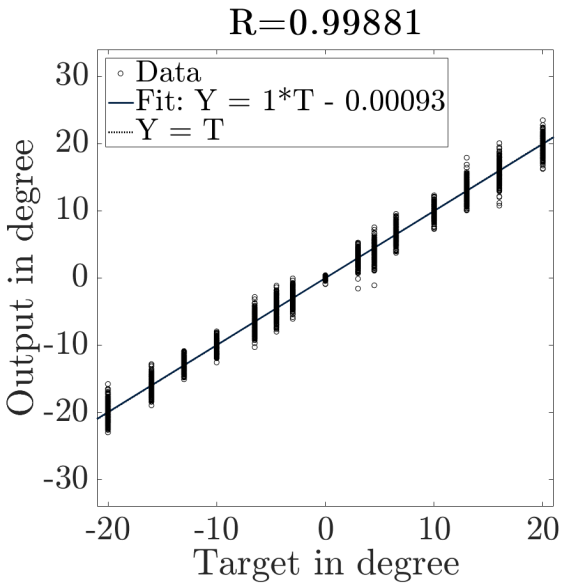

(b) varying alignment

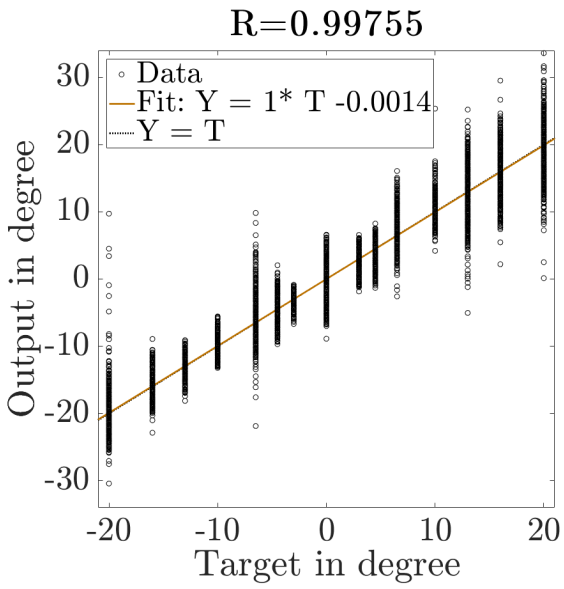

(c) varying both parameters

Figure 8.6: Response of the fully trained artificial neural networks on the simulated environment for the three conditions varying weight, varying alignment and their combination. The strength of the output neuron is interpreted as substrate inclination angle in degree marked as circles over the actual angle in degree on the x-axis. The coloured line represents the linear regression fit. The model parameters are found in the legend and the correlation coefficient R at the top of the graph. As additional interpretation aid the line of equality is also marked. Points along this line represent perfect answers of the ANN.

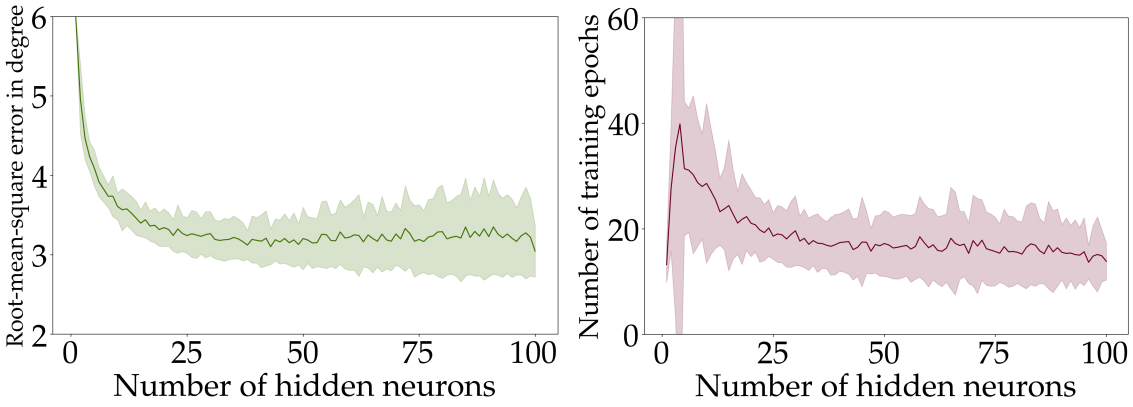

(a) all time steps

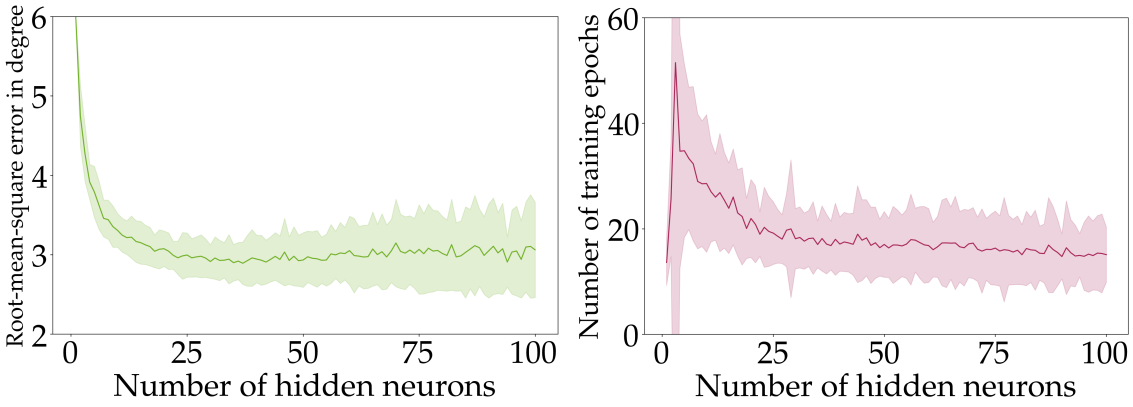

(b) all time steps with extra step cycle information

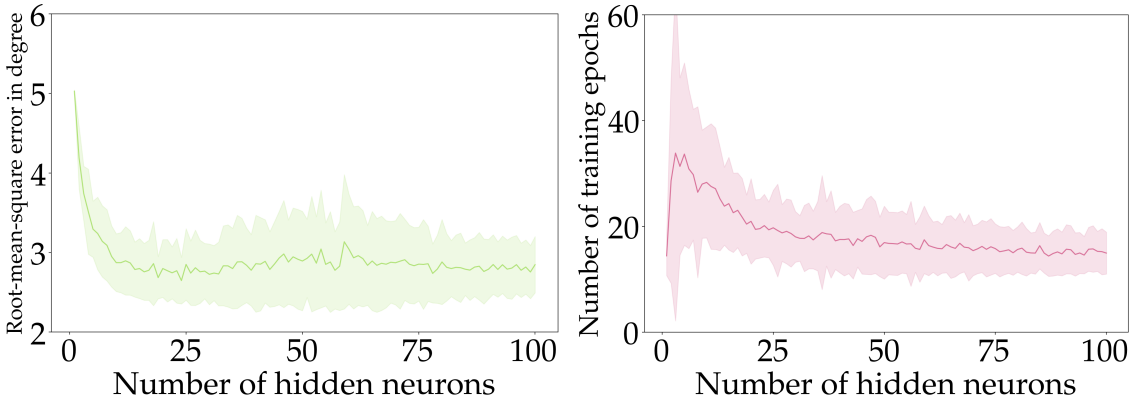

(c) time steps of double support phase

Figure 8.7: Performance as measured by root-mean-square error (RMSE) and necessary training epochs to reach stop criterion in dependence on the number of hidden neurons in the artificial neural network. For each of the three training conditions of the real world data 100 ANNs are randomly initialized and then fully trained. The lines show the means and shadows indicate the standard aberration.

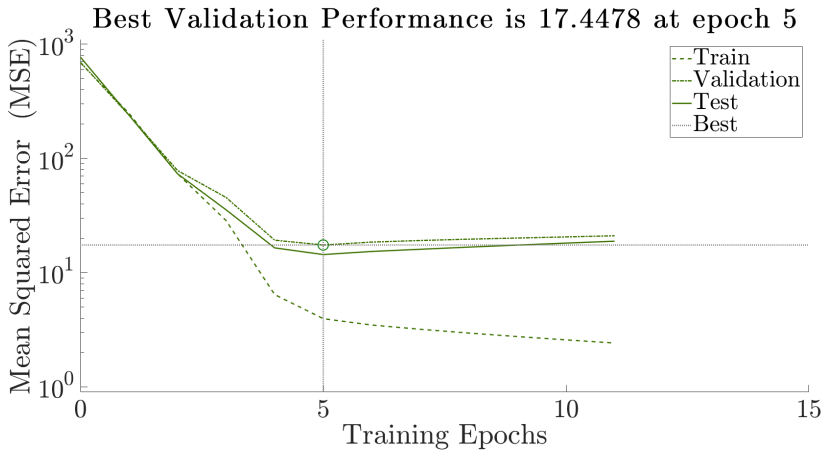

(a) all time steps

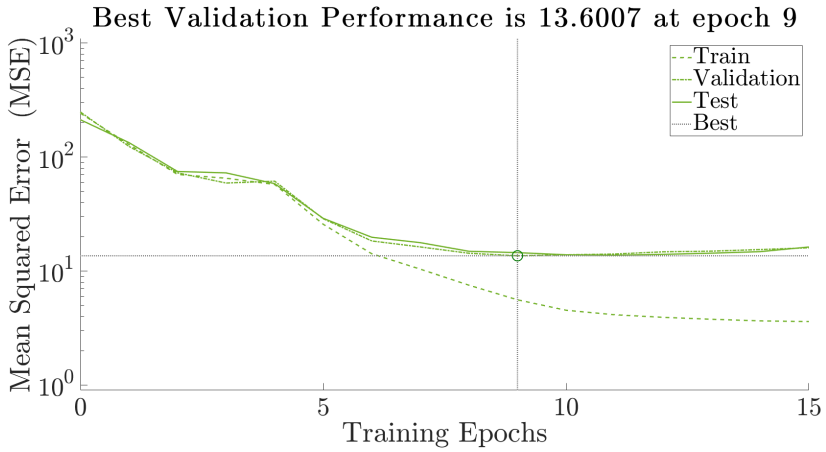

(b) all time steps with extra step cycle information

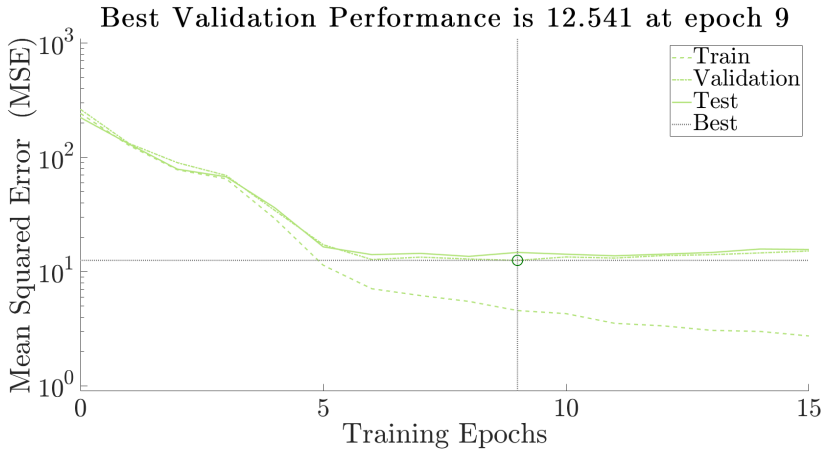

(c) time steps of double support phase

Figure 8.8: Training sequences for the fully trained artificial neural networks with optimal topology for the real world data for the three conditions. The performance as measured by the mean squared error for the data subsets training, validation and test are shown. The best validation performance is marked by a green circle and dotted lines.

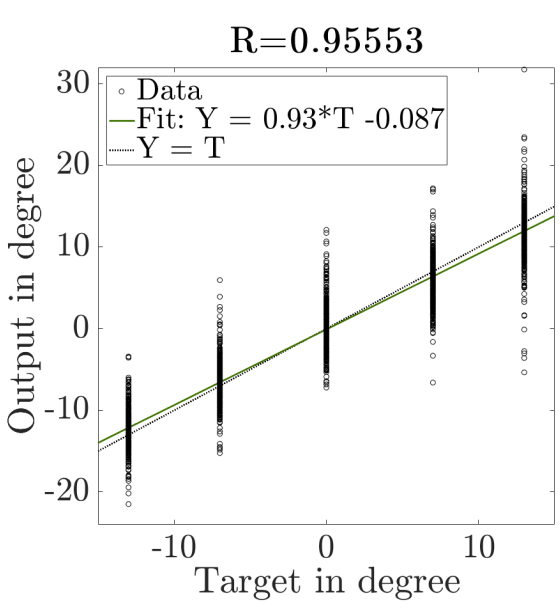

(a) all time steps

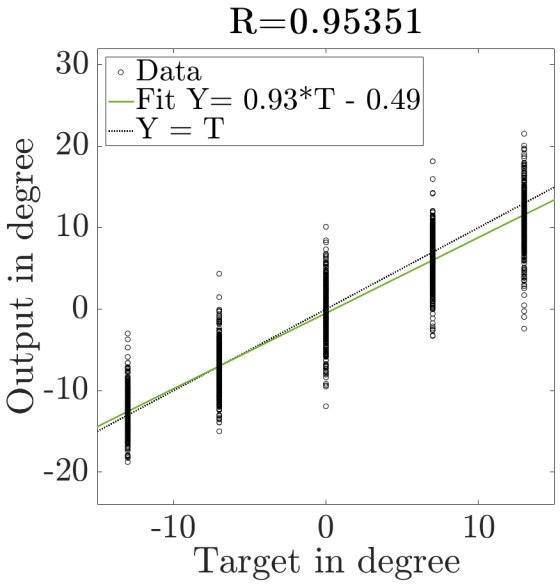

(b) all time steps with extra step cycle information

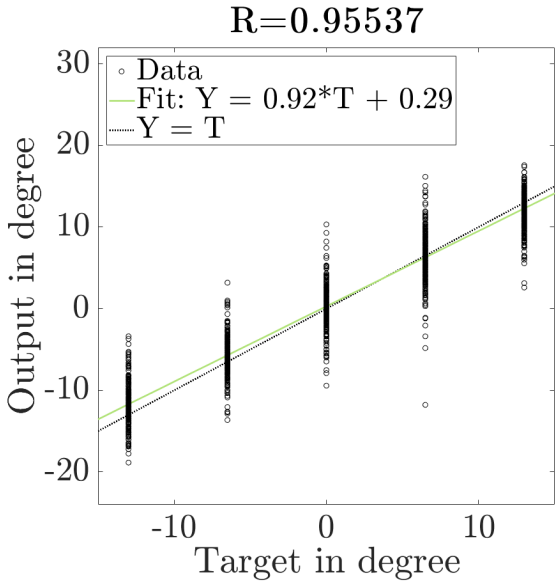

(c) time steps of double support phase

Figure 8.9: Response of the fully trained artificial neural networks with optimal topology for the real world data for the three conditions. The strength of the output neuron is interpreted as substrate inclination angle in degree marked as circles over the actual angle in degree on the x-axis. The coloured line represents the linear regression fit. The model parameters are found in the legend and the correlation coefficient R at the top of the graph. As additional interpretation aid the line of equality is also marked. Points along this line represent perfect answers of the ANN.

Table 8.1: Comparison of the best performance of all described artificial neural networks in this chapter. The performance is evaluated by the lowest root-mean-square error. The topology is characterised by the number of hidden neurons. The number of training epochs indicate the speed to fully train the ANN. For the experimental data mean and standard deviation over 100 randomly initialized ANN of the same topology is shown.

Data	condition	hidden neurons	training epochs	RMSE
Simulated	weight	87	1451	0.174°
	alignment	95	681	0.569°
	Weight & alignment	100	552	0.840°
Experimental	all time steps	100	(13.9 ± 3.5)	$(3.03 \pm 0.32)°$
	additional info step cycle	37	(17.1 ± 5.7)	$(2.88 \pm 0.27)°$
	double support phases	24	(19.4 ± 5.3)	$(2.63 \pm 0.29)°$

8.4 Conclusions

Compared to the manual analysis approach as sketched in Chapter 7 the solution using ANNs proves to be easier. Still the manual approach serves to verify the general validity of the correlation of joint torque with substrate inclination. The trained ANNs are able to differentiate the substrate inclination based on the idiothetic cues of the hexapod as the RMSE is smaller than the difference in tested inclinations. The correlation can be drawn independent of changing external influences like fluctuating weight and alignment. This allows loading and unloading of the hexapod without relaying this information to the navigation system as it is irrelevant to its function. The hexapod can also deviate at least up to 35° from a straight alignment with the incline without having to adjust the ANN.

The prominently better prediction of the 0° inclination in the condition of varying alignments stems from the symmetry of this plane. Each alignment is indistinguishable in a perfect environment. Thus this dataset is effectively presented 1 000 times the same. The worse prediction of the same inclination of 0° under the varying weight condition is more ambiguous. The solution may lie again in the symmetry of this plane. If the ANN considers the load variation between the legs on even ground small rocking movements induced by the inertia of the moving legs may confuse the prediction. On the higher inclinations this effect is less prominent as the symmetry is broken and the legs are already unevenly loaded.

The findings of the simulation are validated on the real world data. While less hidden neurons are necessary to reach the optimal performance, the RMSE is greater than on the simulated data, but still small enough to discriminate the presented inclinations. This shows that the approach is robust to noise and imperfect measuring of the joint torque as the data from the physical hexapod consists of a superposition of joint torque and proper movement. To counteract this superposition it is advantageous to only present the measurements during

the double support phase or offer additional information to the ANN about the timing. This offers interesting new hypotheses for verification on the biological model of the desert ant. For application in the real world training several ANNs of the optimal topology and finally deploying the one with the least RMSE promises best results. The resolution of this method is twice per step cycle which is sufficient, as it provides the average inclination on the length scale of half a step.

The manual approach as laid out in Chapter 7 requires establishing a costly and complex expert system. In contrast the ANN approach is faster, accounts for external disturbances and is easily translated to other hexapods. With the information provided by the ANN it is possible to build a navigation system inspired by the desert ant that relies only on the idiothetic cues of the hexapod.

Part IV

Discussion

Contents

This final part concludes the thesis. It summarises all relevant findings and sets the work in a wider scientific context.

Chapter 9 summarises the contents and key findings of the thesis.

Chapter 10 explicitly states the scientific contribution.

Chapter 11 illustrates implications on neighbouring and future research topics. This concerns conclusions that can be drawn on the biological models as well as alternatives and improvements on the frameworks established in this thesis concerning the reconstruction of the shape of the ant legs as well as the digitalization of the kinematics. Furthermore the fit into a generic biomimetic system is sketched.

CHAPTER 9

Summary

This chapter summarises the biomimetic engineering process as conducted in this thesis and presents the essential findings.

The thesis follows the established biomimetic engineering process (Fig. 9.1) in order to translate bio-inspired detection of substrate inclination to a technical application in walking robot odometry and subsequent navigation. Detection of the substrate inclination is an elementary component in earth bound three-dimensional navigation. In the bio-inspired odometer it enables the calculation of the ground projection of walked distances which is necessary for path integration. In an exploratory setting the relative position to the starting point can be determined this way and dead reckoning to return to that point is available as navigational method.

The first step in the biomimetic engineering process is the development of ideas as presented in Part I. The desert ant *Cataglyphis fortis* is chosen as model organism based on their remarkable navigational capabilities even under extreme conditions (Chapter 1). The technical applicability in mobile robot navigation is self-evident. The available research on the biological model organism is reviewed and relevant information is presented (Chapter 2). The research gap is identified as the mechanism to detect the substrate inclination based solely on idiothetic cues as basic element of a bio-inspired odometer (Chapter 3). The pivotal role of the forces on the legs is identified and hypothesized to be the crucial signal to be detected and processed. This hypothesis is then analysed and evaluated in the presented thesis on

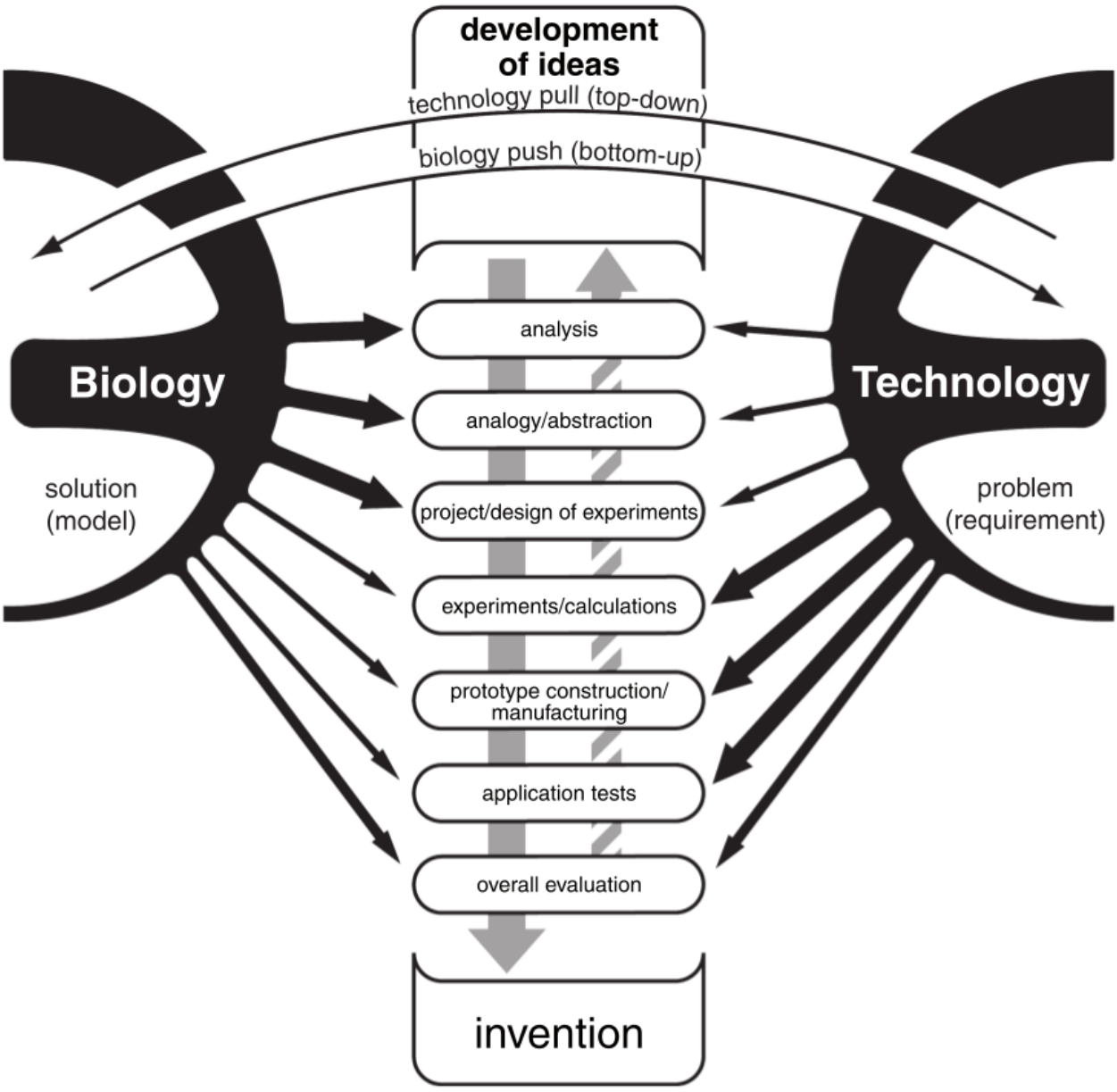

Figure 9.1: Schematic illustration of the biomimetic engineering process after [VDI-Richtlinie 6220, 2012].

the biological model organism as well as on technical platforms emulating the desired final application.

An important step to minimize research efforts later on is the thorough analysis of the biological model organism. In Part II the desert ant legs are investigated with respect to their morphology in particular location and distribution of force sensors and the kinematics.

The campaniform sensilla are the sensors able to detect deformations of the exoskeleton and thus act as measure of the forces acting on the ant leg. The location is determined to concentrate around the joints in particular the coxa-femur joint. Investigations are conducted by scanning electron microscope and validated by synchrotron X-ray microtomography (Chapter 4). Analysing these findings leads to the abstraction that recording the full flow of the force through the entire leg is not necessary but can rather be concentrated on neuralgic points of measurement. These points are identified to be close to the joints. This assumption is later on experimentally verified for the chosen technical application.

Another important aspect to analyse is the movement as it has been determined in behavioural experiments to be essential. The kinematics are extracted from high speed videos and a MATLAB and Simulink model based on average link lengths generates motion models under varying parameters (Chapter 5).

The next important step as set out in Part III is the synthesis in which suitable experiments are designed and prototypes manufactured. Further testing on the application and overall evaluation of the setup is performed. The successive experiments range from a one legged platform over the implementation on a commercially available hexapod platform complemented by testing in a simulated environment.

The one legged platform (Chapter 6) is modelled closely to the biological model to determine permissible levels of abstraction. The results of the analysis of the model organism influence the proportions of the technical leg, the chosen kinematics and the choice of sensors. Several sensors are tested and evaluated. A spring scale acts as validation while the performance of an internal torque sensor and external strain gauges are compared. Although internal and external sensors are similarly suited to determine the inclination, the internal sensors offer the added advantage that no additional components have to be installed.

The results of the one legged platform are generalized to a commercial application. On a six legged mobile robot the internal torque sensors are recorded during movement on inclined planes. The manual analysis of the data allows discrimination of the inclinations in at least 7° steps with a temporal resolution of twice per step cycle (Chapter 7). Thus providing proof of concept under real world conditions.

To facilitate the adaptation process to new situations that arise in exploratory settings the manual approach is substituted by an artificial neural network. Complemented by data acquired in a simulated environment a hyper parameter optimization of a shallow feed forward network is performed (Chapter 8). The adjusted parameter serves to determine optimal

topology to correlate input from the internal torque sensors with the corresponding current substrate inclination. Additional parameters that are varied in the simulation to study the artificial neural network's ability to generalize are weight of the robot model and its alignment on the plane as well as a combination of both factors. The results are verified on the real world data acquired on the physical hexapod platform. The artificial neural network is able to discriminate up to at least 4° on simulated datasets and 7° on real world datasets. Using the artificial neural network eliminates the need to establish expert systems in order to deal with loading and unloading processes and slanted paths.

The final Part IV of the thesis summarises all findings (Chapter 9) and sets them in a wider scientific context. The scientific contribution is laid out in detail (Chapter 10), improvement and further trails to follow in the context of neighbouring research interests are identified for the biological model organism (Section 11.1). Improvements and alternatives to the presented method are proposed (Section 11.2) and the fit into a more general generic biomimetic system of mobile walking robots is sketched to round off the thesis (Section 11.3).

CHAPTER 10

Scientific Contribution

This chapter explicitly states the scientific contribution of the presented thesis.

The biomimetic engineering process is designed to facilitate and structure the scientific discovery of technologically relevant mechanisms in living nature. This way the scientific discovery is guided in the direction of immediate technical applicability. The presented thesis follows this process and in its course touches on several aspects of diverse topics in biology and technological development.

The existing research concerning insect anatomy while extensive is in its nature limited by the sheer amount of distinct species. Known insect species number in the millions [Grimaldi et al., 2005] with over 12 000 being classified as ants [Bolton, 2003]. Thus choosing the specific species of the desert ant *Cataglyphis fortis* as model organism inevitably necessitates original research. The investigations concerning the morphology (Chapter 4) while only conducted on a limited number of specimen are conclusive with previous research of campaniform sensilla. The uniformity found in location and distribution of the sensilla strongly suggests the generalizability to the whole species.

Similarly the findings concerning the kinematics of the legs (Chapter 5) and the necessary number of degrees of freedom to model their movement are novel results. Furthermore the developed system to extract and analyse the motion allows for application in different research topics. Combined with an automated tracking approach (Section 11.2) the established

framework is in principle applicable for an even wider range of different species and novel research questions.

The development of prototypes like the one legged platform (Chapter 6) and the subsequent six legged platform (Chapter 7) and its counterpart in simulation (Chapter 8) provide novel insights on the level of abstraction that is permissible while still preserving the underlying function principle. The modular setup and the implementation in a simulated environment allows a sliding scale of closer to nature or more focussed on technical aspects. Thus findings concerning the biological model as well as the optimization of the technical application and production can be investigated on the same presented setup. In this thesis the development is focussed on the final technical application rather than the in depth exploration of bordering fundamental scientific research questions. Nevertheless the successful implementation on the robotic platform as presented in the thesis suggests that the ant may exploit a very similar mechanism and thus the technical implementation permits drawing basic conclusions on the biological model.

The established method to determine the substrate inclination through recording joint torques using an artificial neural network proves the general feasibility of this approach. It fits smugly with current research in joint torques as well as contributing to the implementation of a more general biomimetic generic autonomous platform (Section 11.3).

CHAPTER 11

Future Directions

The presented work is put in a wider scientific context. Conclusions on the biological model organism are given based on the findings on the technical platform. Improvements and extensions of the methods used are presented and finally the fit into a wider generic biomimetic system is sketched.

11.1 Biological Model Organism

In the biomimetic top-down approach conclusions are usually drawn from the biological model organism and transferred to the technical application, still it is possible to answer biological research questions through technical reconstructions of the model or subsystems or generate new hypotheses on the functionality in the abstracted technical models.

General The starting point of the presented thesis is the hypothesis that through measuring the forces on their legs desert ants *Cataglyphis fortis* are capable of determining the angle of inclination of the substrate which is necessary for successful three-dimensional navigation. All presented results in this thesis are compatible with the hypothesis. No evidence to the contrary could be determined in the investigations concerning the anatomy of the ant leg, the positions of the force sensors or the kinematics. Furthermore the successful implementation

of the assumed function principle suggests the possibility of analogous principles at work in the desert ant. To further ascertain and substantiate this hypothesis experiments on the established robotic system can be designed and tested for systematic failures of the system. Then, if in the desert ant similar failure can be provoked through behavioural experiments, the assumption is corroborated.

Redundancy Behavioural experiments in desert ants *Cataglyphis fortis* suggest that although theoretically unnecessary a redundant system is employed. The forces on each leg change enough to infer the substrate inclination from each leg individually [Wöhrl et al., 2017]. Nevertheless in experiments where single legs are amputated the ants are still able to successfully navigate home [Steck et al., 2009b]. This indicates redundancy in the detection system with the advantage that single legs may get lost to predators without incapacitating the whole ant.

For the robotic system the manual analysis (Chapter 7) reveals that some motors are better suited for the discrimination task but the left-right symmetry still allows a certain degree of redundancy. In a technical application the costs to implement a redundant system have to be weighed. In this specific application through the use of already existing internal torque sensors and the use of an effective shallow artificial neural network no additional costs are added by the redundancy aspect. Thus the full scope of redundancy and its associated benefits of robustness of the system and error minimization can be exploited.

11.2 Improvement on the Framework

In the course of the thesis some topics were touched on that did not prove to be expedient for the development of the final application and thus were not pursued further. They still provide starting points for worthwhile research sketched in the following.

11.2.1 Photogrammetry

In the endeavour to investigate the morphology of the desert ant legs photogrammetry as a low cost alternative to the synchrotron X-ray microtomography was explored. The principle relies on taking pictures of an object from different angles and reconstructing the three-dimensional object from the perspective distortions [Schenk, 2005]. In an object of only a few millimetres like the ant leg the challenges arise through the depth of field of the chosen camera and the surface of the exoskeleton that is almost featureless at the reachable resolution (Fig. C.2). The resolution of a reflex camera like the Nikon D90 (Nikon Corporation, Japan) used in the preliminary testing does not allow for detection of the campaniform sensilla. Reconstruction of two half shells can be achieved in the photogrammetry software ReCap

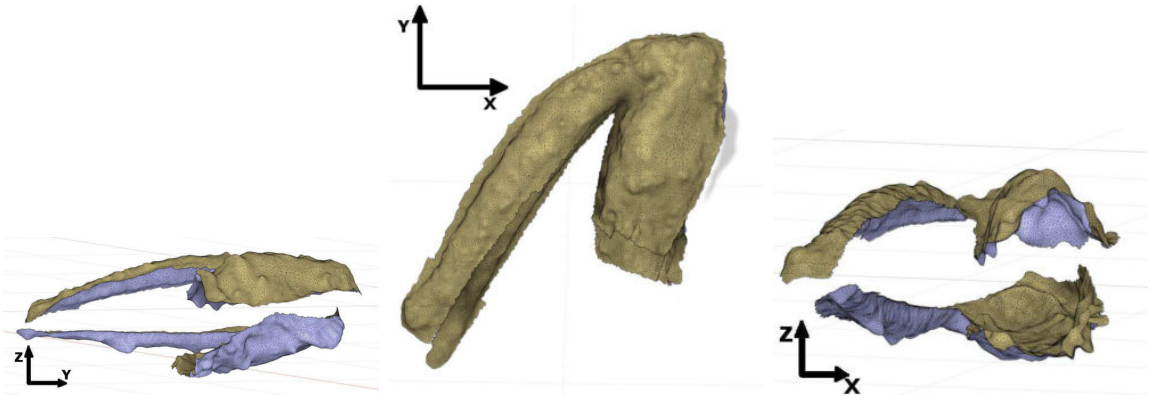

Figure 11.1: Preliminary results of a photogrammetry approach. The reconstructed shell of the desert ant femur and tibia is shown from three perpendicular perspectives. Pictures taken as part of student work [Hügel, 2018].

Photo (v1.4.2.2 Education license, Autodesk Inc., USA) (Fig. 11.1).The rough silhouette that can be achieved through this method could be suitable for designing robotic legs modelled on the ant's proportions and general shape or to get a rough estimate of properties like inertia for simulating a leg close to the biological model and compare it to more abstract designs. This way it can be determined if and what advantages an implementation resembling the biological model more closely has over the presented simplified approach and if increased production costs for customized components is offset by possibly improved performance.

11.2.2 DeepLabCut

In the presented framework to extract and analyse the kinematic data of the desert ant and generating new motion patterns (Chapter 5) a very time consuming element is the manual tracking of unmarked points in the high speed videos. In an automated approach the DeepLabCut software is an efficient method for three-dimensional markerless pose estimation based on transfer learning with deep artificial neural networks [Mathis et al., 2018, Nath et al., 2019].

The method is investigated in a proof of concept on videos of the wood ant and validated on the videos of the desert ant. Restrictions of the software allow for 33 points to be digitized per frame, so only one tripod and the body movement is chosen to include front and hind leg of the left side and middle leg of the right side. For each point the probability to appear at each coordinate of the video frame is calculated. Previous position, direction of the movement and relative position to other points are taken into account. The marker is set at the location with the highest possibility or classified as momentarily hidden if the confidence level is too low. Thus the algorithm is capable of rediscovering points even after they are momentarily obscured. The network is trained for 200 000 iterations or until the loss function stagnates. 5 % of the manually marked frames are reserved for testing the

performance which is measured as mean absolute error (MAE) of the distance in pixel (px) between the manually marked point and the point as predicted by the network.

The DeepLabCut software presents the result of its calculations with the coordinates of all digitized points for all frames and the corresponding probabilities. 4 to 10 videos and varying amounts of frames are labelled manually to discern the influence of different input videos (Tab. 11.1). The best MAE is at (2.8 ± 0.5) px.

Certain aspects of the experimental setup lead to erroneous predictions of the neural network (Fig. 11.3). The setup interferes with the results such that the prediction is disturbed by the outline of a force measuring platform used in other research on the same dataset. The mirror mounts cover parts of the ant in certain frames, this is detected by the network but not in all cases. Ants walking in the opposite direction are not identified correctly. Mirroring the videos before presenting them to the ANN successfully eliminates this effect.

The automated tracking offers substantial time savings in comparison to manual or semi-automated tracking. The use of artificial neural networks eliminates the need for explicit physical markers on the animal body which in the case of desert ants are not feasible due to their small size. The artificial neural network also supersedes the pattern matching algorithms provided in semi-automated tracking in predicting the tracking points next appearance because it takes additional information into account. The precision is comparable to manual tracking but not subject to human inattentiveness in a very repetitive task. Especially challenging situations in which the artificial neural network fails nevertheless can be checked and corrected afterwards. Also additional training to account for these situations can be taken into account later.

Automating the first step of digitizing the animal motion and combining it with the rest of the established framework opens possibilities to quickly generate new motion patterns based also on different species present in the current research like cockroaches [Bailey et al., 2001] and stick insects. For the later for example it would be possible to implement different gaits on the robotic platform HECTOR [Schneider et al., 2014] to compare their respective efficiency depending on the closeness to a natural versus and abstract technical movement.

Another possibility to use this now quickly available dataset lies in the research interest to model insect kinematics close to nature [Guo et al., 2014a].

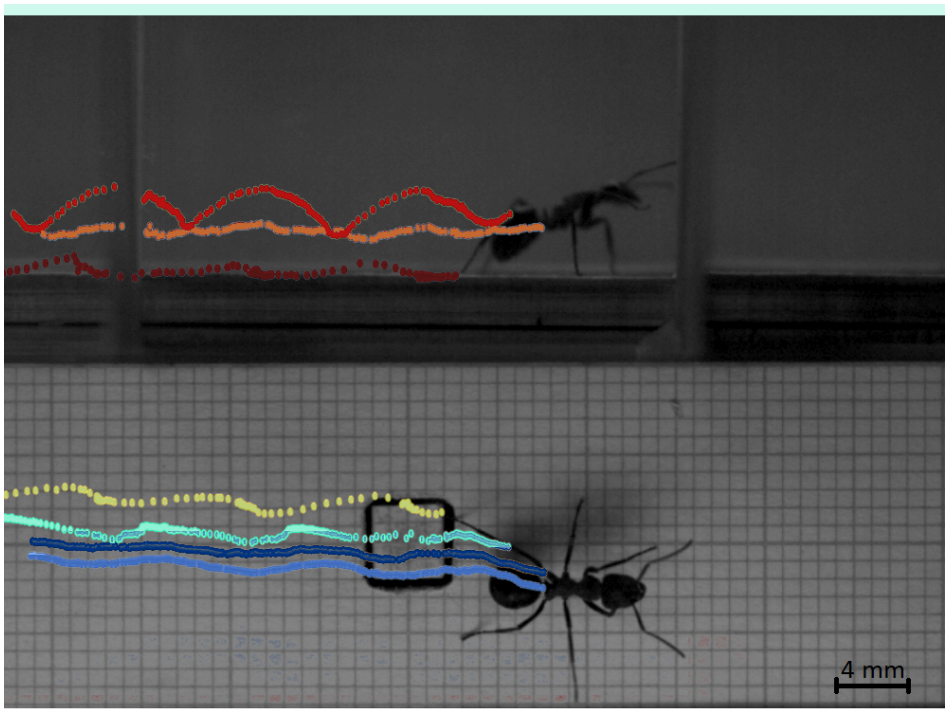

(a) Example of the identified points on the left hind leg. Picture colour corrected.

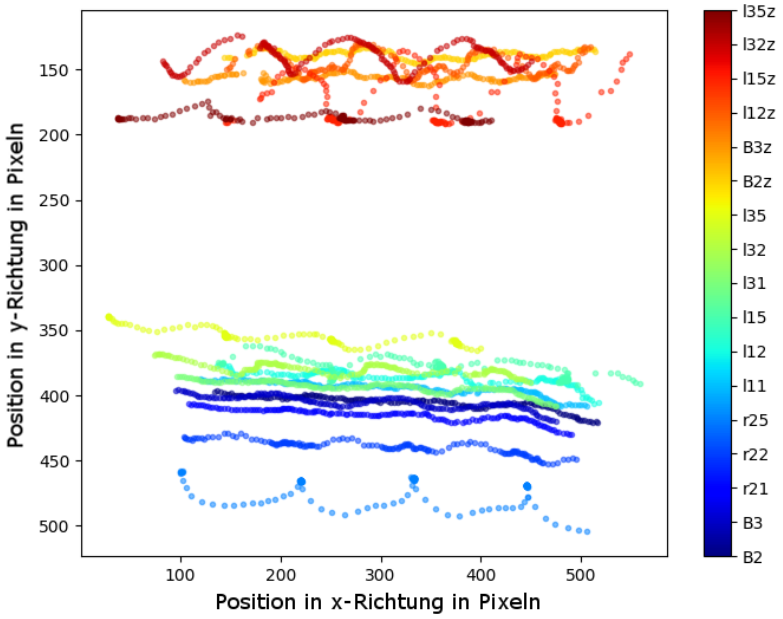

(b) Example of the identified points on all legs of one tripod without video overlay.

Figure 11.2: Exemplary results of the automated digitalization of ant leg movement by an artificial neural network. Pictures taken as part of student work [Martin, 2019], slight modifications.

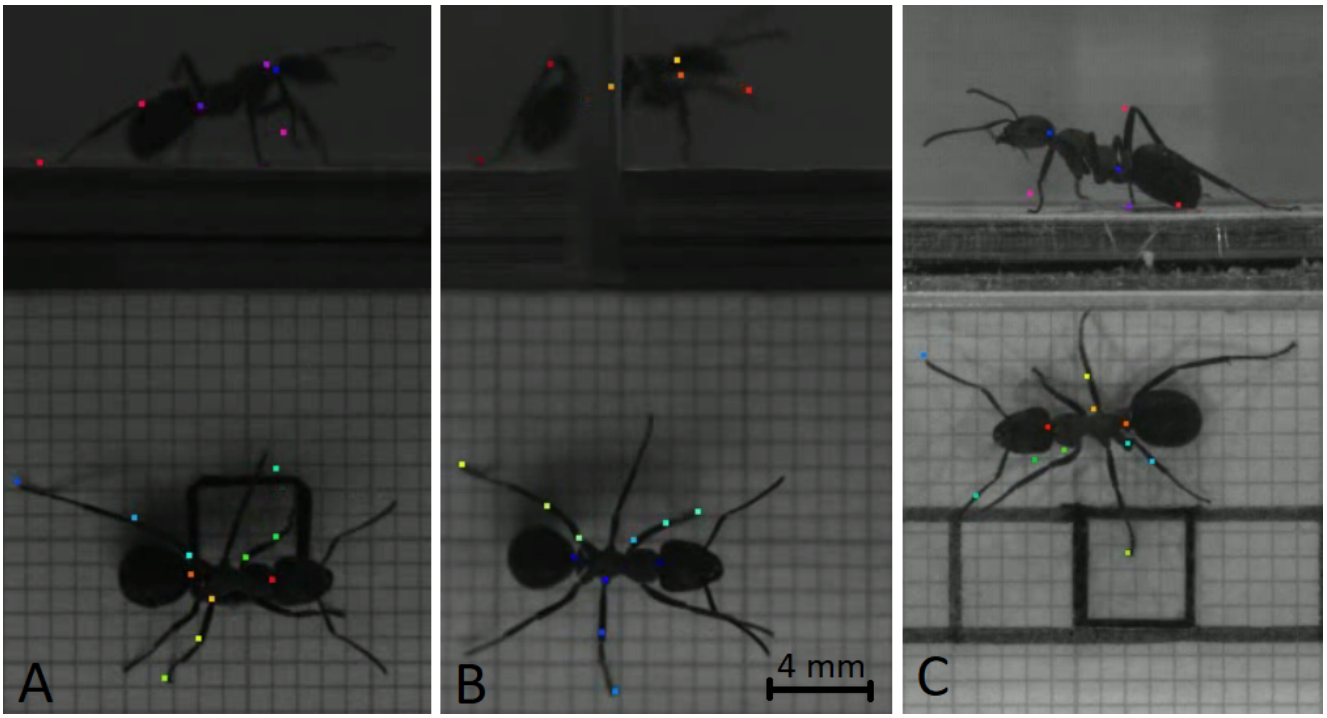

Figure 11.3: Exemplary errors in the prediction of the neural network. (A) The edge of the force measuring platform impedes the discrimination of the leg versus the substrate. (B) The mirror mounts temporarily hides the ant which is not always identified correctly and points in this region are erroneously marked. (C) Due to a rough symmetry of the ant body, ants walking in the opposite direction to the originally trained videos are not identified correctly. Pictures taken as part of student work [Martin, 2019].

Table 11.1: Overview of the performance of the automated digitalization of the movement of the ant legs through DeepLabCut depending on the number of videos used and number of manually labelled frames used in training. The performance is evaluated by the mean absolute error of the position in pixels of the manually labelled points and the points predicted by the network.

									mean
trainings ideos	4	5	5	5	5	6	6	10	5.8 ± 1.7
training frames	146	173	239	263	240	308	279	357	250 ± 64
MAE in px	3.2	3.7	2.6	2.2	2.4	2.4	2.6	3.4	2.8 ± 0.5

11.3 Generic Biomimetic System

The long term comprehensive goal in this biomimetic research is the establishment of a generic biomimetic system that incorporates various bio-inspired components and is capable of autonomous locomotion and operations.

The international bionic award of 2020 was awarded to an autonomous navigating robot based on the desert ant [Berends, 2020]. A sun compass and path integration based on optical flow is implemented and shown to be successful in homing in outdoor environments [Dupeyroux et al., 2019]. To improve the path integration a rudimentary step counter is implemented. This step counter can be significantly improved by the method presented in this thesis. Thus a more refined system can be implemented through the combination of the research results.

Research on the desert ant's path integration has been successfully implemented on a hexapod platform in two dimensions in simulation and experiment [Xiong and Manoonpong, 2018]. The combination with the detection of substrate inclination offers an extension and completion in the third dimension.

The same research group also investigates joint torques. Though their goal is to detect the material of the substrate rather than the inclination [Xiong et al., 2014]. A combination of both systems could be a powerful indicator for terrain condition and structure based on easily accessible sensor readings. This can prove valuable in exploratory settings in unstructured terrain.

Another possibility to employ the system is to use it as a redundant system to secure visual systems used for navigation [Homberger et al., 2016, Bjelonic et al., 2018]. An example would be the weaver hexapod that is developed to visually navigate through unstructured terrain.

As demonstrated by these examples, the system to detect substrate inclination provides a fundamental and multimodal contribution to the improvement of existing robotic systems. A future generic biomimetic system capable of autonomous locomotion and behaviour will also greatly benefit from the implementation of the proposed method.

APPENDIX A

Technical Drawings

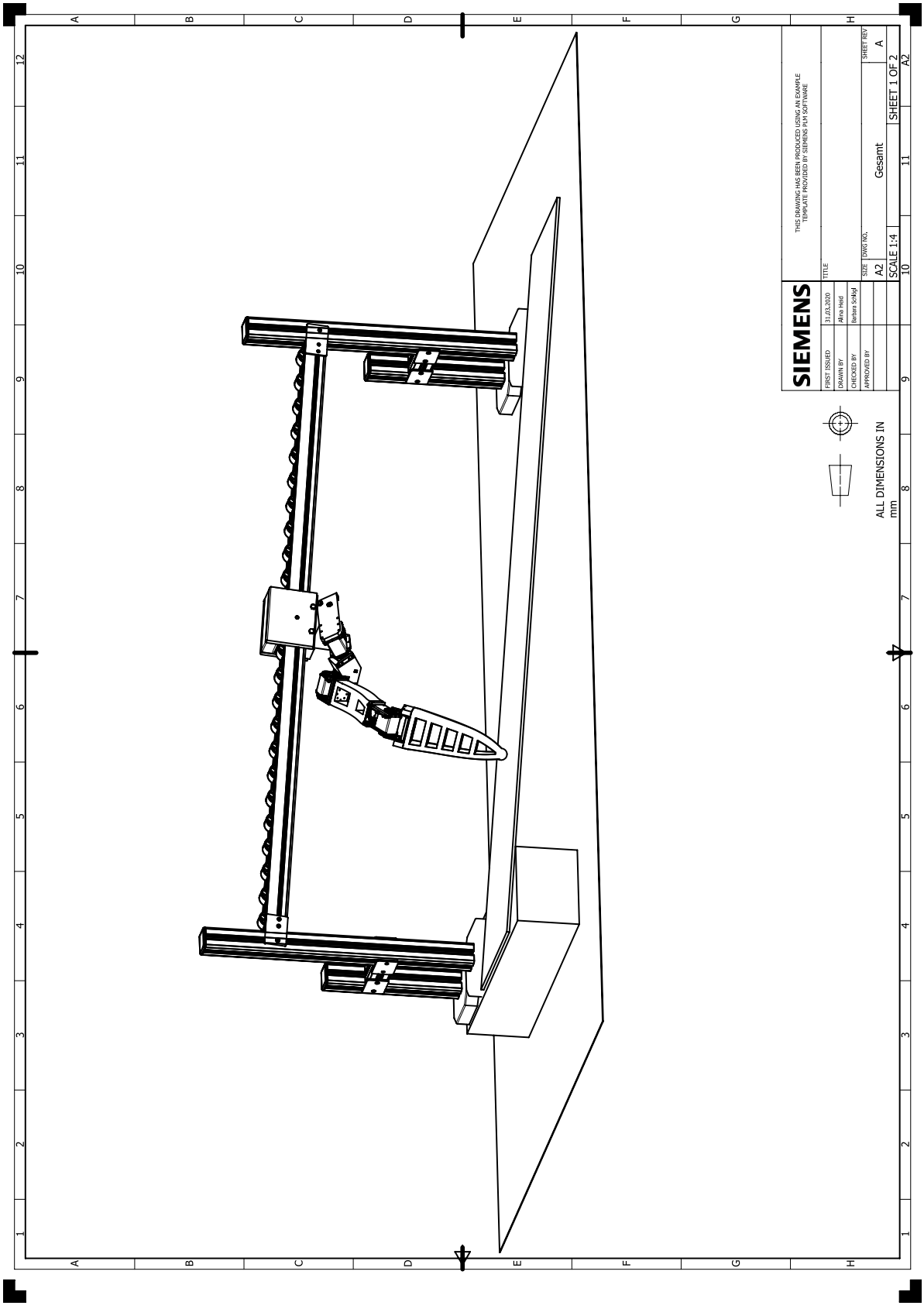

Figure A.1: Technical drawing of the one legged setup.

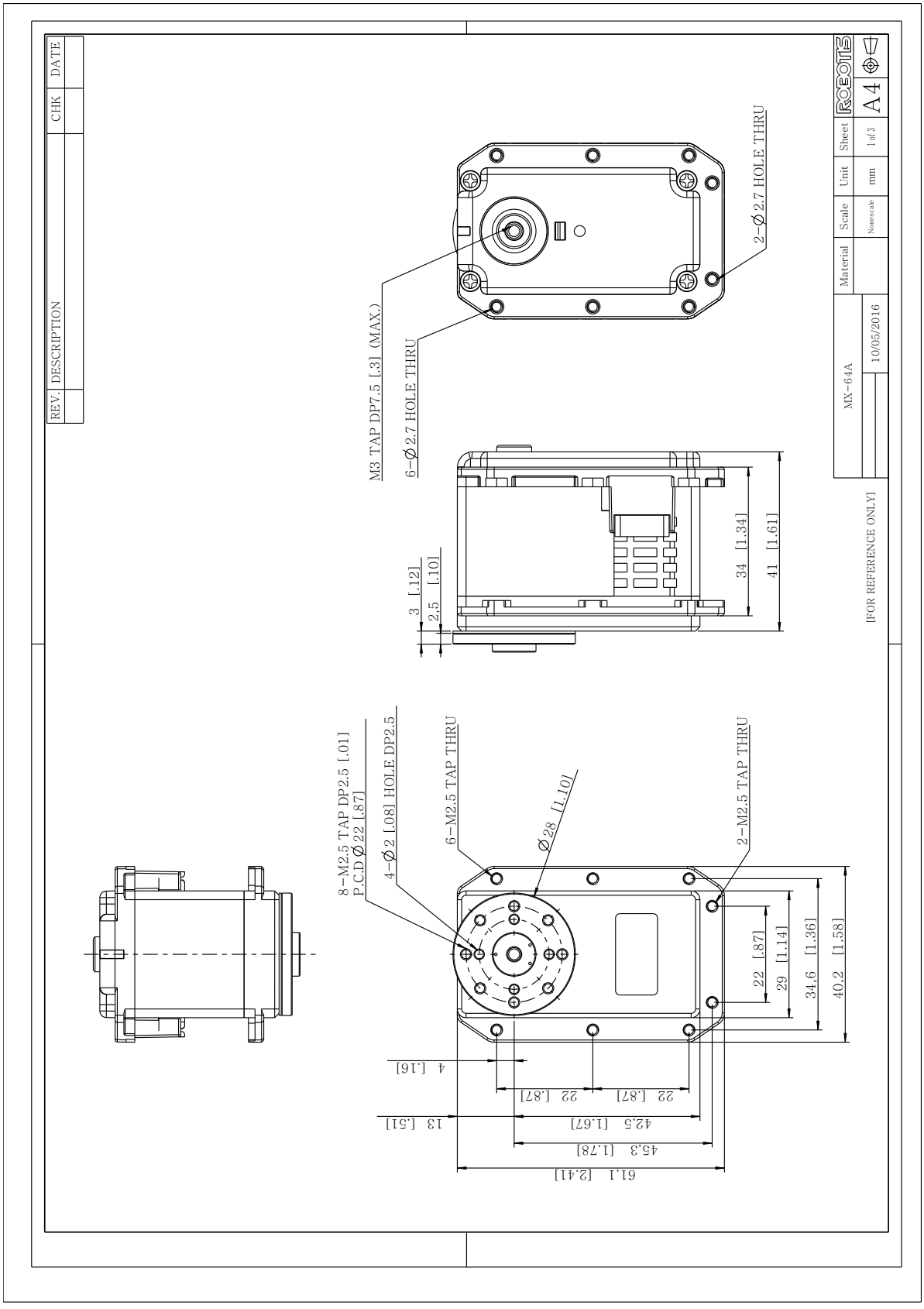

Figure A.2: Technical drawing of dynamixel motors MX-64A.

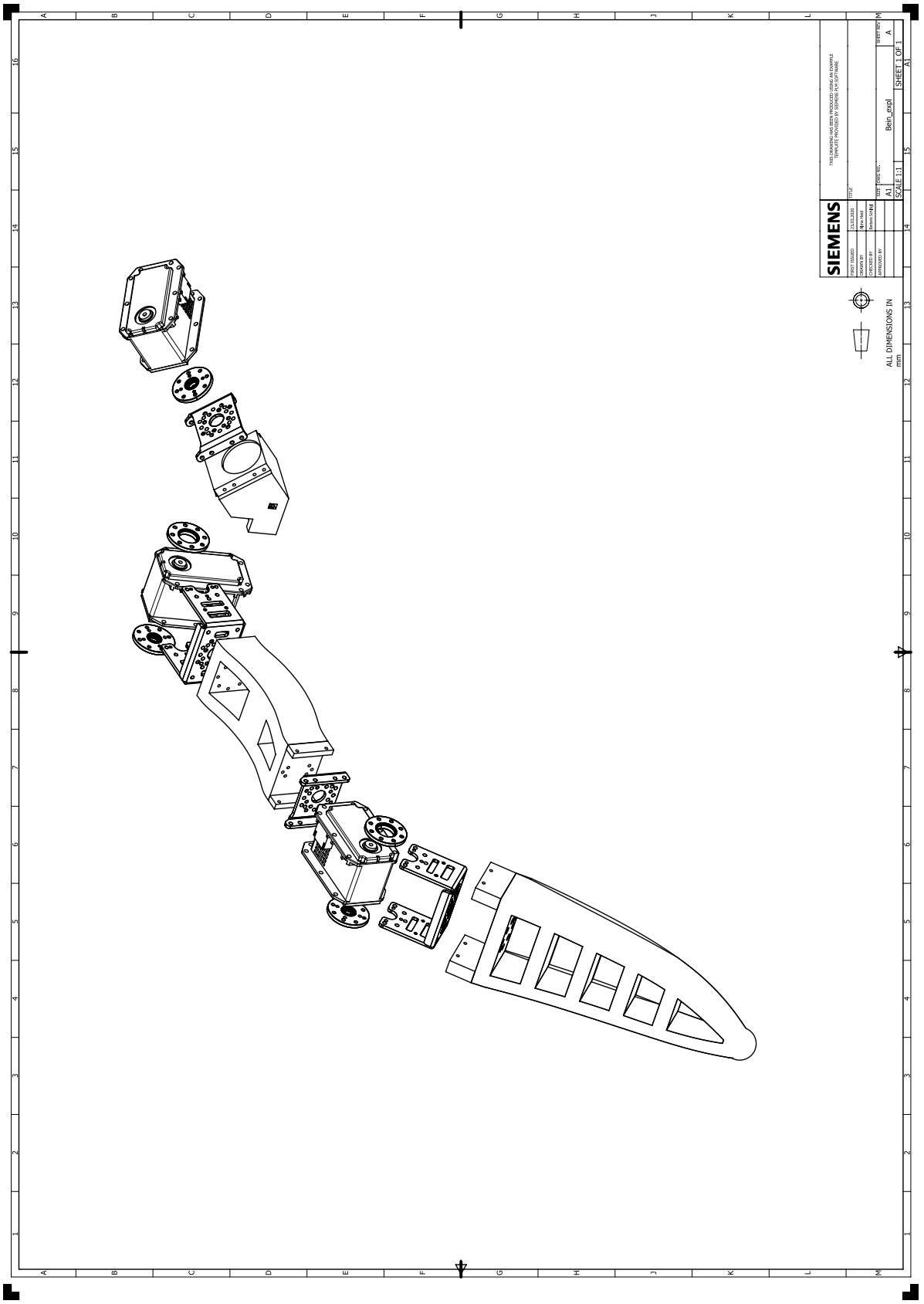

Figure A.3: Technical drawing of the one legged platform. Exploded view.

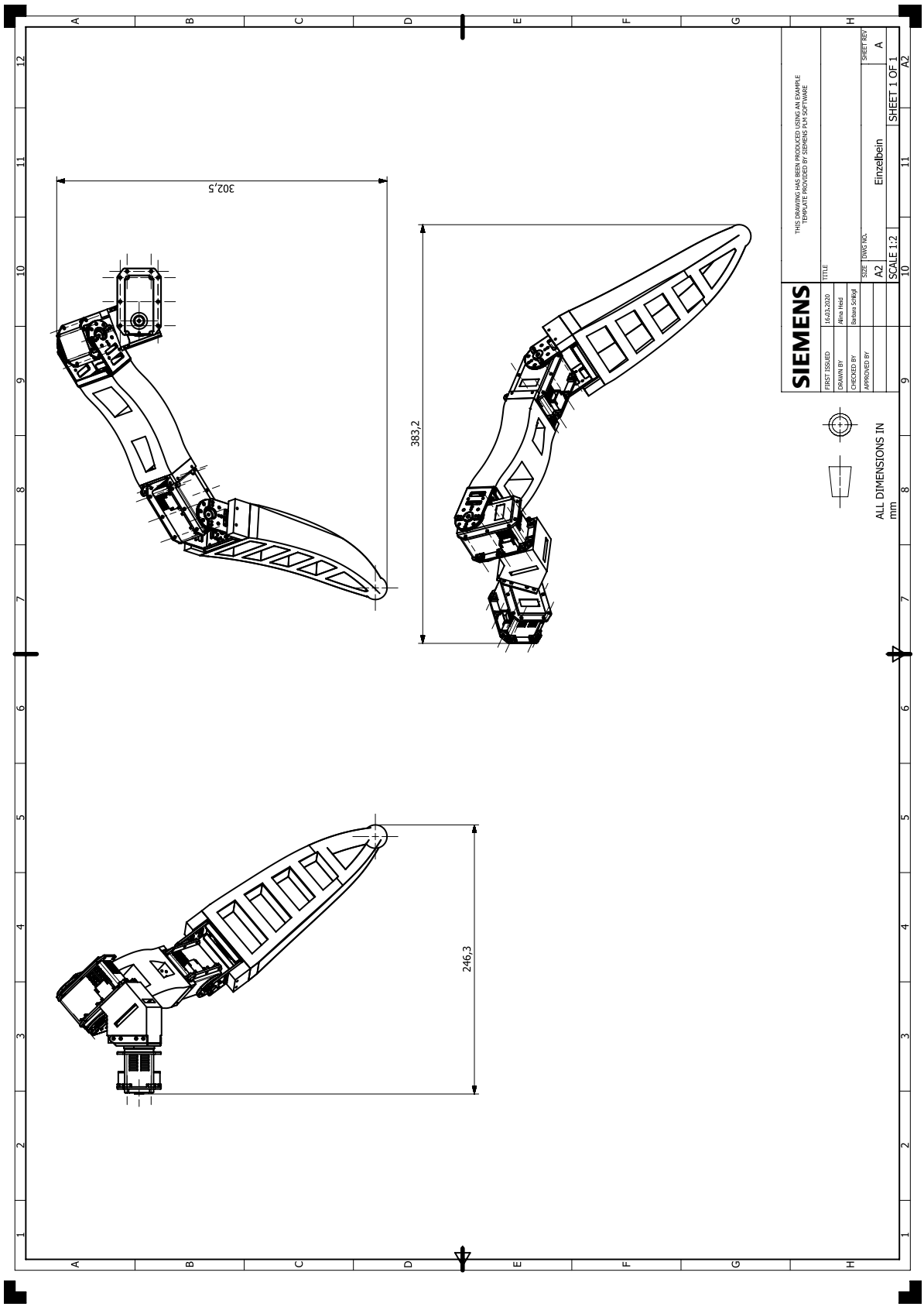

Figure A.4: Technical drawing of the one legged platform illustrated from three perspectives.

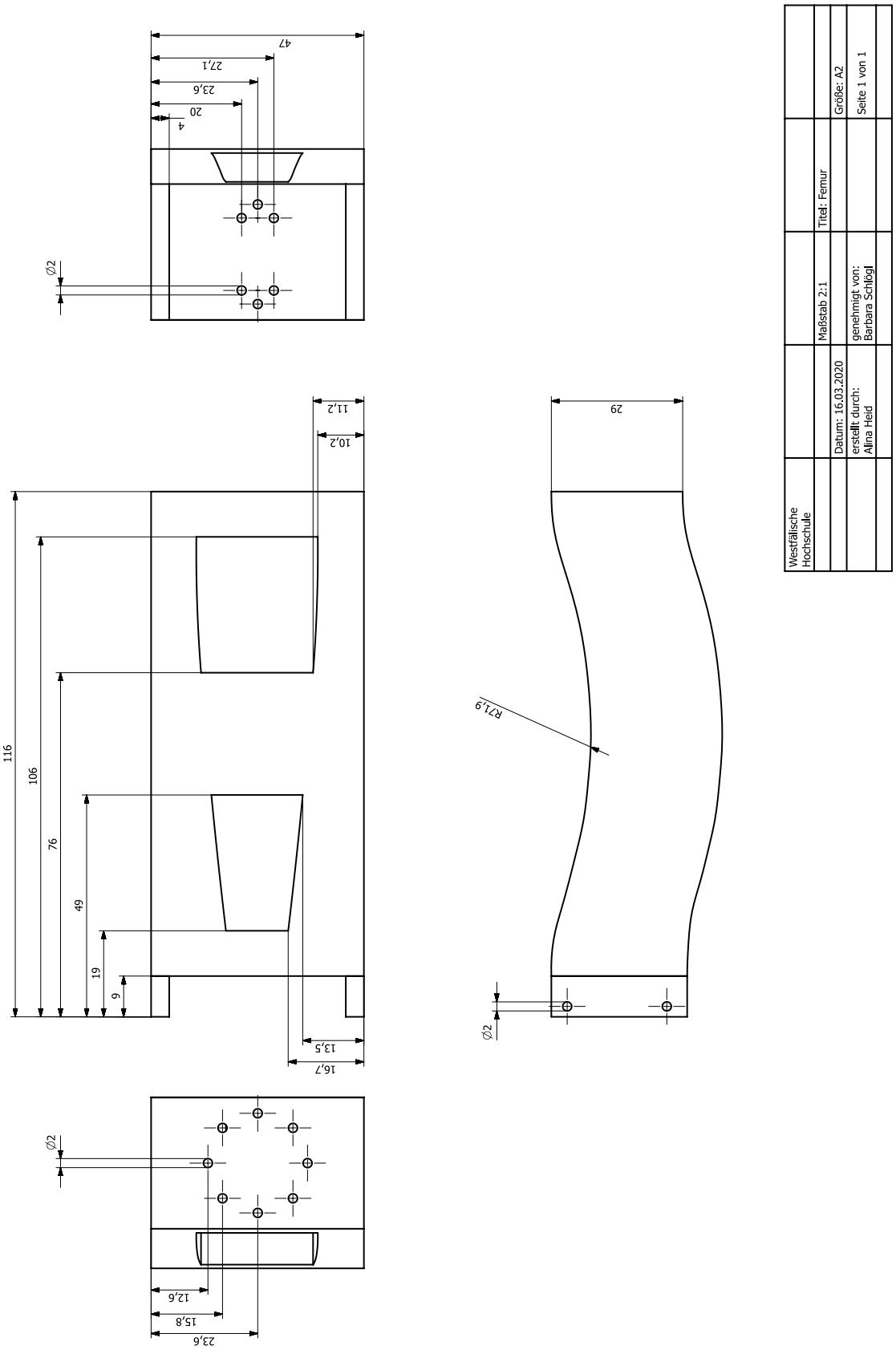

Figure A.5: Technical drawing of the femur of the one legged platform.

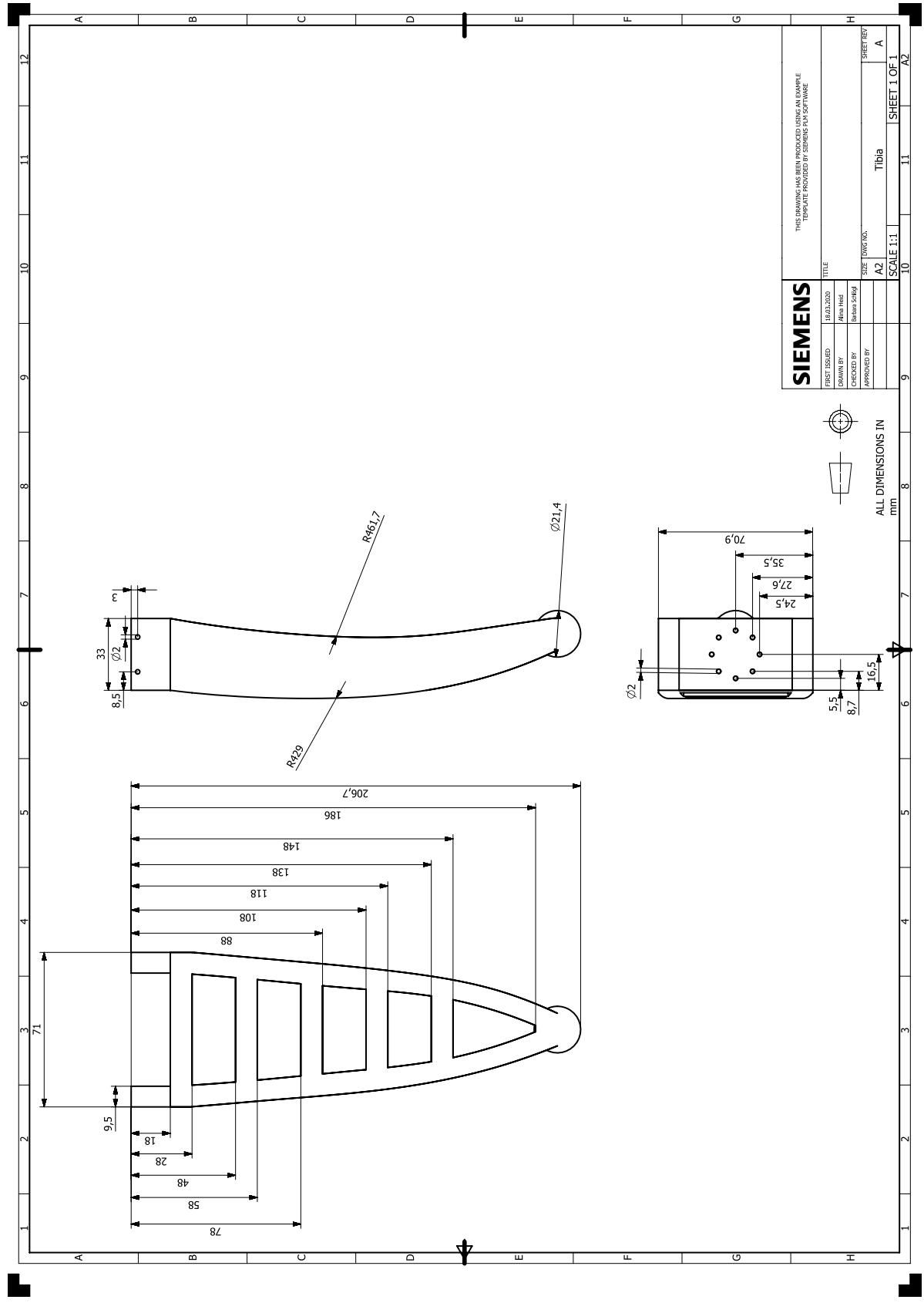

Figure A.6: Technical drawing of the tibia of the one legged platform.

APPENDIX B

Supplementary Statistics

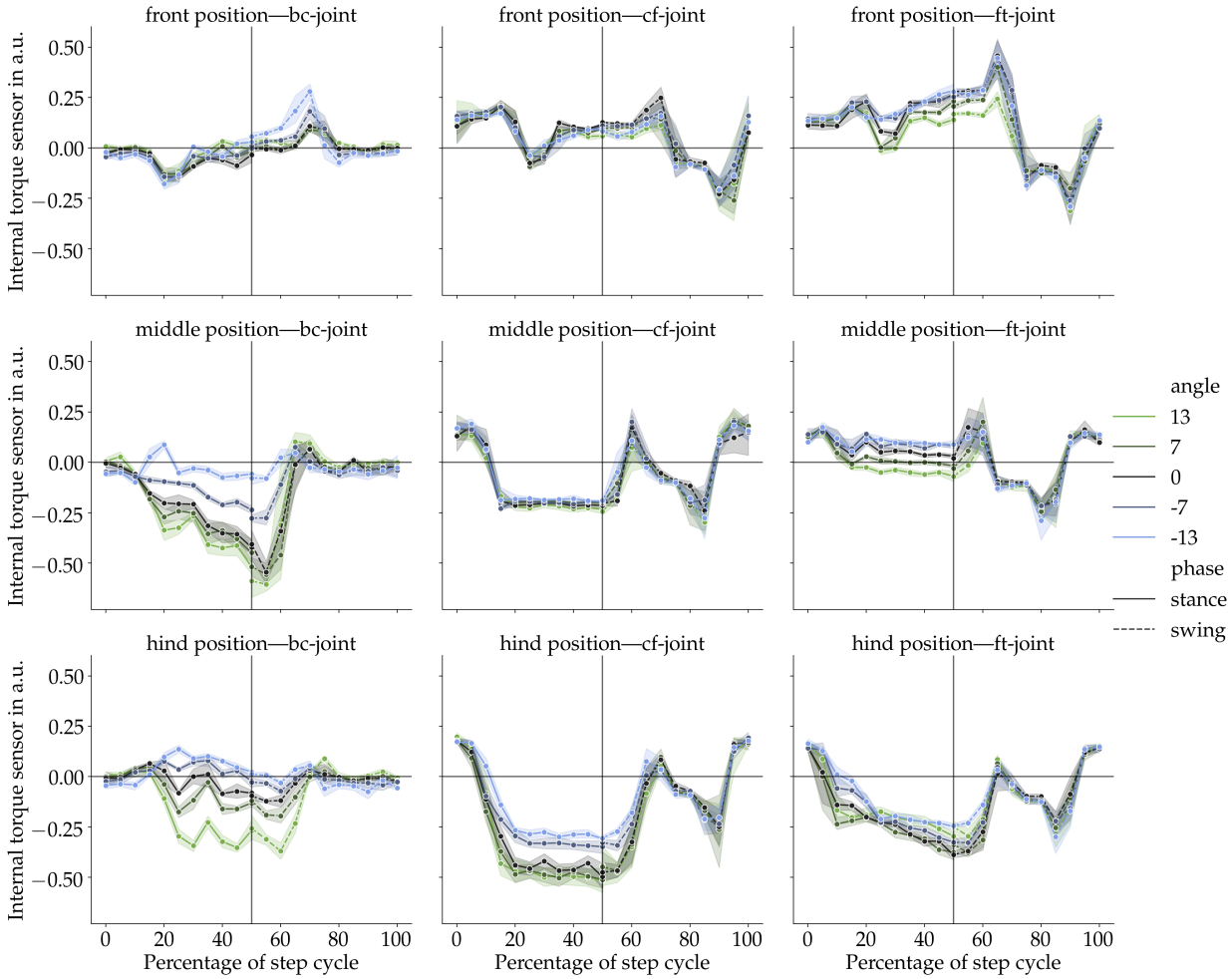

Figure B.1: The internal torque sensor is read in arbitrary units. The course over a whole step cycle is recorded and averaged over all steps and all runs. The shadows indicate the 95 % confidence interval. The results are shown from top to bottom for the left front, middle and hind legs. From left to right the joints are further from the body. Colours indicate the inclination of the ramp. The shift from stance to swing phase is marked with a vertical line. The results for the right leg can be found in (Fig. 7.6).

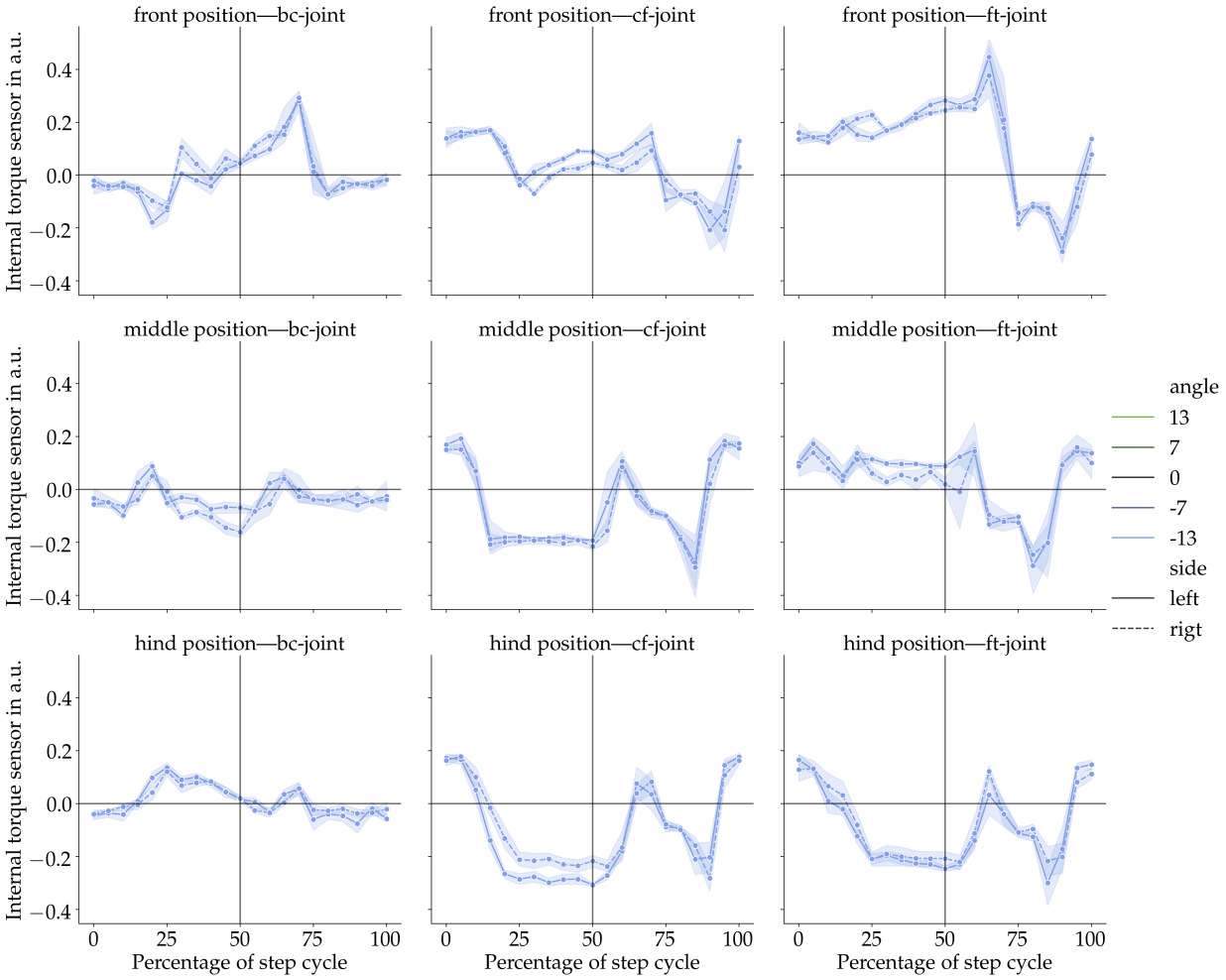

(a) Substrate inclination: $-13°$

Figure B.2: Comparison of the measured internal torque of left and right leg for each inclination. Visual estimation: one-third of the averages are further apart than the 95 % confidence interval and thus significantly distinct and pooling of left and right leg is thus inadmissible. The difference is more pronounced on steeper inclined substrates.

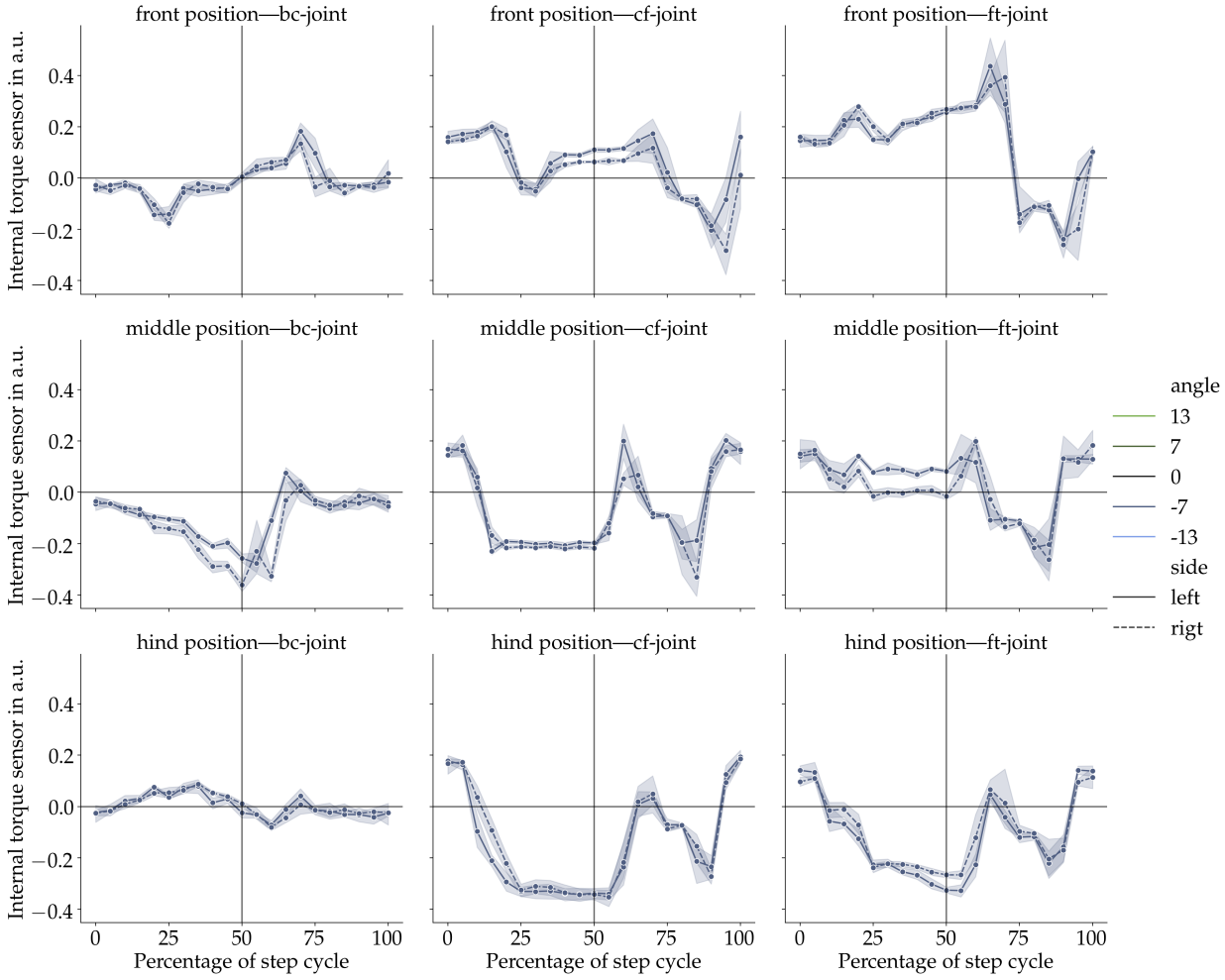

(b) Substrate inclination: $-7°$

Figure B.2: Comparison of the measured internal torque of left and right leg for each inclination. (cont.)

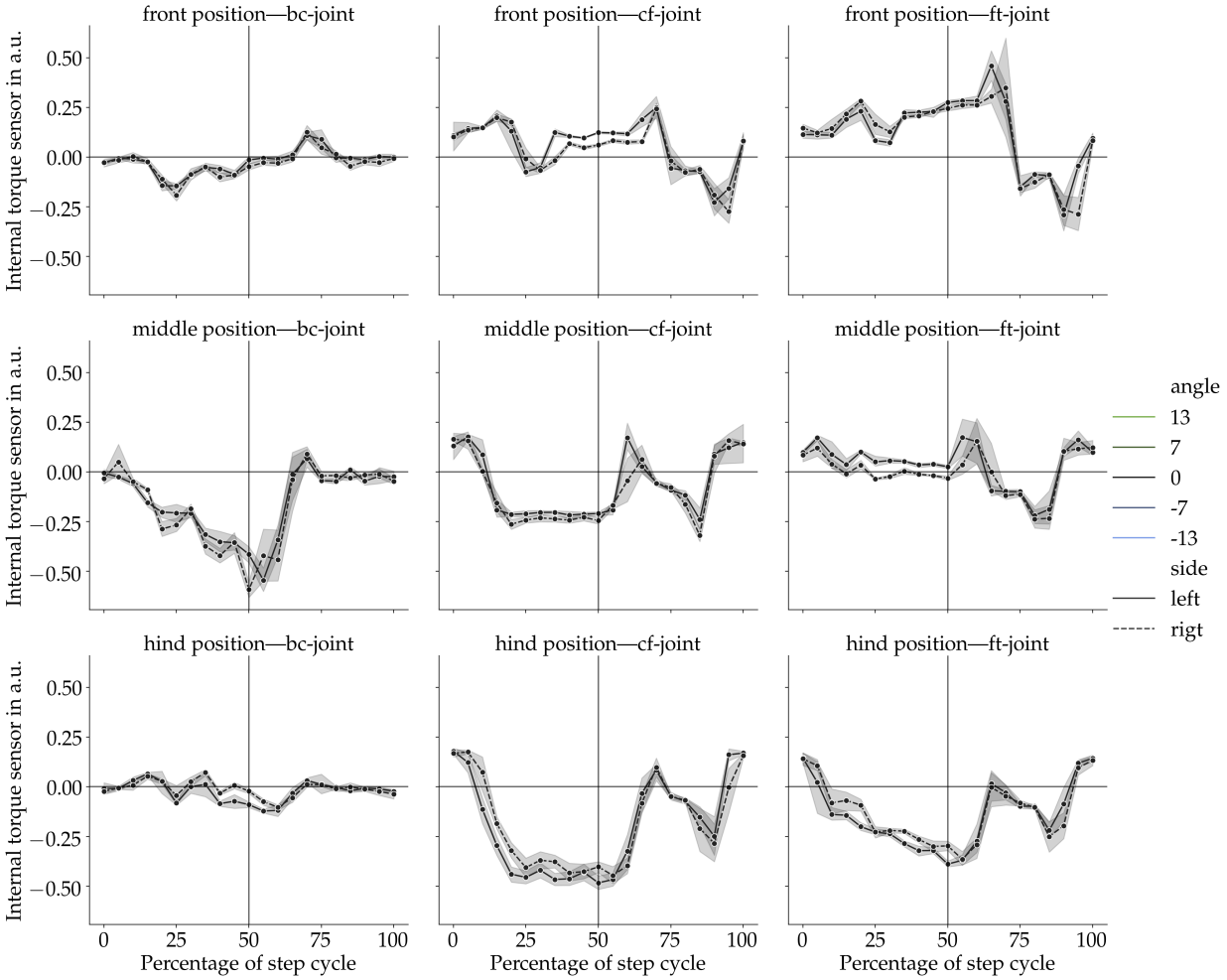

(c) Substrate inclination: 0°

Figure B.2: Comparison of the measured internal torque of left and right leg for each inclination. (cont.)

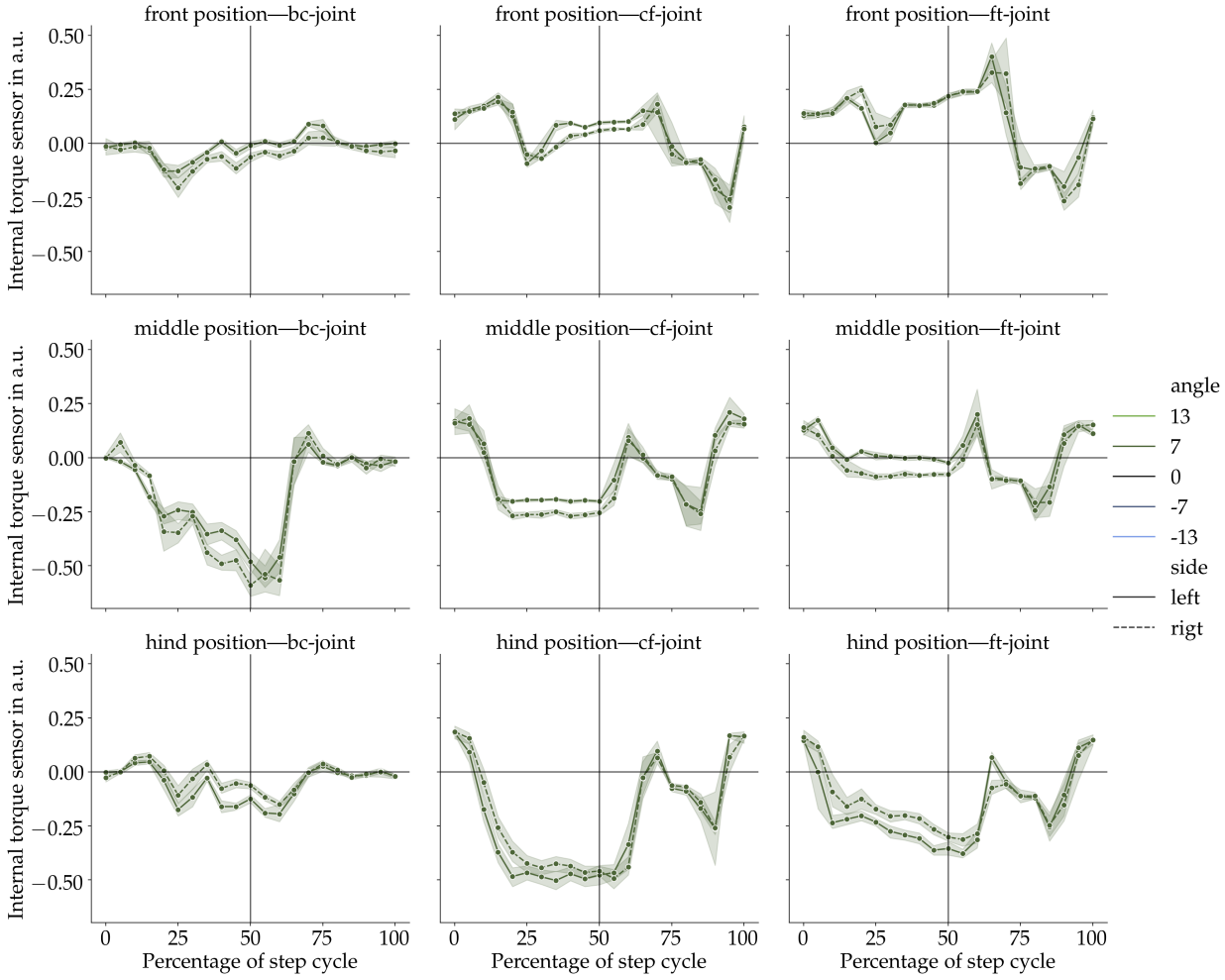

(d) Substrate inclination: 7°

Figure B.2: Comparison of the measured internal torque of left and right leg for each inclination. (cont.)

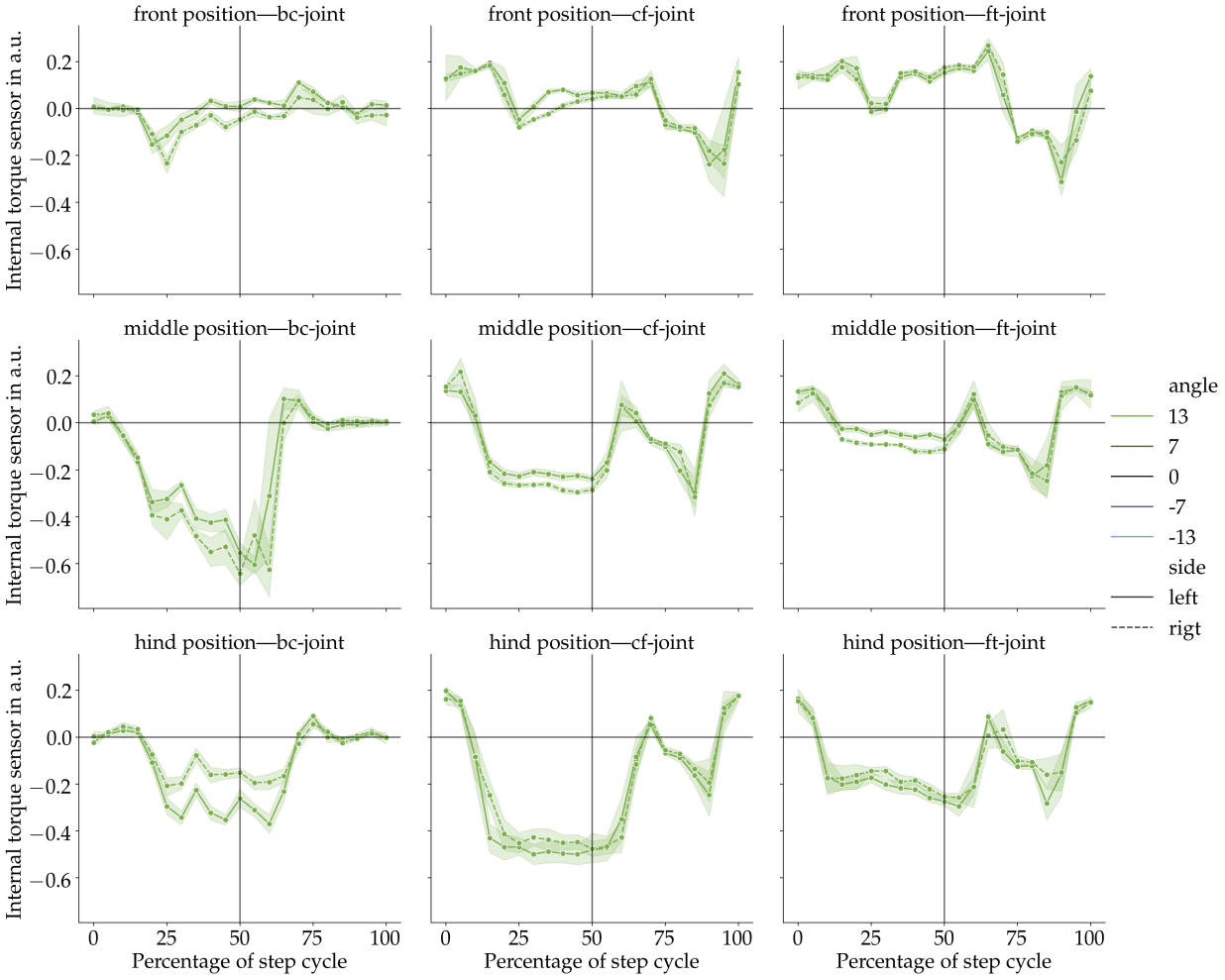

(e) Substrate inclination: 13°

Figure B.2: Comparison of the measured internal torque of left and right leg for each inclination. (cont.)

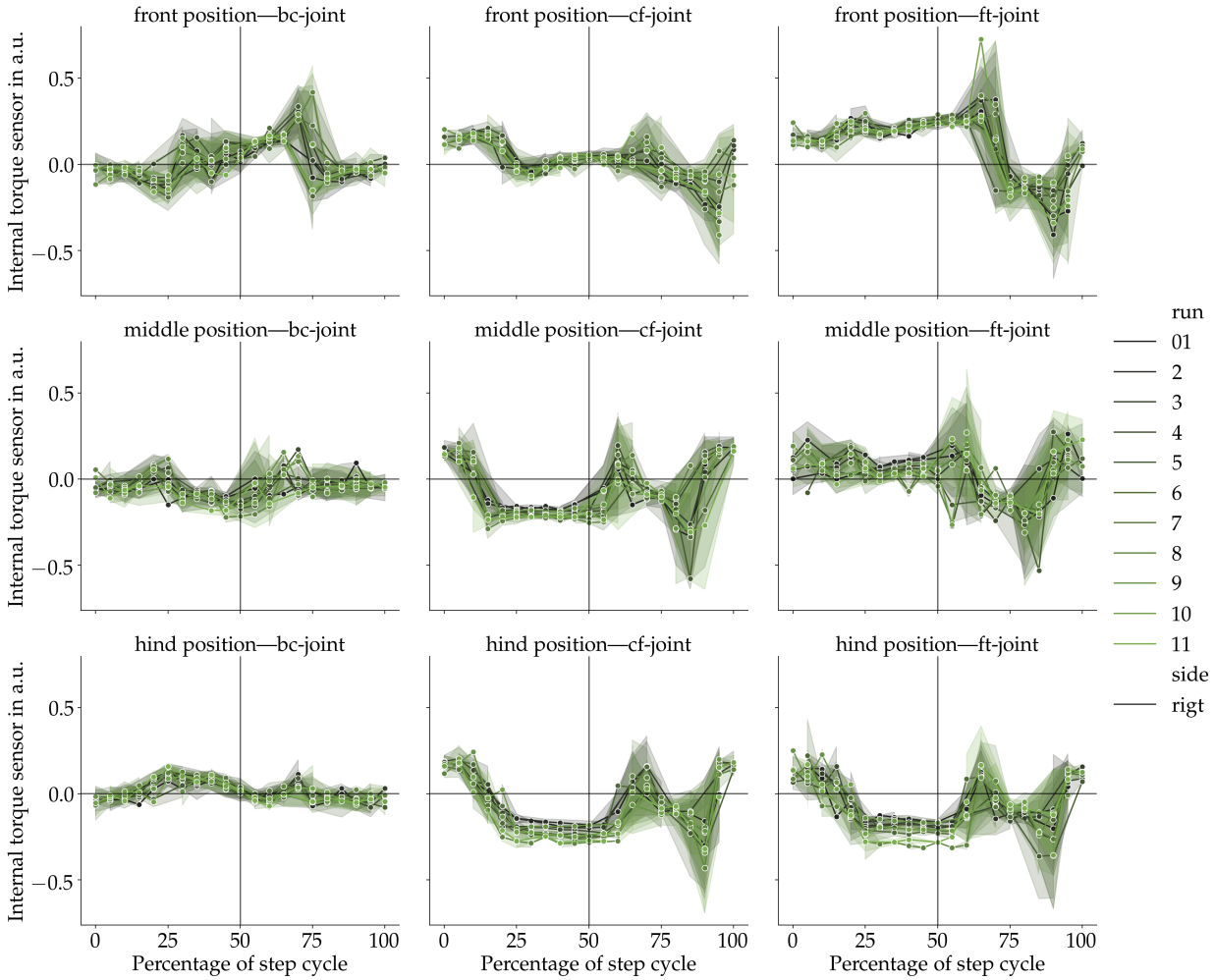

(a) Substrate inclination: −13°

Figure B.3: Comparison of intra-run and inter-run variability in torque measurements for all inclinations. Lines represent the mean over all steps for each run. The shadow indicates the standard deviation. Visual estimation: over 90 % of the torques measured at a certain point in the step cycle are within the range of one standard deviation. Thus, the intra- and inter-run variability is similar and in the further evaluations the separate runs are treated as one long continous run.

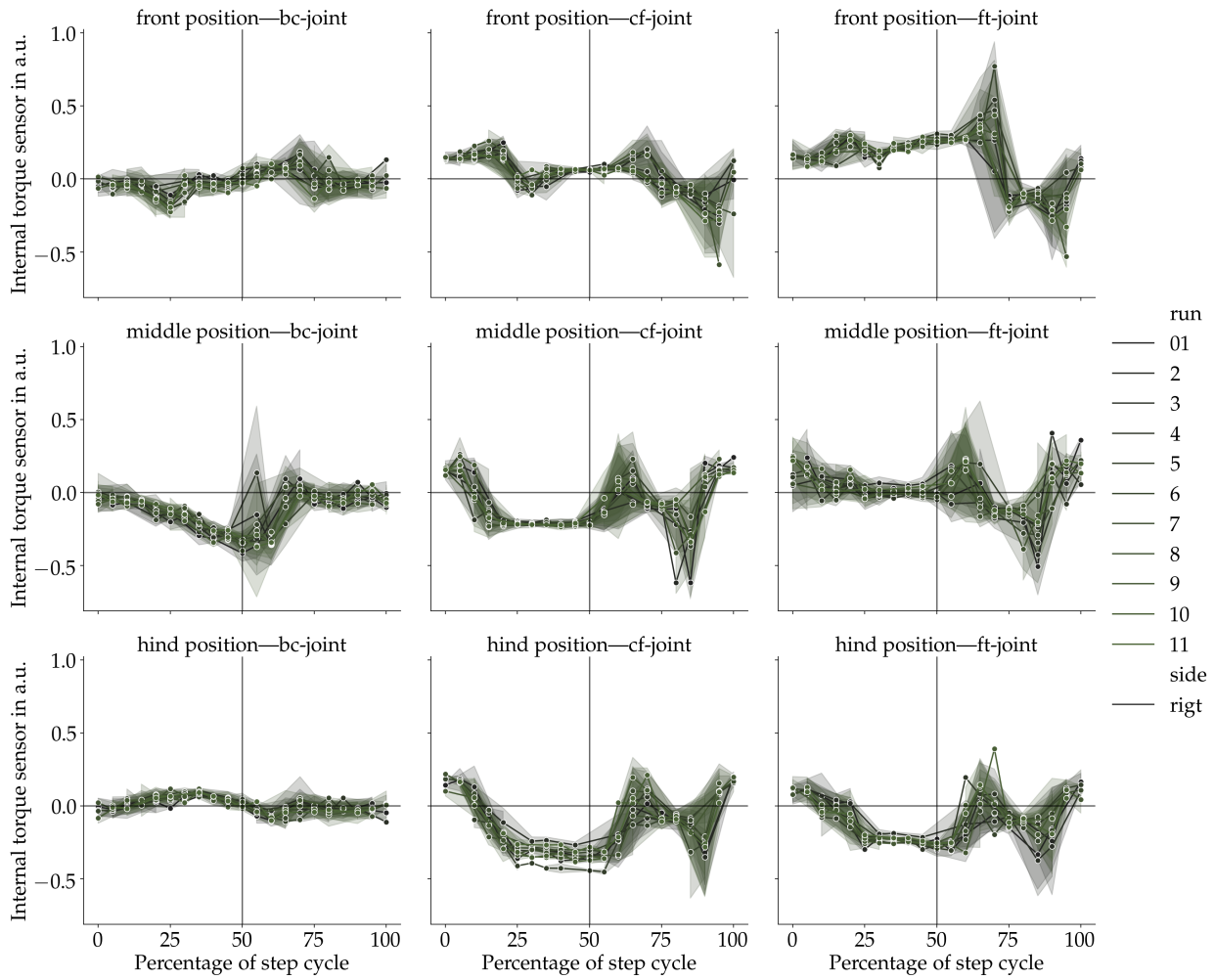

(b) Substrate inclination: $-7°$

Figure B.3: Comparison of intra-run and inter-run variability in torque measurements for all inclinations. (cont.)

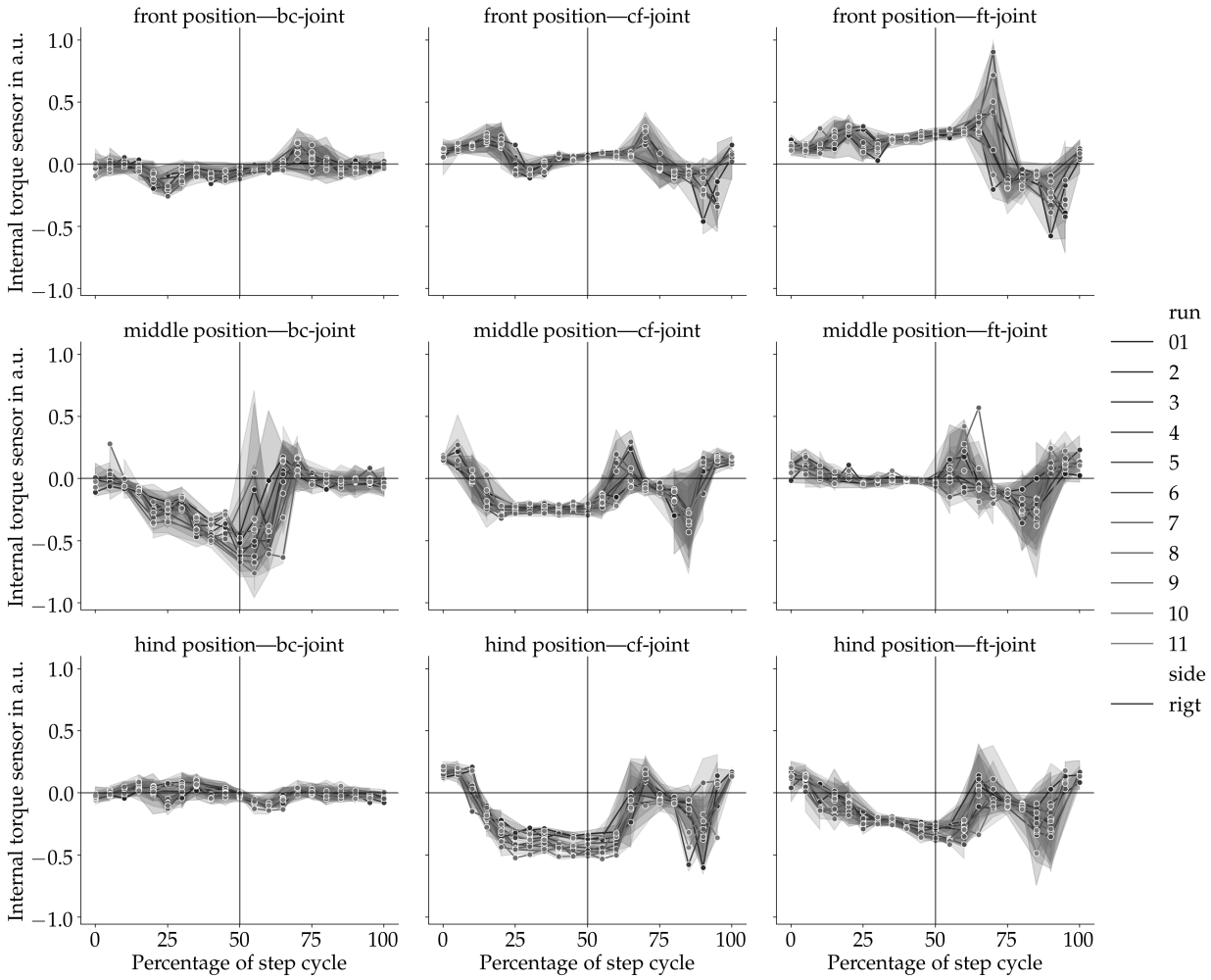

(c) Substrate inclination: 0°

Figure B.3: Comparison of intra-run and inter-run variability in torque measurements for all inclinations. (cont.)

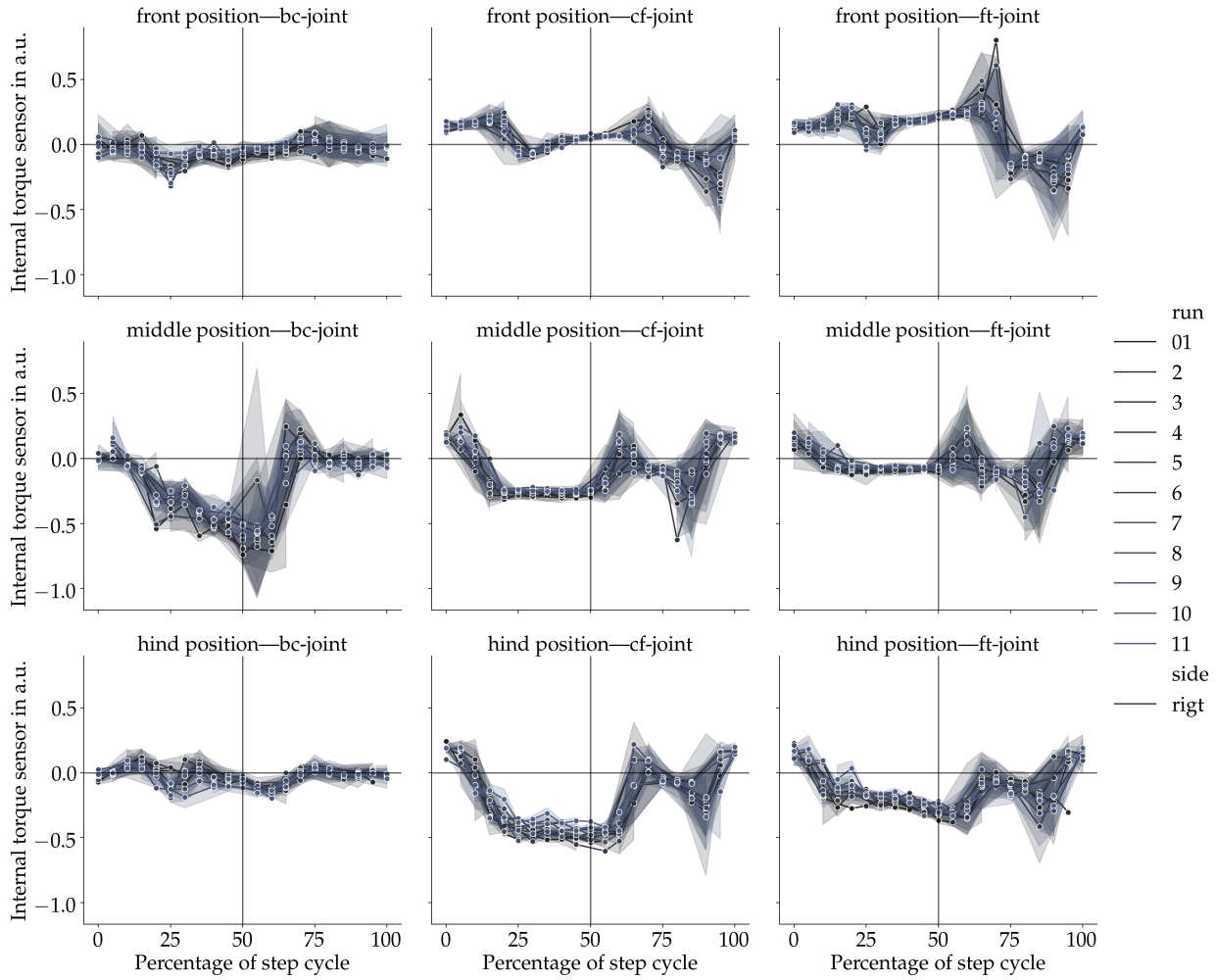

(d) Substrate inclination: 7°

Figure B.3: Comparison of intra-run and inter-run variability in torque measurements for all inclinations. (cont.)

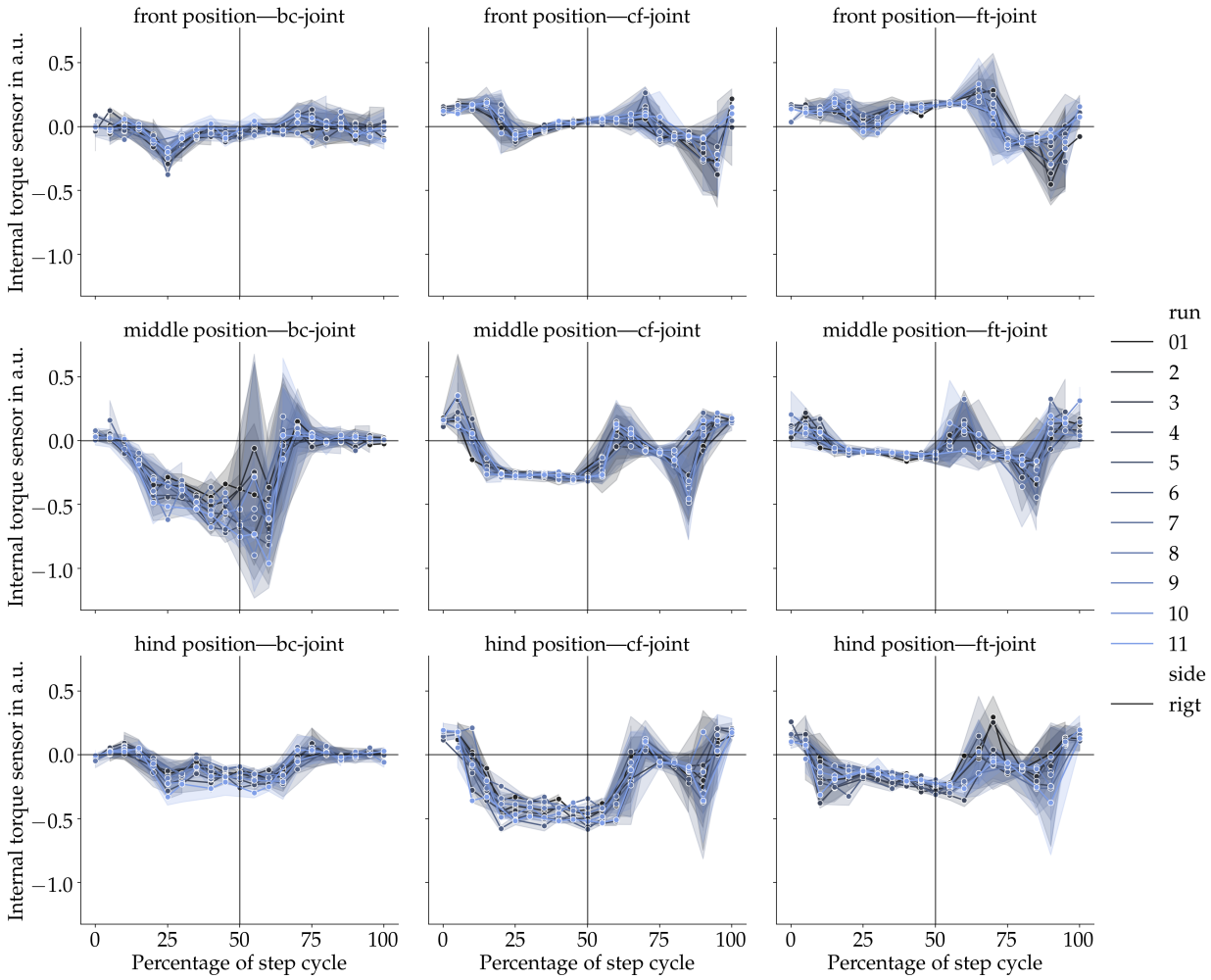

(e) Substrate inclination: 13°

Figure B.3: Comparison of intra-run and inter-run variability in torque measurements for all inclinations. (cont.)

APPENDIX C

Additional Measurements

Figure C.1: Linear correlation between the selected command in ROS and the internally measured value (blue points) and the externally measured force in kg × cm (orange bars). Pictures taken as part of student work [Thuilot, 2017]

Figure C.2: Macro photography of an ant leg used for photogrammetry. Pictures taken as part of student work [Hügel, 2018].

List of Figures

2.1 Path of a foraging desert ant after [Müller and Wehner, 1988]. N denotes the position of the nest, F denotes the position of the feeder. Black line is the foraging path. Blue line is the homing path. 9
2.2 Experimental setup modified after [Seidl and Wehner, 2006]. Training and test channel are set up parallel to each other. After several trips between nest and feeder in the training channel the ants are transferred to the test channel. The position of the turns are recorded to determine the assumed position of the nest. 11

3.1 Structure of the thesis. Numbers denote chapter numbers. The thesis is structured in four parts with Part II and Part III comprising the original research. 14

4.1 Various known shapes of campaniform sensilla as described on the wing and haltere of *drosophila melanogaster*. Modified after [Cole and Palka, 1982]. . . 23
4.2 Prepared scanning electron microscope sample. Double sided tape is stuck to the sample holder and slices for the legs marked. The dried and dissected legs are placed and the whole holder is sputtered with gold. 24
4.3 Anatomical directional reference of the ant. Cranial and caudal describe positions closer or farther from the head. Dorsal and ventral reference the distance to the back or stomach respectively. Proximal and distal denote the closeness to the body. 25
4.4 Three different shapes of campaniform sensilla on the legs of *Cataglyphis fortis*. All pictures taken on right middle legs. Left and middle pictures are from the same specimen, right picture from another specimen. Pictures taken as part of student work [Kreimeier, 2017]. 26

4.5 Overview of one dissected leg under the scanning electron microscope with the segments labelled accordingly. Campaniform sensilla are found mainly in the area marked with the red square. Fig. 4.6 shows magnifications of this area on different samples and thus different perspectives. Pictures taken as part of student work [Kreimeier, 2017]. 27
4.6 All available views of the trochanter on the samples. Views according to the sub-captions. Circles mark fields and single campaniform sensilla with color according to Fig. 4.7. Modified after student work [Kreimeier, 2017]. 28
a caudal view 28
b dorsal view 28
c cranial view 28
d ventral view 28
4.7 Polar projection of discovered fields and single campaniform sensilla. Pictures taken as part of student work [Kreimeier, 2017]. 29
4.8 Reconstructed synchrotron X-ray microtomography images. Holes on the surface (marked with red circles) correspond to the positions of the campaniform sensilla as determined via scanning electron microscope. 29
a Reconstruction via Drishti. 29
b Reconstruction via 3D Slicer. Pictures taken as part of student work [Hügel, 2018]. 29

5.1 Digitized points and fixed reference frame on the desert ant. Green points mark the characteristic points that are identified to digitize the movement. On the body the junction between caput and thorax as well as the junction between thorax and gaster are chosen. Exemplary for all legs the points on the middle leg are marked. The coxa-femur and tibia-tarsus joints as well as the tip of the tarsus are chosen for digitizing. The body-fixed reference frame is centred in the centre of mass. The x-axis corresponds to the cranial direction, the y-axis to the distal direction and the z-axis to the dorsal direction. . . . 34
5.2 Positions of the digitized markers of the front left leg in the body-fixed reference frame of the ant. From top to bottom the coxa-femur joint, femur-tibia joint and tarsus tip are shown. Left to right break down the cranial(x), distal(y) and dorsal(z)-axis. On the x-axis of every graph the progress through the step cycle normalized to 100 % is marked. The y-axis shows the distance from the ant's centre of mass on the axis denoted in the title of the subplot. Grey lines represent data of different steps while the red lines are the respective average over all steps for the marker. 35
5.3 The digitized points are connected to links. The first link (1) connects the head with the ant's centre of mass. A virtual link (2) is drawn from there to the coxa-femur joint to establish the junction of body and respective leg. The next link (3) represents the thigh and runs to the femur-tibia joint. The final link (4) covers tibia and tarsus and ends in the tarsus tip. 36

a Links as located in the ant. 36

b Digitized links over the normalized step cycle in the body-fixed reference frame. Each link is drawn for every 1 % of the step cycle. 36

5.4 Sequence to determine the inverse kinematic. The spatial coordinates of the digitized points are transformed homogeneously and entered into the solver. Two solvers are evaluated: ikine and ikcon and compared with the digitized data (Fig. 5.8). The solver determines the joint angles. For visual screening of undesired behaviour like jerking motions the generated motion is plotted (Fig. 5.7). 37

5.5 Percentage of deviation of the links to their respective averages. 38

5.6 Modified kinematic chain following the Denavit-Hartenberg convention at 95 % of the normalized step cycle. The x-axis follows along the links connecting the digitized points. The origin of the frames is located at the beginning of the links. Green circles denote the digitized points that are connected by the links. 39

5.7 Visual representation of the solution of the inverse kinematic solver. Green circles represent the digitized data. Blue line shows the path of the end effector during the simulation. q_n denote the degrees of freedom. The difference in the paths stem from abstractions assumed in the robotic model, like fixed link length. Blue link corresponds to Link 3 in the ant, red link to Link 4 (Fig. 5.3). The movement is relative to the coxa. The frame of reference denotes the distances to the ant's centre of mass in mm. 40

5.8 Comparison of the performance of the solvers ikine and ikcon. The reference curve "Digitized Data" is generated by the forward kinematics of the digitized points. The four degrees of freedom are shown in degree over the percentage of the step cycle. The closer the curves to the respective digitized data points, the more faithful the reproduction. Another desired trait is a smooth curve to avoid jerking motions in the robot. Pictures taken as part of student work [Giugno, 2016], slight modifications. 41

6.1 Overview of the experimental setup for the one legged platform. The modular leg is movable along the angle-adjustable linear track. The substrate is pictured simplified as an inclined plane. Substrate and track are fixed at the same angle for each run. Dimensioned drawing in appendix (Fig. A.1). . . . 48

6.2 3D-printed connector pieces. The nomenclature follows the established names in hexapod research which is based on the biological counterparts. Dimensioned drawing in appendix (Fig. A.4, A.5 and A.6). 49

6.3 Motors link the connector pieces with each other and to wagon representing the body. The nomenclature denotes which parts are linked. Dimensioned drawing in appendix (Fig. A.2). 50

6.4 Schematic illustration of sensor placement. Sensor sizes are not to scale. The nomenclature of the sensors corresponds to the respective connectors or motors they belong to. 51

6.5 Transfer function showing the correlation of the applied torque and the measured current in the motor (pink line) [ROBOTIS, 2020]. The linearity allows using the current as measure for the joint torque. Also pictured: Efficiency in percent (green) and speed in revolutions per minute (black) as a function of torque. 52

6.6 Simplified overview of ROS nodes. The three joints are summarised to one node in this illustration. Circles represent nodes, squares represent topics. The fixed movement is generated in the *movement* node and published to the *command* topic. This topic is processed in the *dynamixel_manager* node into commands readable by the Dynamixel motors and published to the *motor_state* topic that gets published to the USB port and thus the motors. In the reverse direction the information from the motors via the USB port is read in at the *motor_state* topic and published by the *dynamixel_manager* node to the *state* topic where it is recorded for further analysis. 53

6.7 Forces measured with the spring scale in dependence on the substrate inclination. Mean and standard deviation over 15 repetitions are shown. The line represents the linear regression fit. Precise model parameters can be found in Tab. 6.1. Adding weight to the experimental setup leads to 26 % increase in the slope. 55

a without additional weight 55

b with additional weight 55

6.8 Relative deformation of the strain gauges over the substrate inclinations. Mean and standard deviation over 15 repetitions are shown. The lines represent the linear regression fits. Precise model parameters can be found in Tab. 6.1. Adding weight to the experimental setup results in a steeper slope for all strain gauges. 58

a without additional weight 58

b with additional weight 58

6.9 Internal joint torque over the substrate inclinations. Mean and standard deviation over 15 repetitions are shown. The lines represent the linear regression fits. Precise model parameters can be found in Tab. 6.1. Adding weight to the experimental setup results in a steeper slope for body-coxa and femur-tibia joint. The coxa-femur joint shows no dependance on the substrate inclination. 59

a without additional weight 59

b with additional weight 59

7.1 Dimensions and nomenclature of the PhantomX platform. The walking direction determines the front of the robot. From front to back the legs are numbered consecutively. The sides left and right are determined looking from the top with the walking direction oriented upwards. All legs consist of three connectors labelled from the body outward: coxa, femur and tibia. The joints are labelled with shortened forms of the connectors that they border: body-coxa (bc), coxa-femur (cf) and femur-tibia (ft). This nomenclature is consistent with Chapter 6. 67

7.2 Overview over the experimental setup. The robot is placed on a ramp of varying inclination. Walking upwards is denoted with positive angles, walking downwards is denoted with negative angles. The robot is powered by batteries, the USB cable connects to the laptop controlling the movement and logging the measurements of the internal torque sensors. 68

a top view 68

b side view 68

c inclinations 68

7.3 Sketch of the robot movement. The black arrow indicates the walking direction. Legs in motion are colored red in the top view. Red arrows indicate the motion direction of the legs. The step cycle of one tripod is shown, afterwards the analoguous movement is repeated on the opposing tripod. 69

7.4 Schematic of the wiring. The motors of each leg are daisychained and connected to the microcontroller. The robot is powered by a battery pack indicated by the power plug in this image. The microcontroller is connected through the power hub to the USB2Dynamixel device that allows communication to the laptop via the USB-port. 70

7.5 The internal torque sensor is read in arbitrary units. The course over a whole step cycle is recorded and averaged over all steps and all runs. The shadows indicate the 95 % confidence interval. The results shown are at 0° inclination and for the right front, middle and hind legs. From left to right the joints are further from the body. The shift from stance to swing phase is marked with a vertical line. 73

7.6 The internal torque sensor is read in arbitrary units. The course over a whole step cycle is recorded and averaged over all steps and all runs. The shadows indicate the 95 % confidence interval. The results are shown from top to bottom for the right front, middle and hind legs. From left to right the joints are further from the body. Colours indicate the inclination of the ramp. The shift from stance to swing phase is marked with a vertical line. The results for the left leg can be found in the appendix (Fig. B.1). 75

8.1 Simulated environment in CoppeliaSim. The scene hierarchy is accessible on the left side. On the right side the graphical representation of the simulation is visible. The model of the robot (1) is placed on the model of the ramp (2). The dynamics engine (3), the accuracy (4) and the time step size within the simulation (4) can be chosen in the drop-down menus at the top. 82

8.2 Schematic illustration of the alignment of the robot model on the ramp. The arrow denotes the walking direction of the robot model. The gradient of inclination is oriented along the dotted line. The angle α between these two orientations is used to describe the alignment. Positive angles denote clockwise rotation of the walking direction against the ramp. Negative angles denote a counter clockwise rotation. 83

8.3 Schematic illustration of the artificial neural network. Circles denote neurons, arrows denote connections. All neurons are fully connected and the information is propagated forward through the ANN. The 18 input neurons represent the signals received from each of the 18 motors. In one case an additional input neuron is introduced to represent the current percentage of the step cycle. The number of hidden neurons is varied from 1 to 100 to determine the optimal topology. The output neuron is interpreted as the predicted angle of substrate inclination in degree. 84

8.4 For each of the three conditions of varying weight (light blue), varying alignment (dark blue) and their combination (orange) artificial neural networks are trained for 20 epochs. The ANNs differ in number of hidden neurons. For each condition from 1 to 100 hidden neurons are evaluated after training with respect to the root-mean-square error in degree. The lines serve as guides to identify the general trend but do not represent relation between measured values. 86

8.5 Training sequences for the fully trained artificial neural networks on the simulated environment for the three conditions varying weight, varying alignment and their combination. The performance as measured by the mean squared error for the data subsets training, validation and test are shown separately but run almost identically. The training stops when performance on the validation set is worse than on the training set six times in a row. The best validation performance is marked by a green circle and dotted lines. 88

a varying weight 88

b varying alignment 88

c varying both parameters 88

8.6 Response of the fully trained artificial neural networks on the simulated environment for the three conditions varying weight, varying alignment and their combination. The strength of the output neuron is interpreted as substrate inclination angle in degree marked as circles over the actual angle in degree on the x-axis. The coloured line represents the linear regression fit. The model parameters are found in the legend and the correlation coefficient R at the top of the graph. As additional interpretation aid the line of equality is also marked. Points along this line represent perfect answers of the ANN. 89
a varying weight 89
b varying alignment 89
c varying both parameters 89
8.7 Performance as measured by root-mean-square error (RMSE) and necessary training epochs to reach stop criterion in dependence on the number of hidden neurons in the artificial neural network. For each of the three training conditions of the real world data 100 ANNs are randomly initialized and then fully trained. The lines show the means and shadows indicate the standard aberration. 90
a all time steps 90
b all time steps with extra step cycle information 90
c time steps of double support phase 90
8.8 Training sequences for the fully trained artificial neural networks with optimal topology for the real world data for the three conditions. The performance as measured by the mean squared error for the data subsets training, validation and test are shown. The best validation performance is marked by a green circle and dotted lines. 91
a all time steps 91
b all time steps with extra step cycle information 91
c time steps of double support phase 91
8.9 Response of the fully trained artificial neural networks with optimal topology for the real world data for the three conditions. The strength of the output neuron is interpreted as substrate inclination angle in degree marked as circles over the actual angle in degree on the x-axis. The coloured line represents the linear regression fit. The model parameters are found in the legend and the correlation coefficient R at the top of the graph. As additional interpretation aid the line of equality is also marked. Points along this line represent perfect answers of the ANN. 92
a all time steps 92
b all time steps with extra step cycle information 92
c time steps of double support phase 92

9.1 Schematic illustration of the biomimetic engineering process after [VDI-Richtlinie 6220, 2012]. 100

11.1 Preliminary results of a photogrammetry approach. The reconstructed shell of the desert ant femur and tibia is shown from three perpendicular perspectives. Pictures taken as part of student work [Hügel, 2018]. 107
11.2 Exemplary results of the automated digitalization of ant leg movement by an artificial neural network. Pictures taken as part of student work [Martin, 2019], slight modifications. 109
a Example of the identified points on the left hind leg. Picture colour corrected. 109
b Example of the identified points on all legs of one tripod without video overlay. 109
11.3 Exemplary errors in the prediction of the neural network. (A) The edge of the force measuring platform impedes the discrimination of the leg versus the substrate. (B) The mirror mounts temporarily hides the ant which is not always identified correctly and points in this region are erroneously marked. (C) Due to a rough symmetry of the ant body, ants walking in the opposite direction to the originally trained videos are not identified correctly. Pictures taken as part of student work [Martin, 2019]. 110

A.1 Technical drawing of the one legged setup. 114
A.2 Technical drawing of dynamixel motors MX-64A. 115
A.3 Technical drawing of the one legged platform. Exploded view. 116
A.4 Technical drawing of the one legged platform illustrated from three perspectives. 117
A.5 Technical drawing of the femur of the one legged platform. 118
A.6 Technical drawing of the tibia of the one legged platform. 119

B.1 The internal torque sensor is read in arbitrary units. The course over a whole step cycle is recorded and averaged over all steps and all runs. The shadows indicate the 95 % confidence interval. The results are shown from top to bottom for the left front, middle and hind legs. From left to right the joints are further from the body. Colours indicate the inclination of the ramp. The shift from stance to swing phase is marked with a vertical line. The results for the right leg can be found in (Fig. 7.6). 122
B.2 Comparison of the measured internal torque of left and right leg for each inclination. Visual estimation: one-third of the averages are further apart than the 95 % confidence interval and thus significantly distinct and pooling of left and right leg is thus inadmissible. The difference is more pronounced on steeper inclined substrates. 123
a Substrate inclination: $-13°$ 123
B.2 Comparison of the measured internal torque of left and right leg for each inclination. (cont.) 124
b Substrate inclination: $-7°$ 124

B.2 Comparison of the measured internal torque of left and right leg for each inclination. (cont.) . . . 125
c Substrate inclination: 0° . . . 125
B.2 Comparison of the measured internal torque of left and right leg for each inclination. (cont.) . . . 126
d Substrate inclination: 7° . . . 126
B.2 Comparison of the measured internal torque of left and right leg for each inclination. (cont.) . . . 127
e Substrate inclination: 13° . . . 127
B.3 Comparison of intra-run and inter-run variability in torque measurements for all inclinations. Lines represent the mean over all steps for each run. The shadow indicates the standard deviation. Visual estimation: over 90 % of the torques measured at a certain point in the step cycle are within the range of one standard deviation. Thus, the intra- and inter-run variability is similar and in the further evaluations the separate runs are treated as one long continous run. . . . 128
a Substrate inclination: −13° . . . 128
B.3 Comparison of intra-run and inter-run variability in torque measurements for all inclinations. (cont.) . . . 129
b Substrate inclination: −7° . . . 129
B.3 Comparison of intra-run and inter-run variability in torque measurements for all inclinations. (cont.) . . . 130
c Substrate inclination: 0° . . . 130
B.3 Comparison of intra-run and inter-run variability in torque measurements for all inclinations. (cont.) . . . 131
d Substrate inclination: 7° . . . 131
B.3 Comparison of intra-run and inter-run variability in torque measurements for all inclinations. (cont.) . . . 132
e Substrate inclination: 13° . . . 132

C.1 Linear correlation between the selected command in ROS and the internally measured value (blue points) and the externally measured force in kg × cm (orange bars). Pictures taken as part of student work [Thuilot, 2017] . . . 133
C.2 Macro photography of an ant leg used for photogrammetry. Pictures taken as part of student work [Hügel, 2018]. . . . 134

List of Tables

6.1 Model parameters of the linear regression of the respective sensor reading x and the substrate inclination α 57

8.1 Comparison of the best performance of all described artificial neural networks in this chapter. The performance is evaluated by the lowest root-mean-square error. The topology is characterised by the number of hidden neurons. The number of training epochs indicate the speed to fully train the ANN. For the experimental data mean and standard deviation over 100 randomly initialized ANN of the same topology is shown. 93

11.1 Overview of the performance of the automated digitalization of the movement of the ant legs through DeepLabCut depending on the number of videos used and number of manually labelled frames used in training. The performance is evaluated by the mean absolute error of the position in pixels of the manually labelled points and the points predicted by the network. 110

Bibliography

[Bailey et al., 2001] Bailey, S. A., Cham, J. G., Cutkosky, M. R., and Full, R. J. (2001). Comparing the locomotion dynamics of the cockroach and a shape deposition manufactured biomimetic hexapod. In *Experimental Robotics VII*, pages 239–248. Springer.

[Berends, 2020] Berends, S. (2020). VDI verleiht International Bionic Award. `https://www.vdi.de/news/detail/nachwuchswissenschaftler-gewinnen-mit-autonom-navigierendem-roboter`. (last visited on 4.12.2020).

[Bjelonic et al., 2018] Bjelonic, M., Kottege, N., Homberger, T., Borges, P., Beckerle, P., and Chli, M. (2018). Weaver: Hexapod robot for autonomous navigation on unstructured terrain. *Journal of Field Robotics*, 35(7):1063–1079.

[Bolton, 2003] Bolton, B. (2003). *Synopsis and classification of Formicidae*. American Entomological Institute.

[Bühlmann et al., 2012] Bühlmann, C., Hansson, B. S., and Knaden, M. (2012). Desert ants learn vibration and magnetic landmarks. *Plos one*, 7(3):e33117.

[Carmer and Peterson, 1996] Carmer, D. C. and Peterson, L. M. (1996). Laser radar in robotics. *Proceedings of the IEEE*, 84(2):299–320.

[Cole and Palka, 1982] Cole, E. S. and Palka, J. (1982). The pattern of campaniform sensilla on the wing and haltere of Drosophila melanogaster and several of its homeotic mutants. *Development*, 71(1):41–61.

[Corke, 2002] Corke, P. (2002). Robotics toolbox. `https://petercorke.com/toolboxes/robotics-toolbox/`. (last visited on 18.12.2020).

[Craig, 2009] Craig, J. J. (2009). *Introduction to robotics: mechanics and control, 3/E*. Pearson Education India.

[DeSouza and Kak, 2002] DeSouza, G. N. and Kak, A. C. (2002). Vision for mobile robot navigation: A survey. *IEEE transactions on pattern analysis and machine intelligence*, 24(2):237–267.

[Dumpert, 1972] Dumpert, K. (1972). Bau und Verteilung der Sensillen auf der Antennengeißel von Lasius fuliginosus (Latr.)(Hymenoptera, Formicidae). *Zeitschrift für Morphologie der Tiere*, 73(2):95–116.

[Dupeyroux et al., 2019] Dupeyroux, J., Serres, J. R., and Viollet, S. (2019). AntBot: A six-legged walking robot able to home like desert ants in outdoor environments. *Science Robotics*, 4(27).

[Endlein and Federle, 2015] Endlein, T. and Federle, W. (2015). On heels and toes: how ants climb with adhesive pads and tarsal friction hair arrays. *PloS one*, 10(11):e0141269.

[Federle and Endlein, 2004] Federle, W. and Endlein, T. (2004). Locomotion and adhesion: dynamic control of adhesive surface contact in ants. *Arthropod Structure & Development*, 33(1):67 – 75. Attachment Systems of Arthropods.

[Fedorov et al., 2012] Fedorov, A., Beichel, R., Kalpathy-Cramer, J., Finet, J., Fillion-Robin, J.-C., Pujol, S., Bauer, C., Jennings, D., Fennessy, F., Sonka, M., et al. (2012). 3D Slicer as an image computing platform for the Quantitative Imaging Network. *Magnetic resonance imaging*, 30(9):1323–1341.

[Flannery et al., 1987] Flannery, B. P., Deckman, H. W., Roberge, W. G., and D'AMICO, K. L. (1987). Three-dimensional X-ray microtomography. *Science*, 237(4821):1439–1444.

[Fleischmann et al., 2016] Fleischmann, P. N., Christian, M., Müller, V. L., Rössler, W., and Wehner, R. (2016). Ontogeny of learning walks and the acquisition of landmark information in desert ants, Cataglyphis fortis. *Journal of Experimental Biology*, 219(19):3137–3145.

[Forel, 1902] Forel, A. (1902). Les fourmis du Sahara Algérien. Récoltées par M. le Professeur A. Lameere et le Dr A. Diehl.

[Grimaldi et al., 2005] Grimaldi, D., Engel, M. S., Engel, M. S., and Engel, M. S. (2005). *Evolution of the Insects*. Cambridge University Press.

[Guo, 2015] Guo, S. (2015). *Biologically-inspired control framework for insect animation*. PhD thesis, Bournemouth University.

[Guo et al., 2014a] Guo, S., Chang, J., Cao, Y., and Zhang, J. (2014a). A novel locomotion synthesis and optimisation framework for insects. *Computers {&} Graphics*, 38:78–85.

[Guo et al., 2014b] Guo, S., Chang, J., Yang, X., Wang, W., and Zhang, J. (2014b). Locomotion skills for insects with sample-based controller. *Computer Graphics Forum*, 33(7):31–40.

[Guo et al., 2018] Guo, S., Lin, J., Wöhrl, T., and Liao, M. (2018). A neuro-musculo-skeletal model for insects with data-driven optimization. *Scientific Reports*, 8(1):2129.

[Hertzberg et al., 2012] Hertzberg, J., Lingemann, K., and Nüchter, A. (2012). *Mobile Roboter: Eine Einführung aus Sicht der Informatik*. Springer-Verlag.

[Hoffmann, 1964] Hoffmann, C. (1964). Bau und Vorkommen von proprioceptiven Sinnesorganen bei den Arthropoden. In *Ergebnisse der Biologie/Advances in Biology*, pages 1–38. Springer.

[Hoinville and Wehner, 2018] Hoinville, T. and Wehner, R. (2018). Optimal multiguidance integration in insect navigation. *Proceedings of the National Academy of Sciences*, page 201721668.

[Homberger et al., 2016] Homberger, T., Bjelonic, M., Kottege, N., and Borges, P. V. (2016). Terrain-dependant control of hexapod robots using vision. In *International Symposium on Experimental Robotics*, pages 92–102. Springer.

[Jeffery, 2003] Jeffery, K. J. (2003). *The neurobiology of spatial behaviour*. Oxford University Press, USA.

[Kaib et al., 2010] Kaib, M., Römer, H., Scharstein, H., Stabentheiner, A., and Stommel, G. (2010). Sinnesphysiologie. In *Lehrbuch der Entomologie*, pages 281–344. Springer.

[Kikinis et al., 2014] Kikinis, R., Pieper, S. D., and Vosburgh, K. G. (2014). 3D Slicer: a platform for subject-specific image analysis, visualization, and clinical support. In *Intraoperative imaging and image-guided therapy*, pages 277–289. Springer.

[Knaden and Wehner, 2005] Knaden, M. and Wehner, R. (2005). Nest mark orientation in desert ants Cataglyphis: what does it do to the path integrator? *Animal behaviour*, 70(6):1349–1354.

[Limaye, 2012] Limaye, A. (2012). Drishti: a volume exploration and presentation tool. In *Developments in X-ray Tomography VIII*, volume 8506, page 85060X. International Society for Optics and Photonics.

[Manoonpong et al., 2016] Manoonpong, P., Petersen, D., Kovalev, A., Wörgötter, F., Gorb, S. N., Spinner, M., and Heepe, L. (2016). Enhanced locomotion efficiency of a bio-inspired walking robot using contact surfaces with frictional anisotropy. *Nature Publishing Group*, (April):1–11.

[Markl, 1970] Markl, H. (1970). Die Verständigung durch Stridulationssignale bei Blattschneiderameisen. *Zeitschrift für vergleichende Physiologie*, 69(1):6–37.

[Mathis et al., 2018] Mathis, A., Mamidanna, P., Cury, K. M., Abe, T., Murthy, V. N., Mathis, M. W., and Bethge, M. (2018). DeepLabCut: markerless pose estimation of user-defined body parts with deep learning. *Nature neuroscience*, 21(9):1281–1289.

[McCulloch and Pitts, 1943] McCulloch, W. S. and Pitts, W. (1943). A logical calculus of the ideas immanent in nervous activity. *The bulletin of mathematical biophysics*, 5(4):115–133.

[McNamara, 2008] McNamara, J. (2008). *GPS for Dummies*. John Wiley & Sons.

[Moré, 1978] Moré, J. J. (1978). The Levenberg-Marquardt algorithm: implementation and theory. In *Numerical analysis*, pages 105–116. Springer.

[Müller and Wehner, 1988] Müller, M. and Wehner, R. (1988). Path integration in desert ants, Cataglyphis fortis. *Proceedings of the National Academy of Sciences*, 85(14):5287–5290.

[Nath et al., 2019] Nath, T., Mathis, A., Chen, A. C., Patel, A., Bethge, M., and Mathis, M. W. (2019). Using DeepLabCut for 3D markerless pose estimation across species and behaviors. *Nature protocols*, 14(7):2152–2176.

[Nguyenová et al., 2018] Nguyenová, M. T., Čížek, P., and Faigl, J. (2018). Modeling proprioceptive sensing for locomotion control of hexapod walking robot in robotic simulator. In *International Conference on Modelling and Simulation for Autonomous Systesm*, pages 215–225. Springer.

[Palmer III et al., 2010] Palmer III, L. R., Diller, E. D., and Quinn, R. D. (2010). Design aspects of a climbing hexapod. In *Mobile Robotics: Solutions and Challenges*, pages 197–204. World Scientific.

[Reinhardt, 2014] Reinhardt, L. (2014). *Dynamik und Kinematik der Lokomotion von Formica polyctena*. PhD thesis, Jena, Friedrich-Schiller-Universität Jena, Diss., 2014.

[Reinhardt and Blickhan, 2014] Reinhardt, L. and Blickhan, R. (2014). Ultra-miniature force plate for measuring triaxial forces in the micronewton range. *The Journal of experimental biology*, 217(Pt 5).

[ROBOTIS, 2020] ROBOTIS (2020). ROBOTIS e-Manual MX-64T/R/AT/AR. `https://emanual.robotis.com/docs/en/dxl/mx/mx-64/`. (last visited on 4.12.2020).

[Rohmer et al., 2013] Rohmer, E., Singh, S. P. N., and Freese, M. (2013). CoppeliaSim (formerly V-REP): a Versatile and Scalable Robot Simulation Framework. In *Proc. of The International Conference on Intelligent Robots and Systems (IROS)*.

[Ronacher, 2008] Ronacher, B. (2008). Path integration as the basic navigation mechanism of the desert ant Cataglyphis fortis (Forel, 1902)(Hymenoptera: Formicidae). *Myrmecological News*, 11:53–62.

[Ronacher et al., 2000] Ronacher, B., Gallizzi, K., Wohlgemuth, S., and Wehner, R. (2000). Lateral optic flow does not influence distance estimation in the desert ant Cataglyphis fortis. *The Journal of experimental biology*, 203(Pt 7):1113–1121.

[Ronacher and Wehner, 1995] Ronacher, B. and Wehner, R. (1995). Desert ants Cataglyphis fortis use self-induced optic flow to measure distances travelled. *Journal of Comparative Physiology A*, 177(1):21–27.

[Santschi, 1929] Santschi, F. (1929). Etude sur les Cataglyphis. *Revue Suisse de Zoologie*, 36(2):25–70.

[Schenk, 2005] Schenk, T. (2005). Introduction to photogrammetry. *The Ohio State University, Columbus*, 106.

[Schlögl et al., 2018a] Schlögl, B., Schramm, D., and Seidl, T. (2018a). Using joint-torque for a cost-effective bio-inspired odometer for legged robots. In *Proc. 2nd Int. Youth Conf. Bionic Eng.(IYCBE)*.

[Schlögl et al., 2018b] Schlögl, B., Seidl, T., Wöhrl, T., Bruckmann, T., and Schramm, D. (2018b). Odometrie bei Laufrobotern nach Vorbild der Entfernungs- und Steigungsmessung von Wüstenameisen Cataglyphis spec. In *IFToMM D-A-CH Konferenz*.

[Schneider et al., 2014] Schneider, A., Paskarbeit, J., Schilling, M., and Schmitz, J. (2014). HECTOR, a bio-inspired and compliant hexapod robot. In *Conference on Biomimetic and Biohybrid Systems*, pages 427–429. Springer.

[Seidl, 2008] Seidl, T. (2008). Insect navigation and path finding. *Acta Futura*, 4(february 2008):102–106.

[Seidl et al., 2006] Seidl, T., Knaden, M., and Wehner, R. (2006). Desert ants: Is active locomotion a prerequisite for path integration? *Journal of Comparative Physiology A: Neuroethology, Sensory, Neural, and Behavioral Physiology*, 192(10):1125–1131.

[Seidl and Wehner, 2006] Seidl, T. and Wehner, R. (2006). Visual and tactile learning of ground structures in desert ants. *Journal of Experimental Biology*, 209(17):3336–3344.

[Seidl and Wehner, 2008] Seidl, T. and Wehner, R. (2008). Walking on inclines: how do desert ants monitor slope and step length. *Frontiers in zoology*, 5(1):8.

[Sommer and Wehner, 2012] Sommer, S. and Wehner, R. (2012). Leg allometry in ants: Extreme long-leggedness in thermophilic species. *Arthropod Structure & Development*, 41(1):71 – 77.

[Steck et al., 2009a] Steck, K., Hansson, B. S., and Knaden, M. (2009a). Smells like home: Desert ants, Cataglyphis fortis, use olfactory landmarks to pinpoint the nest. *Frontiers in Zoology*, 6(1):1–8.

[Steck et al., 2011] Steck, K., Hansson, B. S., and Knaden, M. (2011). Desert ants benefit from combining visual and olfactory landmarks. *Journal of Experimental Biology*, 214(8):1307–1312.

[Steck et al., 2010] Steck, K., Knaden, M., and Hansson, B. S. (2010). Do desert ants smell the scenery in stereo? *Animal Behaviour*, 79(4):939–945.

[Steck et al., 2009b] Steck, K., Wittlinger, M., and Wolf, H. (2009b). Estimation of homing distance in desert ants, Cataglyphis fortis, remains unaffected by disturbance of walking behaviour. *Journal of Experimental Biology*, 212(18):2893–2901.

[Talluri and Aggarwal, 1999] Talluri, R. and Aggarwal, J. (1999). Position estimation techniques for an autonomous mobile robot–A review. In *Handbook of Pattern Recognition and Computer Vision*, pages 765–796. World Scientific.

[Thurm, 2001] Thurm, U. (2001). Mechanosensorik. In *Neurowissenschaft*, pages 333–353. Springer.

[VDI-Richtlinie 6220, 2012] VDI-Richtlinie 6220 (2012). Bionik. Konzeption und Strategie. Abgrenzung zwischen bionischen und konventionellen Verfahren/Produkten.

[Vincent et al., 2007] Vincent, J. F., Clift, S. E., and Menon, C. (2007). Biomimetics of campaniform sensilla: Measuring strain from the deformation of holes. *Journal of Bionic Engineering*, 4(2):63–76.

[Vogelgesang et al., 2012] Vogelgesang, M., Chilingaryan, S., dos_Santos Rolo, T., and Kopmann, A. (2012). UFO: A scalable GPU-based image processing framework for on-line monitoring. In *2012 IEEE 14th International Conference on High Performance Computing and Communication & 2012 IEEE 9th International Conference on Embedded Software and Systems*, pages 824–829. IEEE.

[Wahl et al., 2015] Wahl, V., Pfeffer, S. E., and Wittlinger, M. (2015). Walking and running in the desert ant Cataglyphis fortis. *Journal of Comparative Physiology A: Neuroethology, Sensory, Neural, and Behavioral Physiology*, 201(6):645–656.

[Wehner, 1982] Wehner, R. (1982). *Himmelsnavigation bei Insekten: Neurophysiologie und Verhalten*.

[Wehner, 1983] Wehner, R. (1983). Taxonomie, Funktionsmorphologie und Zoogeographie der saharischen Wüstenameisen Cataglyphis fortis (Forel 1902) stat. nov. *Senckenbergiana biol*, 64:89–132.

[Wehner and Räber, 1979] Wehner, R. and Räber, F. (1979). Visual spatial memory in desert ants, Cataglyphis bicolor (Hymenoptera: Formicidae). *Experientia*, 35(12):1569–1571.

[Wittlinger et al., 2006] Wittlinger, M., Wehner, R., and Wolf, H. (2006). The ant odometer: stepping on stilts and stumps. *science*, 312(5782):1965–1967.

[Wittlinger et al., 2007] Wittlinger, M., Wolf, H., and Wehner, R. (2007). Hair plate mechanoreceptors associated with body segments are not necessary for three-dimensional path integration in desert ants, Cataglyphis fortis. *The Journal of experimental biology*, 210(Pt 3):375–82.

[Wohlgemuth et al., 2002] Wohlgemuth, S., Ronacher, B., and Wehner, R. (2002). Distance estimation in the third dimension in desert ants. *Journal of Comparative Physiology A: Neuroethology, Sensory, Neural, and Behavioral Physiology*, 188(4):273–281.

[Wöhrl et al., 2017] Wöhrl, T., Reinhardt, L., and Blickhan, R. (2017). Propulsion in hexapod locomotion: how do desert ants traverse slopes? *The Journal of Experimental Biology*, 220(9):1618–1625.

[Xiong and Manoonpong, 2015] Xiong, X. and Manoonpong, P. (2015). Adaptive and energy efficient walking in a hexapod robot under neuromechanical control and sensorimotor learning. pages 1–14.

[Xiong and Manoonpong, 2018] Xiong, X. and Manoonpong, P. (2018). No need for landmarks: An embodied neural controller for robust insect-like navigation behaviors. Unpublished.

[Xiong et al., 2014] Xiong, X., Wörgötter, F., and Manoonpong, P. (2014). Neuromechanical control for hexapedal robot walking on challenging surfaces and surface classification. *Robotics and Autonomous Systems*, 62(12):1777–1789.

[Zollikofer, 1994] Zollikofer, C. (1994). Stepping patterns in ants-influence of body morphology. *Journal of experimental biology*, 192(1):107–118.

Supervised Student Contribution to the Dissertation

Master thesis

[Giugno, 2016] Giugno, A. (2016). ROS in der Biorobotik - Synthese der Lokomotion von *Cataglyphis fortis*. *Master thesis, Westfälische Hochschule, Deutschland*

Bachelor thesis

[Hügel, 2018] Hügel, A. (2018). Finite-Elemente-Lastanalyse des 3D-Modells eines Insektenbeins. *Bachelor thesis, Westfälische Hochschule, Deutschland*

[Rauscher, 2018] Rauscher, L. (2018). Konstruktion und Vergleich einer lateralen Hilfschiene und eines neigungsverstellbaren Laufbandes als Varianten für die Simulation der Lokomotion eines bionischen Arthropodenbeins. *Bachelor thesis, Westfälische Hochschule, Deutschland*

[Schicks, 2018] Schicks, J. (2018). Vergleich interner und externer Sensoren an einem Laufroboterbein zur Wahrnehmung von steigungsabhängigen Lastunterschieden unter Nutzung des Robot Operating Systems (ROS). *Bachelor thesis, Westfälische Hochschule, Deutschland*

[Schumacher, 2017] Schumacher, T. (2017). Konstruktion und Ansteuerung eines mechanisch-stationären Ameisenbeins. *Bachelor thesis, Westfälische Hochschule, Deutschland*

Project report

[Bongartz, 2017] Bongartz, T. (2017). Analyse der Oberflächenstruktur von Cataglyphis fortis unter Betrachtung der Campaniformen Sensillen. *Project report, Westfälische Hochschule, Deutschland*

[Busch, 2020] Busch, J. (2020). Datenerhebung und -auswertung am Hexapoden-Roboter in Bezug auf wirkende Kräfte bei unterschiedlichen Untergrundsteigungen. *Project report, Westfälische Hochschule, Deutschland*

[Deckers, 2017] Deckers, J. (2017). Projektbericht zu der Gelenkdatensammlung eines hexapoden Roboters. *Project report, Westfälische Hochschule, Deutschland*

[Kaden, 2016] Kaden, N. (2016). Oberflächenstrukturen an den Extremitäten von Cataglyphis fortis. *Project report, Westfälische Hochschule, Deutschland*

[Koepchen-Thomä, 2018] Koepchen-Thomä, L. (2018). Photogrammetrie von biologischen Proben am Beispiel eines Ameisenbeins anhand von REM-Bildern. *Project report, Westfälische Hochschule, Deutschland*

[Kreimeier, 2017] Kreimeier, L.-T. (2017). Die Anordnung Campaniformer Sensillen auf den Beinen der Wüstenameise Cataglyphis fortis. *Project report, Westfälische Hochschule, Deutschland*

[Martin, 2019] Martin, L. (2019). Anwendung und Bewertung von DeepLabCut am Beispiel der Beinkinematik von Ameisen. *Project report, Westfälische Hochschule, Deutschland*

[Rhode, 2017] Rhode, M. (2017). Erstellung eines großformatigen Bildes des Femur und Trochanter von Cataglyphis fortis mittels Rasterelektronenmikroskopie. *Project report, Westfälische Hochschule, Deutschland*

[Sellhorn-Timm, 2020] Sellhorn-Timm, J. (2020). Laufroboter nach Vorbild der Wüstenameisen: Flaches KNN für die Bestimmung der Steigung. *Project report, Westfälische Hochschule, Deutschland*

[Tanai, 2019] Tanai, E. (2019). Projektbericht zu der Gelenkdatensammlung eines hexapoden Roboters. *Project report, Westfälische Hochschule, Deutschland*

[Thuilot, 2017] Thuilot, T. (2017). Evaluation von Servomotoren. *Project report, Westfälische Hochschule, Deutschland*

[Zemela, 2019] Zemela, D. (2019). Dynamische Simulation eines Ameisenbeins von Cataglyphis fortis mit Siemens NX 11. *Project report, Westfälische Hochschule, Deutschland*

DOI: 10.17185/duepublico/74235
URN: urn:nbn:de:hbz:464-20210510-135258-0